Cloud Structure, Microphysics, and Precipitation in Tropical Clouds Inferred From Satellite Data

Terence L. Kubar

A dissertation submitted in partial fulfillment of the
requirements for the degree of

Doctor of Philosophy

University of Washington

2008

Program Authorized to Offer Degree:
Department of Atmospheric Sciences

University of Washington
Graduate School

This is to certify that I have examined this copy of a doctoral dissertation by

Terence L. Kubar

and have found that it is complete and satisfactory in all respects,
and that any and all revisions required by the final
examining committee have been made.

Chair of the Supervisory Committee:

_____
Dennis L. Hartmann

Reading Committee:

_____
Christopher S. Bretherton

_____
Dennis L. Hartmann

_____
Robert Wood

Date:_____

In presenting this dissertation in partial fulfillment of the requirements for the doctoral degree at the University of Washington, I agree that the Library shall make its copies freely available for inspection. I further agree that extensive copying of the dissertation is allowable only for scholarly purposes, consistent with "fair use" as prescribed in the U.S. Copyright Law. Requests for copying or reproduction of this dissertation may be referred to ProQuest Information and Learning, 300 North Zeeb Road, Ann Arbor, MI 48106-1346, 1-800-521-0600, to whom the author has granted "the right to reproduce and sell (a) copies of the manuscript in microform and/or (b) printed copies of the manuscript made from microform."

Signature_____

Date_____

University of Washington

Abstract

Cloud Structure, Microphysics, and Precipitation in Tropical Clouds Inferred From Satellite Data

Terence L. Kubar

Chair of the Supervisory Committee:
Professor Dennis L. Hartmann
Department of Atmospheric Sciences

Satellite cloud and precipitation data are used to show that optically thick high cloud fraction is a good proxy for rain rate. In the ITCZ, the ensemble of high clouds in the East Pacific (EP) induces considerably more net TOA radiative cooling compared to the West Pacific (WP), primarily because of more high, thin cloud in the WP.

We investigate whether anvil cloud temperature is more convectively or radiatively driven. The level of neutral buoyancy seems to influence the temperatures of the coldest, thickest clouds, but has no simple relation to anvil cloud. Instead, median anvil cloud temperature closely follows the temperature of the clear-sky convergence peak. The radiatively-driven clear-sky convergence profiles are consistent with warmer anvil clouds in the EP than the WP.

Cloud radar data are used to investigate the relation of cloud structure and precipitation. Heavily precipitating clouds have high tops that are nearly two km deeper than moderately or non-raining high clouds. As cloud tops rise from 12 km to the tropical tropopause, a nearly tenfold rain rate increase is

observed. Clouds with tops below 9.5 km contribute 38% to *total rainfall* in the WP and 47% in the EP.

The importance of macrophysical variables (cloud thickness, liquid water path LWP) and microphysical variables (effective radius r_e, effective droplet concentration N_{eff}) on warm drizzle intensity and frequency is studied using satellite optical and cloud radar data. Cloud top height and LWP substantially increase as drizzle increases. Droplet radius estimated from MODIS also increases with cloud radar reflectivity (dBZ), but levels off as dBZ>0, except where the influence of continental pollution is present, in which case a monotonic increase of r_e with drizzle intensity occurs.

Drizzle *frequency* increases nearly uniformly when cloud tops grow from one to two km. Drizzle frequencies exceed 90% in all regions when LWPs exceed 250 g m^{-2} and N_{eff} values are below 50 cm^{-3}, even in regions where drizzle occurs infrequently on the whole.

TABLE OF CONTENTS

Page

LIST OF FIGURES

Figure Number Page

LIST OF TABLES

ACKOWLEDGMENTS

I wish to thank the numerous individuals who have not only helped inspired this project, but have also assisted in its direction. First and foremost, I wish to sincerely acknowledge my advisor Dennis Hartmann, who has not only helped develop my potential as a critical thinker, but has also allowed me the longitude in which to strive to become a more independent researcher. The skills that I have acquired under the direction of Dennis will be extensively utilized and deeply appreciated in my research career.

I am also deeply grateful to Robert Wood for his extremely consistent support as role of 'unofficial advisor' since my arrival at the University of Washington in 2003. He has been unquestionably reliable at answering and addressing my innumerable technical and broader research questions, and my journey would not have been complete without his considerate and unwavering guidance. Furthermore, Robert Wood has always seemed genuinely enthusiastic about my work, which has had the effect of initiating and enlarging my passion in atmospheric science research. Robert Wood and I have collaborated closely together on many of the projects that comprise this dissertation, and working with him has been a truly unforgettable experience for me.

Special thanks also to Chris Bretherton for serving on my reading committee, and also for providing insightful feedback over the years about my

work. I also wish to thank Qiang Fu and Stephen Riser for serving on my Ph.D. committee. I also sincerely wish to acknowledge Marc L. Michelsen for his expert and patient computer support over the past five years, for he has allowed a nearly flawless experience as I've acquired, processed, and analyzed many large datasets that comprise this dissertation

I also wish to acknowledge Mark Zelinka, my officemate during the past three years, with whom I've engaged in many stimulating discussions about our research agenda and goals. More personally, Mark has also been a very considerate and respectful officemate, and our many enjoyable conversations about non-science matters as well have made for a very pleasant working environment. I also wish to thank former officemate of three years Mario Lopez, with whom I also participated in countless discussions about both research and non-research topics. I even had several opportunities to extensively collaborate with Mario about projects of mutual interest, which made for an exciting working atmosphere. To continue the appreciation of officemates, I also would likely to explicitly thank former officemate Jian Yuan for his endearing support and friendship for many years. More recent officemates Chaim Garfinkel and Libby Barnes also deserve recognition for making my office an environment very conducive for performing solid and satisfying research.

More broadly, it is also highly worthwhile to thank the many individuals with whom I have met, conversed, and developed scientific and personal connections over the past five years in the UW Department of Atmospheric Sciences. This group includes not only ‘grads 2003’ but many other graduate students and postdocs of which a list would be lengthy. I also greatly appreciate many individuals and groups outside of the department who have helped make my graduate school experience a truly enriching and more diverse one. My love for cooking and baking has been shared with local vegan and vegetarian community groups, from which I have connected closely with multiple individuals. Our potlucks, dining events, and road and hiking trips have helped diversify my life outside of the intense research realm of graduate school.

Chapter 1: Introduction

1.1 Preface

Clouds are an important component of the Earth climate system, as they not only modulate the amount of incoming solar radiation that reaches the surface, but they also emit infrared radiation and therefore control the outgoing longwave radiation. The vertical structure, horizontal extent, and cloud type are important for not only determining surface temperature, but also the location and intensity of precipitation. Distribution of surface precipitation is important for the hydrologic cycle, and even for the general circulation of the atmosphere. The fact that precipitation forms from tiny cloud condensation nuclei and that precipitation distribution is related to the aggregate of many clouds suggests that an understanding of clouds and precipitation requires a spanning of multiple spatial and temporal scales.

1.2 Cloud Types, Scales, and Systems

The visible manifestation of many tiny liquid water and ice particles, which we call clouds, occurs on numerous horizontal and vertical scales. Their visual appearance, horizontal coverage, and vertical extent are a result of the physics and dynamics occurring at the individual cloud droplet level (cloud microphysics) as well as at larger-scales, ranging from cloud scale to mesoscale to synoptic. Clouds of shallow thickness (often around 1 km or less), such as stratus, stratocumulus, altostratus, altocumulus, cirrus, and cirrostratus are characterized by normally weak vertical air motions (1-10

cm s^{-1}) and low water contents (<1 g kg^{-1}) (Houze 1993). These clouds generally only precipitate lightly at most. Convective clouds, on the other hand, often referred to as cumuliform, form under considerably stronger upward air motions than do 'layered' stratiform clouds, a result of moist air becoming less dense than background air. Cumulus clouds are small horizontally and vertically (~1 km), and while they are sometimes idealized to be non-precipitating, they can precipitate. Stratocumulus clouds, though often classified as stratiform, actually contain an ensemble of convective elements, and may transition into cumulus clouds if vertical mixing and/or entrainment become sufficiently strong.

Deeper cumuliform clouds include cumulus congestus clouds, which are also wider and often detrain near or slightly above the 0°C level. Cumulonimbus clouds are very deep and often ascend to near or slightly below the tropopause, formed in areas of vigorous updrafts. Originally referred to as 'hot towers' by Riehl and Malkus (1958), cumulonimbus convective cores are associated with heavy precipitation, and also contain horizontally extensive anvil shields.

While the aforementioned individual cloud elements can appear in isolation, they often form into aggregates of either many nearly *homogenous* cloud elements or a mixture of various different cloud types. An example of the former situation in the subtropics occurs to the west of continents, where persistent warm marine boundary layer stratiform clouds are present in large-

scale subsidence regions of low sea-surface temperatures (SSTs) (Hartmann and Short 1980). These clouds are quite pervasive globally as well, covering nearly one-third of the global ocean surface (Charlson et al. 1987). Another example in the tropics is the nearly ubiquitous tropical trade cumuli, which although individually are quite small, often organize into bands, streets, or patches (Johnson et al. 1999). They are capped vertically by trade inversions, although this capping layer tends to be a bit less strong than the inversions capping stratocumuli (Stevens 2005), ranging from less than 1 km to occasionally greater than 3 km. Trade cumuli themselves also are responsible for the maintenance of the vertical structure of the lower troposphere, and may be an important source of latent heat for deep convection (Riehl et al. 1951; Stevens 2005).

A pervasive type of cloud system in the tropics, particularly within the Intertropical Convergence Zone (ITCZ), is mesoscale convective systems (MCSs) that are organized convective complexes. While MCSs contain multiple convective cores, only 10% of MCS rain areas are convective, while the remainders are horizontally extensive regions of stratiform precipitation (Houze 1993). Numerous MCSs are small, but the relatively few large MCSs comprise much more horizontal area, and precipitation amount in the tropics largely falls from the few large MCSs (Mapes and Houze 1993). This implies a relationship between area of deep convection and precipitation rate, and in fact several studies (see Mapes and Houze 1993 for a brief summary of such

studies) have correlated cold cloud area with precipitation, with threshold cold cloud temperatures ranging from 188 K to 235 K, on the basis that the active convective cores should penetrate furthest into the upper troposphere. Part of this dissertation examines the relationship of cold cloud fraction in tropical convective regions to precipitation rate partitioned by optical depth, so as to separate by the net radiative effect of cold clouds on the climate system.

1.3 Clouds and Radiation

Clouds are also important for the Earth radiation balance, and they can cause both a cooling and a warming of the Earth climate system. Clouds have a cooling effect because they reflect more shortwave radiation than most clear-sky regions, making the planetary albedo higher than clear-sky values. Clouds have a warming effect as they absorb longwave radiation emitted from warmer temperatures, and then re-radiate at lower temperatures, reducing outgoing longwave radiation (OLR) (Harrison et al. 1990). Cloud optical thickness τ primarily determines the albedo, or shortwave effect, whereas cloud top temperature (and optical thickness to a lesser extent) primarily determines the longwave effect. The combination of these two effects determines the net cloud radiative forcing, e.g. Manabe and Wetherald (1967). Following Harrison et al. (1990):

$$\begin{aligned} C_{LW} &= F_{CLR} - F \\ C_{SW} &= S(\alpha_{CLR} - \alpha) \\ C &= C_{LW} + C_{SW} \end{aligned} \qquad (1.1)$$

where the subscripts LW and SW designate longwave and shortwave, respectively, F_{CLR} is clear-sky OLR, F is total sky OLR, S is incoming solar flux, α_{CLR} is clear-sky albedo, and α is total sky albedo. Thus, cold clouds have large values of C_{LW}, a result of F being small compared to F_{CLR}. Also, C_{SW} is usually negative. Aforementioned regimes of warm stratiform marine clouds have small values of C_{LW} and much larger values of C_{SW}, and thus have modest to large negative cloud forcing (Harrison et al. 1990). Individual optically thick stratiform clouds can have a negative forcing lower than -100 Wm^{-2} (Hartmann et al. 2001). On the other hand, deep convective regions of the tropics, such as the ITCZ and South Pacific Convergence Zone (SPCZ) have large C_{LW} and C_{SW} values, such that the net cloud forcing is fairly close to neutral (Hartmann and Short 1980; Harrison et al. 1990; Hartmann et al. 2001). However, where convection is deeper and thus cloud tops are colder, such as in the western Pacific, values of C are closer to zero compared to areas such as the eastern Pacific, where high-topped clouds are warmer and where an abundance exists of warm clouds, making the net cloud forcing negative (Hartmann et al. 2001). In Chapter 2 of this thesis, differences in net cloud radiative forcing will be examined in different regions of the ITCZ.

1.4 Detrainment Level of Clouds

We thus see that the cloud height, or the temperature at which clouds emit radiation, is critical in determining the OLR. In the tropics and subtropics, two primary vertical modes of convective cloud tops are observed;

warm stratiform clouds near marine boundary layer top or trade cumuli near the trade inversion, and deep convective cores that occasionally top out just below or near the tropopause. A secondary mode is often found near or above the 0°C level (~5km). Using Geoscience Laser and Altimeter System (GLAS) data, for instance, Dessler et al. (2006) show the existence of three modes of cloud top heights. These modes of clouds are thought to be related to three prominent stable layers in the tropical troposphere. However, as Johnson et al. (1999) point out, congestus clouds often ascend above the 273K level, due the abundance of supercooled water, such that droplets do not become glaciated until 10-15K colder than the 273K level. This is consistent with the Dessler et al. (2006) analysis, in which cloud tops between 6 and 8km represent a local maxima. The cumulus congestus level, however, may also be related to anvil base evaporative cooling, suggesting connectivity among the various vertical modes.

Important exceptions to these rules are observed. In areas of deep convection, early satellite data analysis by Reed and Recker (1971) showed a peak in stratiform anvil and thin clouds around 175 hPa. This is well below the stable tropopause layer (Hartmann et al. 2001; Hartmann and Larson 2002), and is hypothesized to be related to the decrease in clear-sky cooling rates above this level, due to the rapid decrease of emission from water vapor due to very low temperatures. In clear-sky regions, subsidence heating is balanced by radiative cooling, so that mass converges at the level of the drop-off in

radiative cooling. This convergence in clear-sky regions is balanced by divergence in deep convective regions, so that anvil cloud detrainment should be related to the level where cooling by water vapor precipitously decreases in clear sky regions. This notion of radiative driving of convective high-topped clouds will be examined thoroughly and quantified in Chapter 2 of this thesis.

1.5 Vertical Structure of Clouds and Precipitation in Deep Convective Regions

In the tropical Pacific ITCZ, where convective clouds are prevalent, buoyant parcels of air ascend, cool, condense, and precipitate. In simple energy balance arguments, if convective heating via latent heat release in cloudy convecting regions is largely balanced by radiative cooling in clear-sky regions, precipitation should be related to convection strength. As convection strength is intimately tied to buoyancy, of which a quantitative measure is convective available potential energy (CAPE), deep convection should be collocated with regions of high CAPE. Thus, we might expect that convective precipitation intensity be related to cloud thickness or even cloud top height, since the lifting condensation level (LCL) can be assumed nearly constant in tropical regimes. Stratiform anvil clouds and precipitation also cover a large fraction of the ITCZ, but as their source is convection, we might also expect their rain rates to be connected to cloud top heights.

The height, or temperature, of clouds, is also, as we mentioned in section 1.3, enormously important for modulating OLR. What controls the

amount of CAPE, which surely must be related to depth of convection? In the tropics, temperatures above the boundary layer or trade inversion vary only slightly horizontally, so static stability is largely determined by absolute SST (Back and Bretherton 2008a). From a first approximation, we thus might expect clouds to be deepest where CAPE is highest.

Indeed, CAPE is relatively high throughout the ITCZ, owing to the warm SSTs there. But as convection is not uniformly deep throughout the ITCZ, other mechanisms are surely also responsible for ascent. Regions of low-level convergence allow warm and moist low-level air to rise, and this ascending air is buoyant (though not nearly as much as in continental convective air). Over the tropical oceans, Back and Bretherton (2008b) show that convergence is largely determined by the SST gradients. In the western Pacific ITCZ, SSTs are higher than the eastern Pacific ITCZ, but SST gradients are smaller in the western Pacific. The large-scale dynamics as well as the SST distributions lead to a vertical velocity profile in which ascent is more concentrated in the upper troposphere in the western Pacific and more in the lower troposphere in the eastern Pacific (Back and Bretherton 2008b). Though it seems plausible that the vertical structure of convection may respond to the large-scale vertical-velocity profiles of the tropics, such that more low and mid-level convection would be expected in the eastern Pacific, the large-scale vertical motion profile may simply be a reflection of the average convection profile. Determining causality is indeed an ongoing challenge.

The overarching objective in Chapter 3 of this thesis is to examine the structure of convective clouds in two differing dynamic and thermodynamic regimes of the western versus eastern Pacific with a satellite-borne cloud radar platform (CloudSat). Since precipitation is intimately related to the strength of convection, we will use microwave-derived rain rate data to investigate how the depth of precipitating clouds differs from non-precipitating clouds. We will attempt to quantify the association of convection depth with precipitation intensity.

1.6 Warm Clouds and Rain in the Tropics and Subtropics

The negative radiative forcing of warm clouds, a result of their strong albedo effect compared to their IR effect, and extensive coverage of them across much of the tropics and subtropics, makes them an important subset of clouds to understand (Hartmann and Short 1980). Indeed, increasing warm stratiform cloud fraction by 4% could offset warming by doubling CO_2 (Randall et al. 1984). Klein and Hartmann (1993) show a strong positive correlation between lower tropospheric stability (θ_{700}-SST) and stratocumulus cloud amount, where we can consider the lower tropospheric stability as a reflection of inversion strength. This makes physical sense not only because an inversion is necessary to cap stratiform clouds in the boundary layer, but also because the longwave cooling by warm clouds at cloud top below the thermal inversion reinforces the inversion. Sufficient longwave cooling at cloud top creates instability and makes stratocumulus clouds convective in

nature (Lilly 1968; Nicholls 1984; Klein 1995). While radiative cooling from the clouds themselves help maintain the inversion necessary for marine stratiform clouds in the first place, it is important to note that on short timescales, the cloud does not really control the lower tropospheric stability. In the tropics and subtropics, the inversion strength may also be related to the large-scale dynamics, including the strength of the subtropical highs, which may be connected to the strength of the Hadley Circulation (Klein and Hartmann 1993).

The stratocumulus-topped boundary layer (STBL) is normally fairly well-mixed, and thus the lapse rate is near-neutral. The formation of stratus clouds begins when the top of the mixed layer reaches saturation. As clouds expand vertically, radiative cooling at cloud top becomes more important, which both strengthens the inversion and the drives the convective dynamics of the cloud layer. Maintenance of a saturated layer between the lifting condensation level and the inversion base height is necessary to maintain a stratocumulus cloud layer. The LCL is determined by both surface temperature and humidity, so changes in these values will have an impact on the thickness of the cloud, assuming an unchanged inversion height (Wood 2008). Similarly, changes in the strength or height of the inversion have implications for the thickness and possibly coverage of stratiform clouds. If subsidence from above becomes sufficiently strong, the inversion base could lower to near the LCL, eliminating the saturation layer and thus the cloud

altogether (Klein 1995; Randall and Suarez 1984). Other physical mechanisms of weakening the inversion strength, such as enhanced vertical mixing or entrainment of warm, dry air aloft, could also potentially help dissipate stratocumulus clouds, or perhaps allow for the transition to trade cumuli (De Roode and Duynkerke 1997). In terms of radiative forcing, the transition to trade cumuli is important as aggregates of trade cumuli are generally much more patchy than stratocumuli, meaning that trade cumuli have a smaller net negative cloud radiative forcing.

Another possible dissipation mechanism of warm stratiform clouds may be related to processes occurring within cloud, such as drizzle production. Using a simple one-dimensional model, Albrecht (1989) examines the dependence of cloud fraction, water content, and relative humidity on precipitation efficiency. As the precipitation efficiency increases by reducing the cloud condensation nuclei (CCN), the water content decreases, there is less evaporation and consequently a decrease in relative humidity. The combination of decreasing cloud water and relative humidity results in a marked decrease in cloud fraction. The crux of the Albrecht (1989) effect is that an increase (decrease) in aerosols will reduce (increase) the propensity of drizzle, thereby increasing (decreasing) cloud lifetime and thus negative cloud forcing. In this context, Albrecht (1989) hypothesizes this feedback to be applicable for both marine stratocumuli and trade cumuli.

In Albrecht's (1989) study, only cloud fraction, rather than cloud albedo, was considered as a function of droplet concentration and thus precipitation. However, warm cloud microphysics is also important for cloud radiative forcing. When cloud liquid water is held constant, as CCN increase, the mean cloud droplet size, or radius, decreases, and consequently the surface area of cloud droplet and cloud albedo increases (Pincus and Baker 1994). In fact, an order of magnitude increase of CCN can increase albedo by 30% (Charlson et al. 1987). Using a simple model of the marine boundary layer, Pincus and Baker (1994) investigate the sensitivity of cloud thickness and albedo to changes in droplet concentration N_d. This study uses a parameterization for precipitation in stratocumulus clouds, in which precipitation formation occurs as a result of autoconversion, or the collision of cloud droplets. In this case, precipitation P, cloud thickness h, and cloud droplet concentration N_d are related by $P \approx h^{4/3} N_d^{-1}$. Pincus and Baker (1994) show that cloud thickness increases with N_d, since droplet size and precipitation decrease with N_d, and also that cloud albedo is *enhanced* more for clouds with low N_d. Increasing aerosols in low background N_d regimes thus has a larger impact on increasing cloud reflectivity compared to more polluted regimes. This emphasizes the importance of both aerosol concentration and precipitation processes in the shortwave effect of stratocumulus clouds.

Other studies suggest that the cloud response to increasing N_d may not be as straightforward or unidirectional as proposed by Albrecht (1989) or

Pincus and Baker (1994). For example, Ackerman et al. (2004) point out that though some observations indicate enhanced cloud liquid water in ship track regions (high N_d regions), other measurements indicate depressed LWP in such regions. To better understand this behavior, Ackerman et al. (2004) use model simulations based on three stratocumulus field projects, and investigate how cloud liquid water changes with N_d. In their simulations, precipitation reduces entrainment of air aloft, consistent with arguments that precipitation dries air and reduces evaporative-cooling induced downdrafts. Simulations of the Atlantic Stratocumulus Transition Experiment (ASTEX) show increasing LWP with N_d, but in that experiment the relative humidity above the boundary layer is 70%. When air above the boundary layer is very dry (i.e. relative humidity 10%), then increased entrainment due to precipitation suppression with increased N_d actually reduces LWP. For intermediate relative humidity aloft, LWP increases with N_d, but only when N_d is less than 225 cm^{-3}. Thus, whether the air above the boundary layer is relatively moist or dry seems to be an important factor on how perturbing N_d may change cloud liquid water.

Using a simple mixed layer model (MLM) to capture the dynamics of the STBL, Wood (2007) shows that the cloud thickness response to increasing N_d is determined by a balance between cooling and moistening of the boundary layer due to suppressed precipitation and warming and drying as a result of enhanced entrainment of air above the boundary layer. The balance is sensitive to cloud base, in which cloud thickness increases with increasing N_d

for a lower cloud base, which is consistent with the Albrecht (1989) hypothesis, but cloud thinning with increasing N_d occurs for elevated cloud bases. Over sufficiently long time scales of more than a few days, cloud thickness increases with N_d. This suggests that sensitivity of cloud thickness and/or lifetime effects to aerosol changes involves a complex balance of processes.

Other studies examining the mesoscale structure of stratocumulus clouds reveal further insight about both cloud radiative forcing and the propensity for precipitation. Closed-cellular stratocumuli, for instance, may be more homogeneous thermodynamically and also less likely to drizzle (Stevens et al. 2005; Comstock et al. 2005). These studies have examined that pockets of open cells (POCs), which may be embedded within close-cell stratocumuli, are linked to higher drizzle rates, and also that replenishment of water via boundary layer evaporation may help maintain drizzle and the mesoscale organization of POCs. This is important as open-celled stratocumuli have a lower mean-cloud albedo compared to closed stratocumuli with the same liquid water. Other studies such as Sharon et al. (2006) indicate that drizzle itself may help dissipate stratocumuli into open patches. They show that the existence of rifts in stratocumulus clouds, which are persistent areas of broken, cellular clouds within closed stratocumuli and decreased albedo, may originate from drizzling portions of closed stratocumuli. Sharon et al. (2006) propose a positive feedback whereby low CCN areas, which promote collision and

coalescence and therefore drizzle, and are consequently cleansed, maintaining low CCN and therefore drizzle and rift regions.

Objectives of recent large-eddy simulation modeling work by Savic-Jovcic and Stevens (2008) include quantifying the vertical structure of drizzling versus nondrizzling stratocumulus clouds as well as the horizontal extent and organization of these two types. Their simulations are able to capture realistic mesoscale features seen in observations, such as that the clouds in the nondrizzling simulation are closed-cell and have a high domain-averaged albedo of 0.75. In contrast, the drizzling simulation has a much lower mean reflectivity of 0.35, and exhibits increased variability in cloud cover, with more evident open-cellular nature. Only approximately one-third of the lower albedo for the drizzling domain can be attributed to the lower droplet concentration (and thus larger cloud drops) of 25 cm^{-3} for drizzling cases versus 200 cm^{-3} for the nondrizzling cases, while the majority of the difference stems from the redistribution and reduction of cloud water. Individual drizzling elements may be optically thicker than nondrizzling counterparts, but the overall cloud fraction is considerably reduced in the drizzling simulation, so that the domain-averaged albedo is smaller. Reduced cloud as a result of precipitation is consistent with the Albrecht (1989) hypothesis.

Given the negative net radiative forcing of warm reflective clouds, understanding possible maintenance and dissipation mechanisms of them is of

utmost importance for the climate system. Since warm rain precipitation may be a dissipation mechanism of warm clouds, particularly for stratocumuli, or perhaps even a cloud-building mechanism for cumuli, a better understanding of the distribution of warm rain as it relates to cloud properties seems relevant. As suggested in observational and modeling studies of drizzle, it is both a microphysical diabatic process and also a player as a potential organizer of mesoscale structure. It follows that warm rain production may be a function of both the microphysics of individual cloud elements, such as the number density and size of cloud droplets, as well as to the bulk macrophysical cloud structure, such as cloud liquid water and thickness. In Chapter 4 of this thesis, we seek to quantify the propensity of warm clouds to drizzle in the tropics and subtropics based on their micro- and macrophysical structure, using satellite radiometer and cloud radar observations. By quantifying the sensitivity of warm drizzle probability and intensity to micro- and macrophysical regime, one can also infer the importance of natural or anthropogenic aerosol to precipitation in warm clouds.

1.7 Research Questions and Common Themes

As all of the chapters of this thesis had been originally prepared in the form of peer-reviewed journal articles, with the content of Chapters 2 and 3 having already been published (Kubar et al. 2007; Kubar and Hartmann 2008), the material from one chapter to the next is fairly independent. Nonetheless, common themes among the chapters are present. In this thesis we wish to

better understand deep and shallow convection vertical structure because of its importance on the radiative balance of the atmosphere, and also because convection depth is closely tied to precipitation intensity. Even though Chapter 4 deals exclusively with warm clouds, of which there is a collection of both cumuliform and stratiform, we also find a relationship with warm cloud thickness and drizzle intensity. In Chapters 2 and 3, we focus closely on clouds and precipitation in deep convective regions from a perspective of relating the large-scale dynamics to mean cloud and precipitation statistics. We downscale from the large-scale to the microscale and cloud-scale in Chapter 4, as we look at how drizzle in nonfreezing clouds is sensitive to both the concentration and mean size of individual cloud drops (e.g. the microphysics) and to the total cloud liquid water (macrophysics). In Chapter 4, we also broaden our analysis away from solely deep convective regions to include multiple meteorological regimes in the tropics and subtropics.

The overarching questions that are addressed in each of the chapters include:

•How much variability in net cloud radiative forcing is there across the ITCZ, and how does the ensemble of cloud types, defined by their optical thickness and emission temperature, control this variability? Are anvil clouds, many of which are convectively generated, found at the same temperature as deep convective cores? Does the undilute level of neutral buoyancy in the upper troposphere control convection depth, or is convection depth more strongly

related to longwave cooling profiles determined by humidity and temperature profiles? (Chapter 2)

•How does the vertical structure of convective clouds vary from the western to eastern ITCZ, and how does precipitation modulate the structure? How does precipitation intensity relate to cloud depth, and how does the vertical distribution of cloud tops correspond to mean precipitation? (Chapter 3)

•How does the geographic variability of warm cloud height, LWP, droplet radius, and N_d relate to the distribution of warm cloud drizzle frequency and intensity? What relative role do warm cloud macrophysics and microphysics play in drizzle frequency and intensity? Among tropical and subtropical regions of different meteorological regimes and background aerosol loads, how universal is drizzle frequency as a function of both LWP and N_d? (Chapter 4)

Chapter 2: Radiative and Convective Driving of Tropical High Clouds

2.1 Introduction

Upper-tropospheric clouds associated with tropical convection have large shortwave (SW) and longwave (LW) cloud radiative forcing (CRF). Clouds reflect SW radiation, which cools the planet, and the size of the effect is determined primarily by cloud optical depth. Clouds trap LW radiation, which tends to warm the climate, and primarily depends on cloud top temperature, except for relatively thin clouds (visible optical depth $\tau \leq 4$), in which the LW effect increases with optical depth as well. The ensemble of convective clouds is such that the SW and LW effects come fairly close to canceling (Harrison et al. 1990). Using International Satellite Cloud Climatology Project (ISCCP) data, Hartmann et al. (2001) show that in an area of the West Pacific, the net CRF is on the order of about -10 Wm^{-2}, and a considerably larger negative net CRF in a portion of the East Pacific ITCZ region of about -45 Wm^{-2} is observed. It is suggested that this is because clouds are warmer and optically thicker in the East Pacific. Berg et al. (2002) and Schumacher and Houze (2003) have also studied structural differences, and infer the existence of shallower rainfall systems with more stratiform precipitation in the East Pacific.

We construct temperature-optical depth (T-τ) histograms to better understand differences in high-topped cloud properties in the West Pacific (WP) (5°-15°N, 120°E-160°E), Central Pacific (CP) (5°-15°N, 160°E-160°W),

and East Pacific (EP) (5°-15°N, 150°W-100°W). These histograms are then used in conjunction with a radiation model in order to quantify radiative effects of convection across the ITCZ, in a similar spirit as Hartmann et al. (2001), but with much higher vertical resolution afforded by MODIS data. We also are interested in the driving mechanisms behind the structure of these histograms, and thus we composite high-topped cloud fraction with rain rate. Composites by rain rate normalize convective intensity, so that we can then examine more subtle effects on convection, such as those from SST, SST gradients, and ITCZ structure across the North Pacific.

We also wish to address the claim that cloud systems are shallower in the EP, but in doing so we ask the question how high tropical clouds get and what controls their detrainment level. Reed and Recker (1971) analyzed satellite data composites that revealed a peak in stratiform anvil and thin cloud around 175 hPa, which corresponds to approximately 13 km. They also made upper-level divergence calculations, which suggested a peak at around the same level. Other studies have also suggested convective detrainment well below the tropopause. Folkins et al. (1999, 2000) suggest that convective detrainment occurs below 14 km, based on O_3 concentrations that begin increasing towards stratospheric concentrations at this level.

So, what determines the top of the tropical convective layer, and why is this top apparently well below the tropopause? The 'Hot Tower' concept of Riehl and Malkus (1958) and Riehl and Simpson (1979) assume that

convection occurs such that saturated ascending parcels are undiluted, and become negatively buoyant around 150 hPa, making this a cap for convection, which again is below the tropopause. Folkins et al. (1999 & 2000) also state that undiluted parcels become negatively buoyant once they reach the level in the upper atmosphere in which environmental Θ_E is the same as Θ_E at the LCL. We refer to these ideas as the 'PUSH' mechanism, as high-topped clouds are convectively driven by energy present in low-level air. An alternative perspective, which we refer to as the 'PULL' mechanism, is that clear-sky radiatively-driven upper-level convergence determines the level at which detrained cloud is maximum. Clear-sky radiative cooling drops off quickly in the upper troposphere where water vapor levels rapidly decrease, since saturation vapor pressure is dependent only on absolute temperature, per the Clausius-Clapeyron relationship. Hartmann and Larson (2002) have argued that the PULL mechanism implies an essentially fixed anvil cloud temperature.

In order to evaluate the PULL mechanism, we use a radiative transfer model to calculate clear-sky cooling rates and the corresponding upper-level convergence. We then examine to what extent anvil outflow occurs at this level, as evidenced by cloud temperatures measured by MODIS. We will quantify the relationship between clear-sky convergence and cloud temperature. The goal is to characterize the mechanisms that determine the altitude of convective clouds in the ITCZ.

2.2 Data for Cloud T-τ Histograms

We use data from *Collection 4* Aqua MODIS, which is a sun-synchronous satellite with local daytime overpass time at the equator of 1:30 p.m. The MODIS cloud products include cloud mask (which assesses the probability that there is a cloud in a given pixel), cloud top properties (i.e. temperature, pressure), cloud optical depth, and cloud phase. The horizontal spatial resolution of five km of the Joint Level-2 MODIS dataset is higher than other remote-sensing instruments of similar spatial coverage (Platnick et al. 2003). The nature of a sun-synchronous satellite, however, does preclude the observation of the diurnal cycle.

Cloud optical depth retrievals are based on solar reflectance. Clouds are assumed to be homogeneous, and ice and liquid cloud look-up tables are used (King et al. 1997). A non-absorbing wavelength band (0.86 μm) is used to allow for an independent retrieval from particle size (King et al. 1997).

To estimate cloud top temperature, the Joint Level-2 dataset is used, which has the same horizontal resolution for cloud top temperature and cloud fraction (5 km) as the full Level-2 data. Though the Joint dataset has lower resolution for τ (5 km versus 1 km) than the standard Level-2 swath product, its smaller data volume is an advantage. For clouds above 700 hPa, a CO_2-slicing method is used (Platnick et al. 2003). This method utilizes the partial absorption in each of two different MODIS infrared bands. Within the 15-μm CO_2 absorption region, the ratio pairs used by MODIS are 14.2/13.9 μm,

13.9/13.6 μm, 13.6/13.3 μm, 13.9/13.3 μm, and 13.3/11 μm (Platnick et al. 2003). Each MODIS band senses a different atmospheric layer. Upward infrared emission is measured in each of the different bands, and cloud pressure is then determined. With use of the National Center of Environmental Prediction (NCEP) reanalysis tables, cloud top temperature is then estimated. In the lower troposphere (below 700 hPa), the CO_2-slicing method is less effective, and is replaced with band temperatures within the 11-μm atmospheric window. One major advantage of CO_2-slicing is that it is relatively insensitive to emissivity, so that the temperature of thin clouds can be sensed more accurately compared to estimates based on brightness temperatures alone (Platnick et al. 2003).

Because our interest is in tropical oceanic convection, only areas over the open ocean are considered. Also, because we are interested in both thermal and optical properties, only daytime data are used. Data influenced by sunglint are not used.

Instantaneous satellite retrievals are aggregated into three-day averages and 1° latitude by 1° longitude regions. This averages together individual convective events occurring on short time (less than one day) and small spatial scales (less than about 100 km). These temporal and spatial scales are small enough to capture variability in convection. (We do in fact test the sensitivity of different temporal and space scales, and determine that it is quite low.)

We use weekly sea-surface temperature (SST) data from the Climate Diagnostics Center, which contain National Oceanic and Atmospheric Administration (NOAA) Optimum Interpolation (OI) SST version two data. These data are global, have 1° x 1° resolution, and are derived from a combination of *in-situ* and satellite measurements (Reynolds et al. 2002). These data are interpolated onto the same temporal scale as the MODIS data.

Daily rain rate data on a grid of 0.25° by 0.25° comes from the Advanced Microwave Scanning Radiometer (AMSR), which is also aboard the Aqua satellite. The obvious advantage of this is the collocation (in space and time) with MODIS. Its microwave frequencies can see larger raindrops through smaller cloud particles, and it becomes saturated for precipitation rates of 25 mm/hr. We use the version five rain rates, which have an improved rain algorithm in which freezing levels have been revised, lowering calculated rain rates in the tropics compared to older versions (Updates to AMSR-E V05 Algorithm 2006). Like the SST data and MODIS data, rain rate data are aggregated into three-day averages for compositing purposes with MODIS cloud data.

To further ensure the statistical robustness of the MODIS data, we use only aggregated three-day 1° latitude by 1° longitude data that contain at least 200 good 5km boxes. These include boxes that are well-removed from land, free of sunglint, and have a determined cloud mask (land/water, sunglint, and cloud mask quality flags are used). During a three-day period, a maximum of

1200 good boxes are possible, since 1° of latitude/longitude near the equator is about 100km, and the horizontal resolution of Joint Level-2 MODIS is 5km. The threshold of 200 good boxes to define data that are good that meet the above criteria perhaps is somewhat arbitrary, but does filter out three-day periods in which relatively few good boxes exist. To examine the sensitivity to the given temporal and spatial resolution, calculations are also performed with one-day periods, and the results are largely unchanged (figures not presented in this report). The same is also true when 5˚ latitude by 5˚ longitude boxes are chosen. Thus, the results are not sensitive to the spatial or temporal resolution.

To understand both qualitatively and quantitatively the structure of clouds across the ITCZ, cloud fraction histograms, categorized by temperature (ordinate) and optical depth (abscissa) are constructed, which we will refer to as T-τ histograms. The three regions, namely the WP, CP, and EP have different SST distributions, with the WP representing the large warm pool region, the CP a transition zone of sorts, and the EP a narrow ITCZ, with strong SST gradients on its edges. A composite SST map from September 2003 through August 2005 is given in Fig. 2.1. It should be noted that the median SST in the WP during this period is 28.9°C, 28.5°C in the CP, and 27.9°C in the EP. For the T-τ histograms, 26 temperature bins of five degrees and 10 optical depth bins are used, the latter of which follows a nearly logarithmic scale with the following bins: (0-0.125, 0.125-0.25, 0.25-0.5, 0.5-1.0, 1.0-2.0, 2.0-4.0, 4.0-8.0, 8.0-16.0, 16.0-32.0, 32.0-64.0). We have a total

of 260 possible cloud bins, which provides much greater resolution than the 42 ISCCP pressure/optical-depth bins. However, it is primarily in the vertical that MODIS T-τ histograms are superior to ISCCP. For example, in the upper troposphere, the ISCCP pressure bins are 440 hPa to 310 hPa, 310 hPa to 180 hPa, and 180 hPa to 30 hPa. These correspond to approximate temperature ranges (based on GPS data) of 260 K to 240 K, 240 K to 215 K, and 215 K to 193 K (at 100 hPa), which are coarse compared to the 5 K bins used here. These histograms are discussed in a later section.

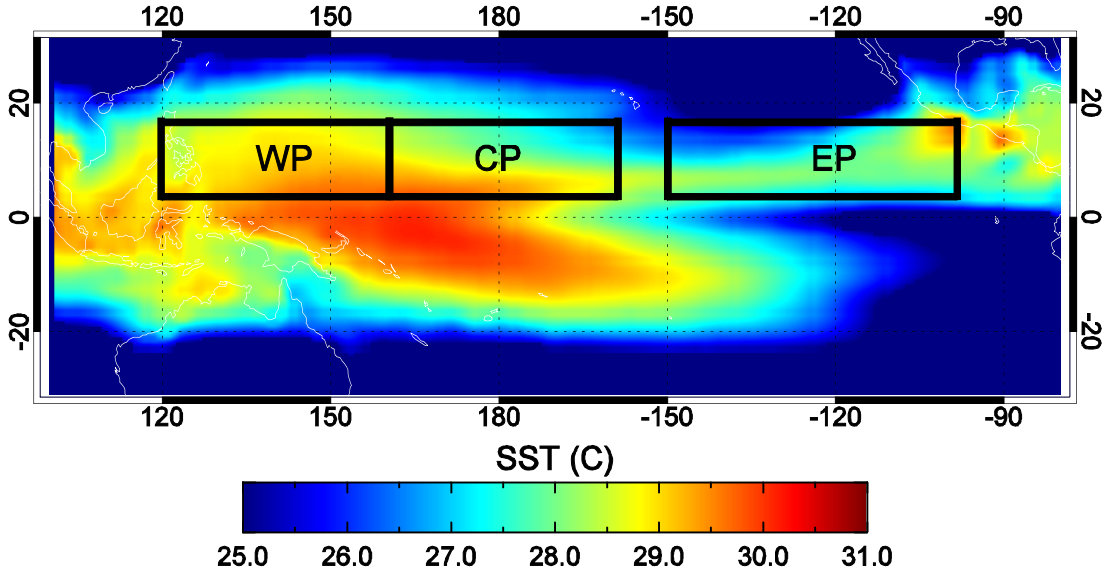

Fig. 2.1. Map of Composite SSTs over the tropical Pacific for September 2003-August 2005, indicating the three regions selected for study.

2.3 Radiative Transfer Model/T-τ Histogram Methodology

We employ the same radiation model as used by Hartmann et al. (2001), namely the Fu and Liou (1993) delta-four-stream, k-distribution scheme. The purpose of a radiative transfer model is twofold; we calculate

radiative energy budgets for each of our cloud categories, and we also use clear-sky heating rates (to be discussed later) for calculation of clear-sky convergence profiles. We focus on the former in this section.

For each of the aforementioned cloud types, cloud radiative forcing is calculated, assuming 100% cloud cover in each bin. These are computed every hour for the centers of the WP, CP, and EP, with zenith angles corresponding to day 90 of the year. Ice water content (IWC) is calculated by the relationship

$$IWC = \frac{2}{3}\frac{r_{ice}\tau_{ice}}{\Delta z} \qquad (2.1)$$

where r_{ice} is the effective radius of ice, τ_{ice} the optical depth, and Δz the geometric thickness of the cloud. An analogous relation is used for liquid water content (LWC); cloud is assumed to be all ice at temperatures below 263 K. No mixed clouds are included, but this is not seen as a major problem, since the emphasis of this study is that of tropical high-topped cloud. Also, as is done in Hartmann et al. (2001), r_{ice} is assumed to be 30μm, and r_{liquid} 10μm. According to Korolev et al. (2001), the dependence of particle size on temperature is quite weak. Thus, without further detailed information about an exact dependence of particle size on temperature, selecting one value for ice and one for liquid seems to be a good assumption. A more quantitative analysis of this assumption is examined in a later section. Geometric cloud thickness Δz is based on climatology from Liou (1992), which contains nine thickness categories, depending on cloud height and optical depth. Concentrations of CO_2, CH_4, and N_2O are assumed to be 330 ppmv, 1.6 ppmv,

and 0.28 ppmv, respectively, and the surface albedo is 0.05 (a reasonable value for the ocean). (Calculations were also made using more current greenhouse gas values, and there was very little sensitivity of radiative calculations to greenhouse gas concentrations.)

In Fig. 2.2, contours of shortwave, longwave, and net top-of-atmosphere radiation are shown in T-τ coordinates. Optical depth matters more for SW cloud forcing, and cloud top temperature has only a marginal effect, so that clouds have a much stronger SW cooling effect as their optical thickness increases. On the other hand, cloud top temperature and cloud optical depth are both important for LW cloud forcing for optically thin clouds ($\tau<4$ or so). For such clouds, as optical thickness increases, so does the LW warming effect. For all clouds, the LW effect increases with decreasing cloud top temperature, and for clouds with an optical thickness greater than four, *only* cloud top temperature matters. The net CRF is positive for thin cloud colder than 260 K, and reaches a peak (of +94.3 W m^{-2}) for very cold cloud at around $\tau=1$, and then decreases with increasing τ. It becomes negative for larger optical depths, but becomes negative at lower optical depths for warmer clouds. We choose our high-topped cloud to include clouds colder than 245 K, as this represents a temperature at which high-topped cloud amount is well separated from other cloud modes (a relative minimum in cloud amount appears at approximately this temperature). Low, thick clouds have a negative forcing with a value of about -216 Wm^{-2}.

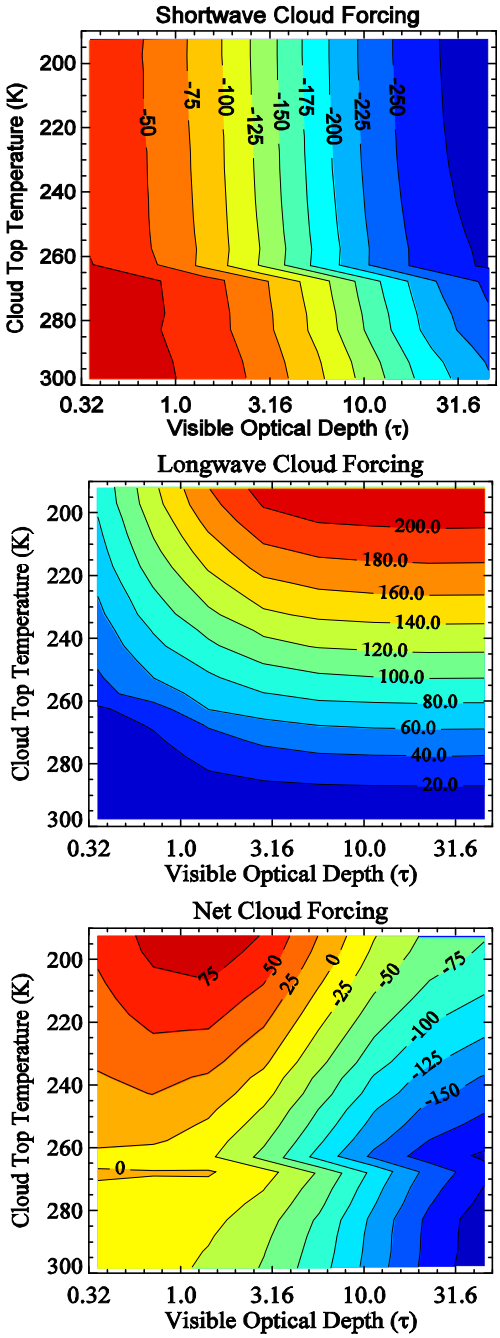

Fig. 2.2. West Pacific shortwave (top), longwave (middle), and net (bottom) cloud top-of-atmosphere radiative forcing, assuming 100% cloud percent in each T-τ bin (Wm^{-2}).

2.4 Cloud Fraction Histograms and Radiative Flux Histograms

2.4.1 Histogram Cloud Types

Cloud fraction histograms are presented in Fig. 2.3 for the period September 2003 through August 2005, and suggest three modes of clouds in the WP, CP, and EP. One mode is that of low, marine boundary layer cloud, with top temperatures generally warmer than 280 K. As described by Sarachik (1978), these have bases approximately at 600m that extend vertically to about 2 km. Yanai et al. (1973) note that the vast majority of the moisture is contained within this shallow cloud layer, and water vapor and liquid water are transported upward via deep convection. Another dominant mode is that of high-topped cloud, which shows optical depths with a wide range of values. The observation of high-topped cloud of a wide range of optical thickness, ranging from thick convective cores to anvil clouds to thin cirrus, is consistent with observations from ISCCP in Hartmann et al. (2001). Subtle differences exist in this cloud type, however, namely that high-topped cloud peaks slightly higher up in the troposphere (lower cloud top temperature) in the WP and CP compared to the EP. Also, the median optical depth of all high-topped cloud in the EP is slightly higher.

Mid-level clouds represent a third, though arguably less important mode, that are particularly prevalent in the EP. This cloud peaks around 260 K in the EP, and at slightly lower temperatures in the WP and CP. Less attention

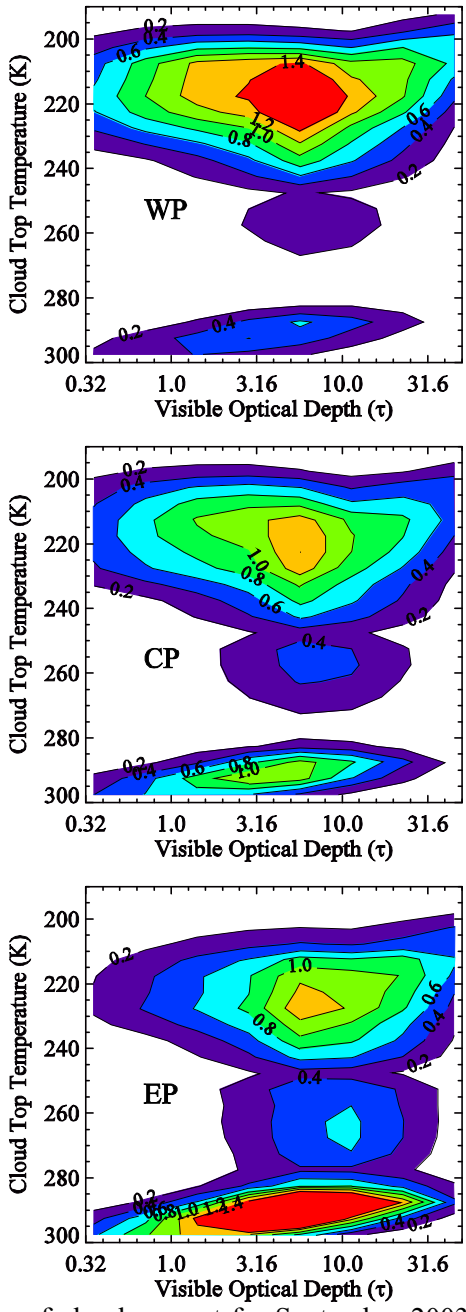

Fig. 2.3. T-τ histograms of cloud percent for September 2003-August 2005, for WP, CP, and EP (top to bottom).

has been drawn to this population of clouds, and some studies, particularly more conceptual ones, have primarily underscored the two aforementioned modes. Early observational studies, however, such as that by Malkus and Riehl (1964), documented the presence of cumulus congestus clouds at or slightly above the 0°C level. Later studies, such as that by Johnson et al. (1999), highlight this middle population of clouds as an important one. Even a two-dimensional cloud modeling study by Liu and Moncrieff (1998) reveals three cloud modes, one of which is located between about six to seven km, coincident with the melting layer.

To explain the reasons for these three modes, Johnson et al. (1999) suggest that the three layers; one near 2 km, another near 5 km (near 273 K), and the third in the vicinity of 15-16 km (about 1-2 km below the tropopause) represent three prominent stable layers of the tropical atmosphere (see Fig. 2.4 for GPS temperatures, corresponding heights, and differences between WP and EP). The enhanced stability in these areas, according to Johnson et al. (1999), stunts vertical cloud growth and promotes divergence and detrainment. As Fig. 2.4 shows the *averaged* temperature profiles from September 2004 through July 2005, however, these stability layers are *not* seen. In MODIS, we see the middle congestus clouds peaking considerably colder than 273 K, at 255 K to 260 K. Johnson et al. (1999) suggests that overshooting above the 0°C level occurs because supercooled droplets are in abundance, especially in the ITCZ, and droplets do not become glaciated until 10-15 K colder than

273K. This is quite consistent with the MODIS identification of a middle cloud population colder than the 273 K level. It is less clear, however, why the population of congestus is more prominent in the EP. It may have to do with the fact that SST gradients are stronger in the EP, driving stronger surface convergence, and a profile of vertical velocity such that vertical velocity peaks much lower in the troposphere compared to regions such as the WP, where the SST gradients are relatively weak (Back and Bretherton 2006). Even when we examine the conditional probability of seeing congestus cloud given no high-topped cloud (plot not shown), the EP still has more congestus cloud for a given rain rate.

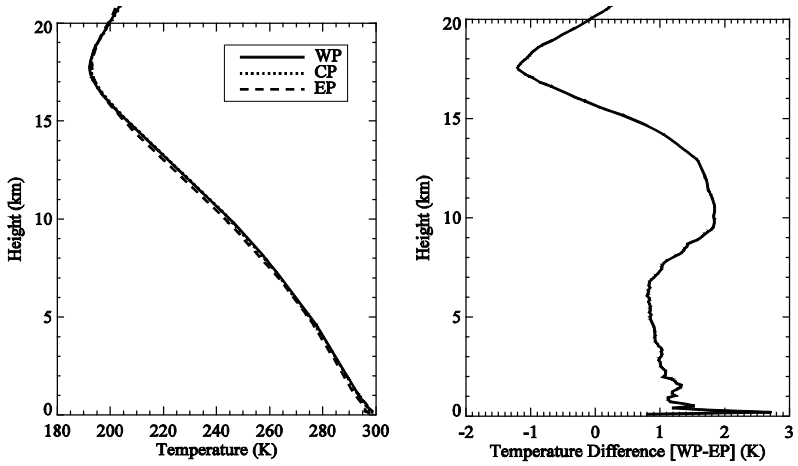

Fig. 2.4. GPS temperature profiles (top) and WP-EP temperature differences (bottom) for September 2004-July 2005.

2.4.2 Cloud Forcing by Type

Earlier, we presented T-τ histograms of SW, LW and total cloud radiative forcing, assuming 100% cloud cover in each T-τ bin. We now use the T-τ cloud fraction histograms constructed from MODIS data to calculate

average-sky cloud forcing (the term used by Hartmann et al. 2001), to provide information about the actual radiative impact of clouds for the WP, CP, and EP. Multiplying the corresponding overcast cloud forcing histograms (Fig. 2.2) with actual cloud fraction in each T-τ box (Fig. 2.3) gives the average cloud radiative effect.

We define high thin, anvil, and high thick cloud based on their net radiative effects. These clouds all have tops colder than 245 K, and the optical depth ranges are thin (0-4), anvil (4-32) and thick (32-64). Defined in this manner, thin clouds have a TOA warming effect, and anvil and thick cloud a TOA cooling effect. We reserve a separate category for thick cloud because these likely represent deep convective cores.

The *average-sky* cloud forcing histograms, which hereafter we will refer to as net CRF, are presented in Fig. 2.5 for the WP, CP, and EP. The net CRF in the EP is much more negative (-51 W m^{-2}) than the CP (-22 W m^{-2}) or WP (-16 W m^{-2}) net CRF, partly due to the larger population of low, thick cloud there. Also, the WP (and CP, to a slightly lesser extent) contains much more high, thin cloud, which contributes to a *smaller negative* net CRF.

Figure 2.5 also gives the net CRF value for only *high-topped cloud* in each of the three regions, including only clouds colder than 245 K. The WP and CP have similar high net CRFs, at -7.5 and -8.4 W m^{-2}, respectively. This contrasts with the EP, which has a high net CRF of -18.2 W m^{-2}. The less negative high-topped cloud forcing in the WP stems from differences in thin

cloud amount, which will be more clearly demonstrated in the next section. Differences in anvil and thick cloud net CRF will also be addressed later on.

It is also noteworthy at this point to briefly elaborate on the particle size assumptions used in our calculations. As mentioned before, r_{ice} is assumed to be 30μm, and r_{liquid} 10μm. To quantitatively assess the sensitivity to particle size, high net CRF calculations are also performed with r_{ice}=50μm and r_{ice}=15μm. The net high CRF values with r_{ice}=50μm are -2.5 Wm^{-2} for the WP, -4.3 Wm^{-2} for the CP, and -14.5 Wm^{-2} for the EP, respectively. For r_{ice}=15μm, the values are -14.0 Wm^{-2} for the WP, -13.9 Wm^{-2} for the CP, and -22.7 Wm^{-2} for the EP. It is not surprising that increasing r_{ice} makes the net high-topped cloud CRF less negative, as a larger particle size is less reflective. However, what is important is that the difference between the WP and EP is not affected strongly by assumptions of particle size, and regional differences, as opposed to absolute differences, are at the crux of this study.

2.5 High-Topped Cloud Amount Versus Convective Strength

Simple energy balance indicates that net heating by precipitation in convecting regions is balanced by radiative cooling in adjacent subsidence regions. Deep cumulonimbus clouds carry water vapor from the shallow cloud layer to the upper troposphere, and as they do, the water vapor condenses. It is these cumulonimbus towers that precipitate most heavily, and thus it should

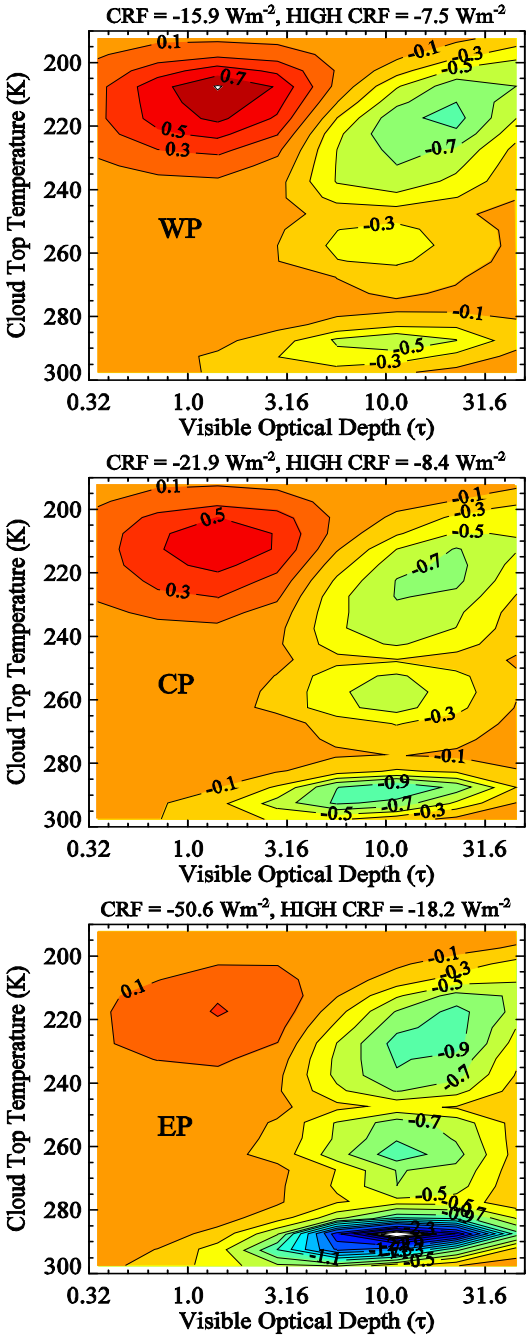

Fig. 2.5. Cloud radiative forcing contour plots binned by T-τ for WP, CP, and EP (top to bottom) for September 2003-August 2005.

follow that rain rate is a good proxy for convection strength. We have composited high-topped cloud with rain rate, with the hope of revealing possible regional differences in characteristics of convection along the ITCZ. By compositing with rain rate, we effectively remove convection strength from the equation, such that differences in structure for a given convective regime can be compared. In Fig. 2.6, thin, anvil and high thick cloud amount are presented as a function of rain rate, averaged over the two-year period of September 2003 through August 2005. Each point represents the following rain rate percentiles ranges: 1) 2.5th-10th, 2) 10th-25th, 3) 25th-50th, 4) 50th-75th, 5) 75th-90th, and 6) 90th-97.5th. Each error bar represents the observed value ±3 times the sampling error. The sampling error S_E is given by

$$S_E = \frac{\sigma}{\sqrt{N}} \qquad (2.2)$$

where σ is the standard deviation of all 1° by 1° boxes (three-day aggregates) within each rain rate percentile regime that have nonzero precipitation rates and at least 200 good data points, and N the number of 1° by 1° boxes (three-day aggregates) that fall within each rain rate regime. Sampling error bars encompassing ±3 times the sampling error represent the 99% confidence interval, assuming normally distributed data. It is important to note that the 1° by 1° boxes are assumed to be independent of one another, which may not necessarily be the case, such that the error bars might be underestimates.

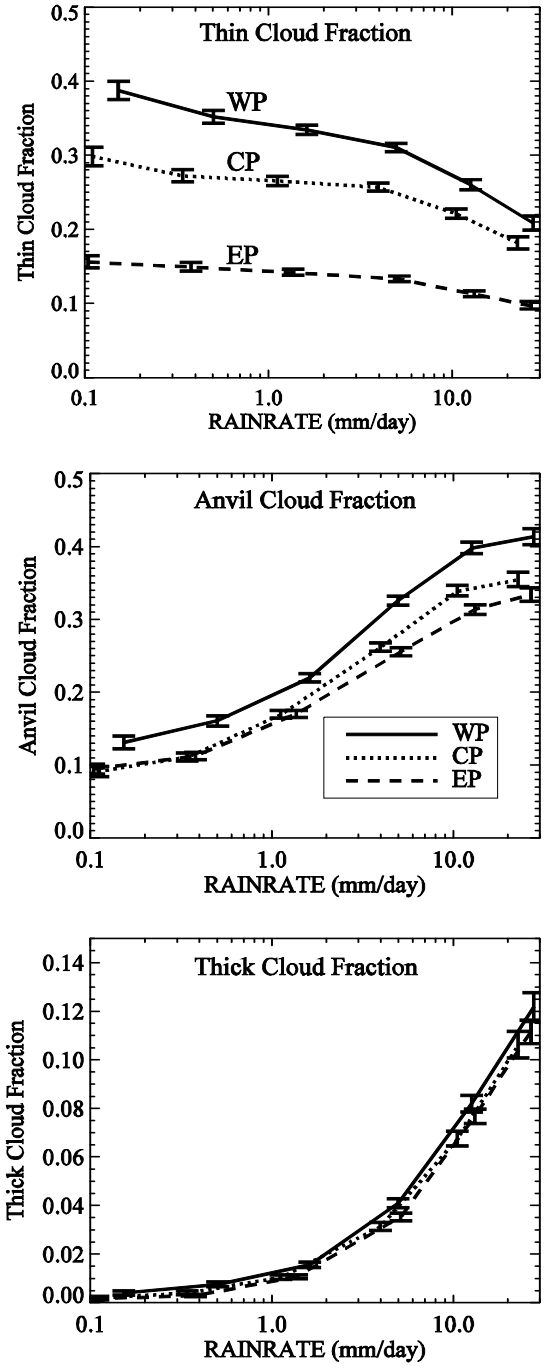

Fig. 2.6. Thin, anvil, and thick cloud fraction versus rain rate for September 2003-August 2005 (note the different scale for thick cloud fraction).

On the top panel of Fig 2.6, we see that for a given rain rate, thin cloud is more than twice as abundant in the WP as in the EP. Also, thin cloud is nearly independent of rain rate. The observed thin cloud fraction decreases slightly with rain rate as anvil and thick cloud increases with rain rate, and this is because as there is more opaque cloud, thin cloud is not as detectible by MODIS, even if it is present.

Anvil cloud is more abundant in the WP than the CP or EP for a given rain rate, though the differences are less dramatic than for thin cloud. Finally, thick cloud in the WP, CP, and EP increases in a very similar manner with rain rate, and it is difficult to distinguish between the three regions. This suggests that thick cloud amount is a very good proxy for rain rate, which could be quite practical for remote sensing purposes, as using OLR alone as a proxy for rain rate can give fallacious results (Berg et al. 2002).

The fact that combined anvil plus thin cloud is much more abundant in the WP per unit of precipitation, despite thick cloud being the same, implies important structural differences in convection in the WP versus the EP. If we understand convective cores to be manifested as thick, high-topped cloud that then spreads and thins out with time, then the thick cloud in the WP that spreads out into thinner cloud shields is sustained over larger geographical regions. In a later section, we will show that relative humidity is higher in the WP in the upper troposphere, and perhaps the moister upper troposphere there slows the evaporation of the ice compared to the EP. It is probable that

convection contributes to the observed upper-level relative humidity profiles (Udelhofen and Hartmann 1995). The EP ITCZ is considerably narrower than the WP ITCZ, so that the EP is surrounded by a much drier upper-level environment. The EP is thus more readily influenced by the surrounding dry regions, which could be less conducive to maintenance of anvil and thin high-topped cloud. Entrainment of non-ITCZ air into the EP in the upper troposphere could partly explain the lower anvil and thin cloud amount. At present, we cannot compute accurate moisture budgets for these regions, however.

We also examine the TOA radiative impacts of thin, anvil, and thick cloud by compositing them with rain rate. Figure 2.7 shows that thin cloud increases TOA radiation, and anvil and thick cloud reduce the TOA energy budget. For a given rain rate, the CRF of thin high-topped cloud is approximately 10 W m^{-2} higher in the WP versus the EP. With increasing rain rate, the CRF of anvil and thick cloud becomes more negative, as these cloud types become more abundant. The anvil and thick net CRF in the WP and EP are nearly indistinguishable from one another, however, despite the presence of more anvil cloud in the WP. This is because even though the SW effect is *stronger* for anvil cloud (because the anvil cloud fraction is greater) for a given rain rate in the WP (not shown), the LW effect is also *stronger* (also not shown), since anvil cloud is slightly colder in the WP.

Finally, the bottom right panel of Fig. 2.7 shows that the total high CRF is considerably more negative for the EP for a given rain rate, which we can safely say is mostly due to much less thin, high-topped cloud there, since the CRF due to the other high-topped cloud types (anvil and thick) is very similar in the WP and EP for a given rain rate. Thus, the structural differences in convection in the WP and EP also have significant implications for the energy balance at the top of the atmosphere.

2.6 High-Topped Cloud Top Temperature Versus Rain Rate

We now present thin, anvil, and thick cloud top temperature versus rain rate in Fig. 2.8. It is clear that all high-topped cloud types in the WP and CP are systematically about 5 K colder than the EP, for a given rain rate. Once again, for quality assurance purposes, these data only include each three-day 1° by 1° box for which at least the cloud fraction is greater than zero, at least 200 good 5-km data points are present, and the rain rate is nonzero. For all rain rates during the September 2003 through August 2005 period, the median cloud top temperatures of thin clouds are WP= 217.4 K, CP=217.6 K, and EP=222.8 K. For anvil cloud, the respective temperatures are 219.4 K, 220.8 K, and 224.3 K, and for thick cloud 212.1 K, 214.3 K, and 218.5 K. Thus, WP thin and anvil clouds are approximately 5 K colder than in the EP, and thick cloud about 6 K colder.

A few points can be made about these observations. First, as expected, thick convective cores penetrate highest in the atmosphere, and anvil clouds

detrain from these cores at a lower level. Thin cloud is only slightly colder than the anvil cloud, which seems to lend credence to a notion that it is related

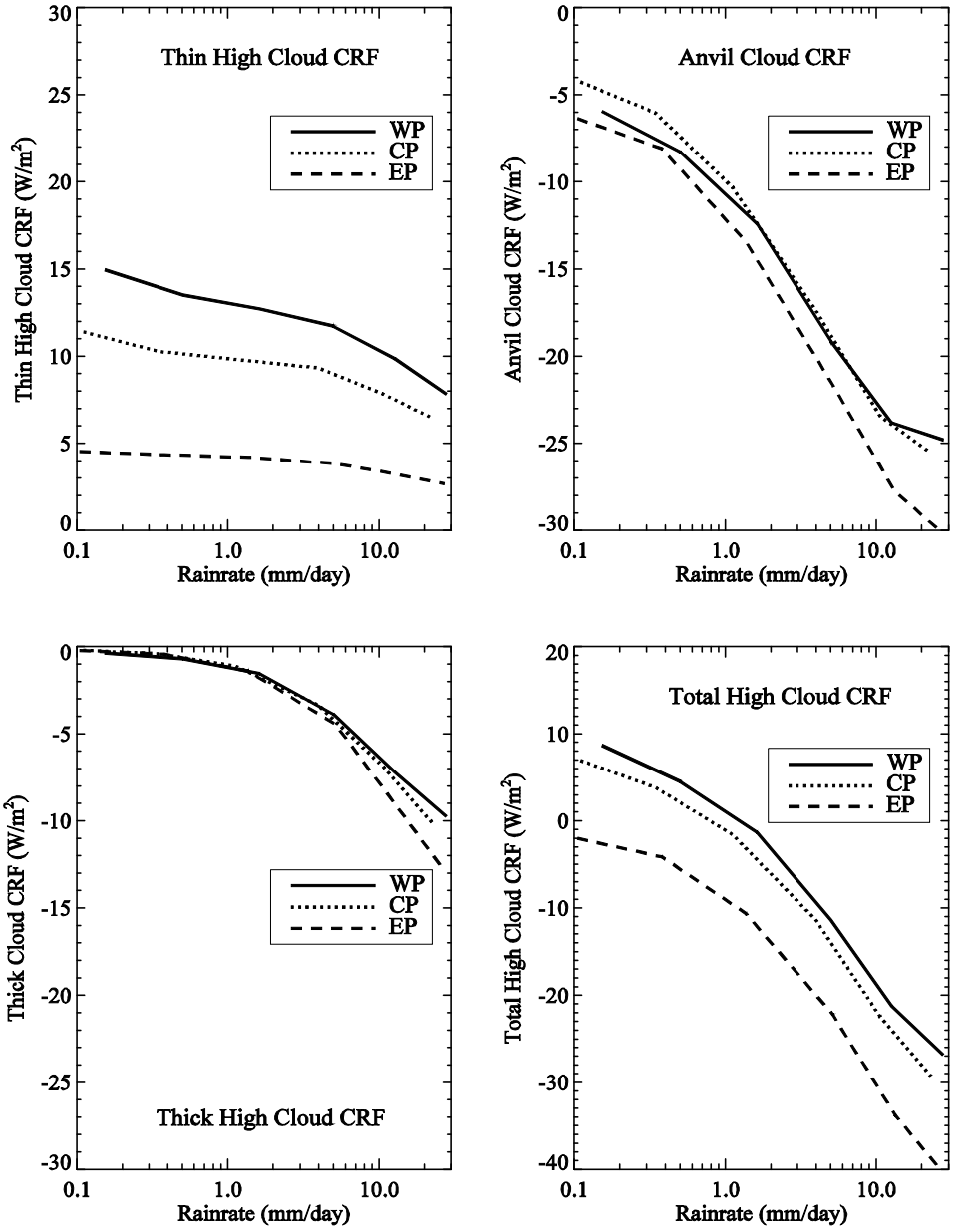

Fig. 2.7. High-topped cloud radiative forcing versus rain rate for the same period as Fig. 2.6.

to the anvil cloud. It is important to note, however, that MODIS does not see tropopause cirrus at all, as it is too optically thin. According to Dessler and Yang (2003), the optical depth cutoff for MODIS is 0.02, and while the subvisual tropopause cirrus have optical depths less than 0.03 (McFarquhar et al. (2000)), they are often *optically thinner* than that. One can view the evolution of convection such that anvil cloud detrains from core clouds, and over time, thin cloud is the residual of the anvil cloud as it spreads and thins out away from the convective cores, although some high thin cloud can be generated by waves (e.g. Boehm and Verlinde 2000). It seems that MODIS can detect thin cloud at realistic temperatures, compared to satellite estimates based on thermal imaging alone, for which the temperature depends on emissivity. The CO_2 slicing method utilized by MODIS, on the other hand, does not require an emissivity estimate.

It is noteworthy that anvil and thin cloud top temperature seem to show no clear relationship with rain rate, whereas thick cloud (save the lowest rain rates in the WP) seems to get colder with increasing rain rate. This perhaps is consistent with the notion that the thick cloud is convectively driven, and since rain rate is a proxy for convection strength, we might expect the strongest convection to penetrate deeper.

2.7 Clear-Sky Divergence Calculations in the Upper Troposphere

We wish to better understand cloud top temperature differences in the WP and EP, and to ask how the cloud top temperature is determined. We

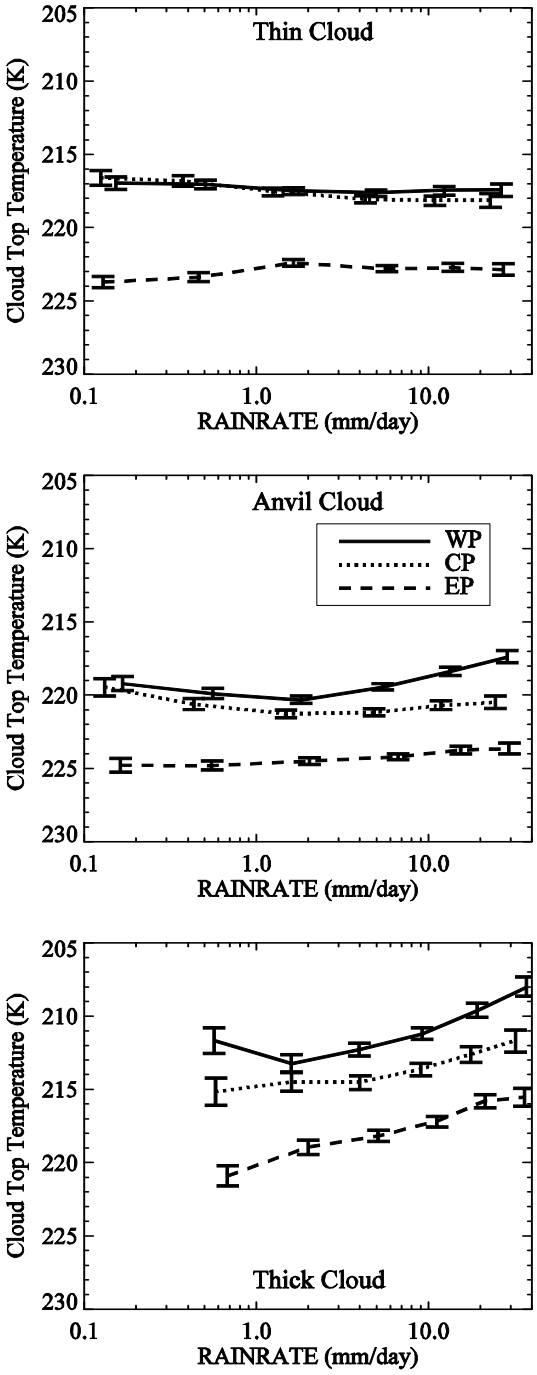

Fig. 2.8. Cloud top temperature versus rain rate for thin (top), anvil (center), and thick (bottom) high-topped cloud for September 2003-August 2005.

explore both the 'PUSH' and 'PULL' mechanisms; the former suggests that the altitude of anvil and thick clouds is driven by buoyancy, while the latter argues for clear-sky radiation being the key factor. In this section, we focus on data used to explore the PULL mechanism. Calculation of clear-sky convergence profiles requires moisture and temperature profiles, that are then used to calculate clear-sky cooling rates and vertical velocity (ω) profiles.

The Microwave Limb Sounder (MLS), aboard the Aura satellite, uses the 190 GHz channel to measure upper-level water vapor mixing ratios. There are 22 levels between 316 hPa and 0.1 hPa, with measurements made in the upper tropospheric region of interest at 316 hPa, 215 hPa, 147 hPa, and 100 hPa (Livesey et al. 2005). This corresponds to a vertical resolution range of 2.7-3.0 km. This resolution in the upper troposphere with MLS is superior compared to more conventional measurements of upper-level relative humidity from radiosondes, whose spatial resolution is spotty, and satellites, whose vertical resolution is coarse (Sassi et al. 2001). Vertical resolution in the upper troposphere is important for moisture for clear-sky divergence calculations. Also, MLS can measure upper tropospheric moisture in clear and cloudy regions, as opposed to nadir satellite measurements using thermal infrared, which are limited to clear skies. Data from MLS aboard the Aura satellite are available from September 2004 onward.

Vertical temperature profiles are available from Global Positioning System (GPS) data, with 0.5 K precision. Though GPS data are available well

before September 2004, we start from September 2004 to overlap with the Aqua data. This is a navigation system which contains 24 satellites. Major advantages of GPS include long-term stability, good vertical resolution, all-weather capability, and global coverage. Atmospheric refractivity fields are utilized, allowing conversion to profiles of temperature and pressure (Schmidt et al. 2004). The largest temperature errors occur near the surface and at 8 km, and are 0.5 K and 0.2 K, respectively. Errors fall to 0.1 K in the majority of the stratosphere (Kursinski et al. 1997).

The same radiative transfer model used for CRF calculations is used to compute atmospheric profiles of clear-sky radiative longwave cooling rates, which require temperatures and mixing ratios as inputs. GPS temperatures are interpolated onto the 1000 pressure levels in the model; the layers between each level contain approximately equal mass. Between 0.1 hPa and 147 hPa, MLS mixing ratios are interpolated onto the model pressure levels. For mixing ratios between 147 hPa and 316 hPa, a polynomial fit of order three is used to interpolate data onto the model pressure levels. Between 316 hPa and 375 hPa, a linear fit is made, and below this, an idealized tropical profile (with specific humidity) is used, from McClatchey et al. (1971).

Once the longwave cooling rates are calculated, they are used to calculate the diabatic omega (ω) profiles from the following relationship, which is derived from the thermodynamic energy equation (Holton 1992):

$$\omega = \frac{-Q(p)pc_p}{R_D T}\left[1 - \frac{pc_p}{R_D T}\frac{\partial T}{\partial p}\right]^{-1} \qquad (2.3)$$

In (3), Q(p) is the longwave cooling rate as a function of pressure, c_p is the specific heat at constant pressure [=1004 J K^{-1} kg^{-1}], R_D the dry air gas constant [=287 J K^{-1} kg^{-1}], T the absolute temperature, and ω the vertical velocity in pressure coordinates.

Next, the horizontal divergence is calculated from the continuity equation, which is given by

$$Div_H = -\frac{\partial \omega}{\partial p} \qquad (2.4)$$

In (4), $Div_H = \partial u/\partial x + \partial v/\partial y$. Because of the derivative, the estimated divergence is quite noisy, and a smoothed divergence profile is computed for each region by averaging divergence into five-degree temperature bins (temperature being the vertical coordinate) corresponding to the temperature bins used for the MODIS data. Vertical profiles of relative humidity, cooling rates, ω-profiles, and smoothed divergence profiles are discussed in more detail in section 2.8.

2.8 Relative Humidity, Cooling rate, ω, and Clear-Sky Convergence Profiles

Composite relative humidity profiles from September 2004 through July 2005 for the WP, CP, and EP are shown in Fig. 2.9. The focus here is in the temperature range where anvil clouds detrain, which occurs between about 215 K and 225 K. In the EP and WP profiles a secondary peak in relative humidity occurs at about these temperatures. The peak in relative humidity in

the WP is larger in magnitude and peaks at a lower temperature than the EP. These differences in relative humidity peak temperature and amplitude are interesting, and might be related to the fact that there are simply more anvil and thin cloud in the WP compared to the EP.

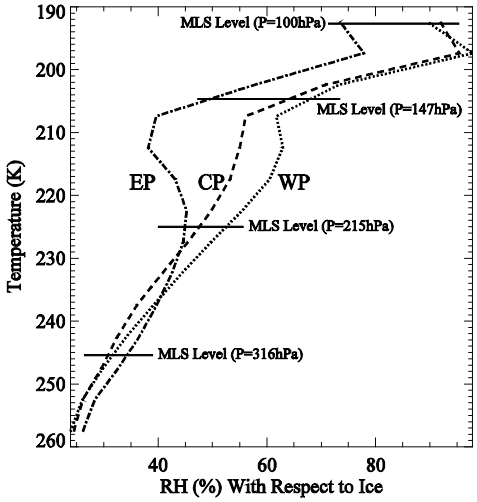

Fig. 2.9. September 2004-July 2005 relative humidity with respect to ice for WP, CP, and EP. Also shown are MLS levels.

Longwave clear-sky radiative cooling rate profiles are presented in Fig. 2.10, and show that below 250 hPa, cooling rates are roughly constant at around 2 K day^{-1}. Above this layer, longwave cooling rates drop off sharply. Hartmann and Larson (2002) argue that this is because of the Clausius-Clapeyron relationship, which states that the saturation vapor pressure depends only on temperature. Clear-sky emission from the upper troposphere comes from the rotational lines of water vapor, and depends strongly on vapor pressure. The sharp decreases of longwave clear-sky radiative cooling rate profiles above 250 hPa occur because of low absolute temperatures there and consequently low vapor pressures. The large decrease in clear-sky radiative

cooling rates corresponds to a mass convergence at this temperature, and this balances divergence from convective regions at the same temperature. It is this circulation that corresponds to the detrainment of the majority of anvil cloud.

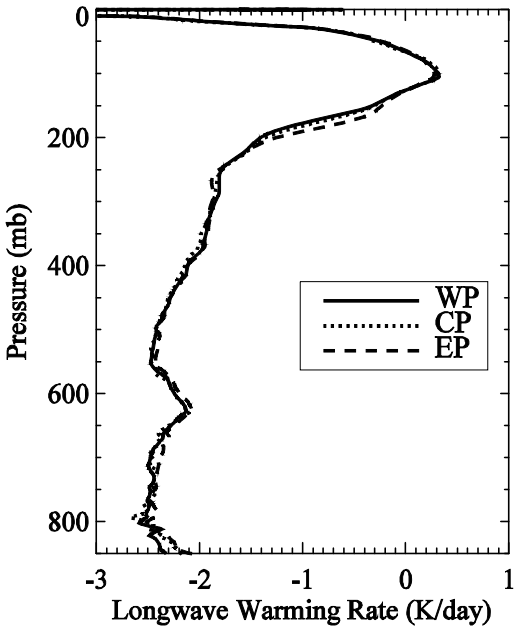

Fig. 2.10. Calculated longwave clear-sky radiative warming rates for WP, CP, and EP.

Profiles of clear-sky ω are shown in Fig. 2.11, and indicate fairly strong subsidence below about 250 hPa (on the order of 40 mb/day), and decreasing sinking motion above this level. The Q=0 level, which is the level at which clear-sky radiative cooling is zero, is around 125hPa (see Fig. 2.10). This is below the tropopause, which is at approximately 95 hPa in all three regions.

Smoothed clear-sky convergence profiles are shown in Fig. 2.12. Clear peaks appear in the upper-troposphere in the WP and EP, roughly corresponding to the peaks in upper-level relative humidity. To quantify the

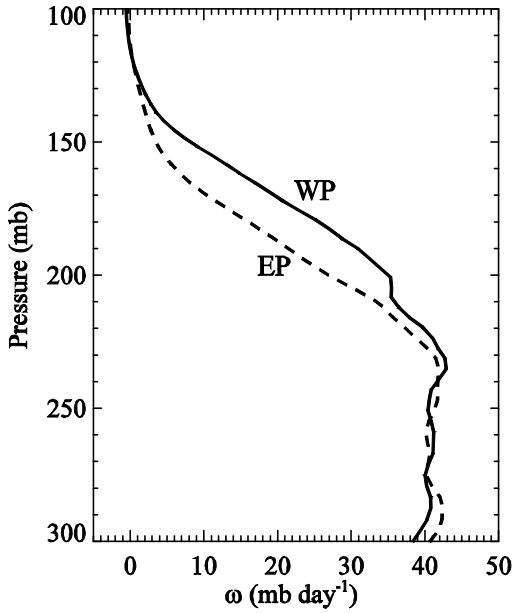

Fig. 2.11. Vertical velocity in pressure coordinates (ω) necessary to balance clear-sky radiative cooling for September 2004-July 2005.

differences in the WP and EP, a convergence-weighted temperature (T_C) is calculated from the following relationship:

$$T_C = \frac{1}{\overline{C}\Delta T}\int_{190K}^{240K} C(T)TdT \qquad (2.5)$$

where C(T) is the smoothed convergence, $\overline{C}$ is the mean convergence in the layer from 240 K to 190K, and ΔT=50 K. T_C provides a quantitative measure of the temperature at the peak of convergence, and is 216.6 K in the WP and 220.2 K in the EP for the period of September 2004 through July 2005. As we shall see in a later section, these differences in clear-sky convergence correspond rather well with differences in anvil cloud top temperature measured by MODIS.

In an attempt to quantify why T_C is about 3.6 K warmer in the WP versus the EP, we explore the relative importance of specific humidity and temperature profiles. We use specific humidity as it is directly related to water vapor content. We pair WP and EP temperature and specific humidity profiles in all possible combinations and compute the corresponding T_C. Table 2.1 indicates that the specific humidity difference is more important than the temperature, but the temperature is also a factor. Figure 2.4 shows that the WP has a larger lapse rate in the region above 12 km, or colder than about 225 K.

An idealized tropical profile, from McClatchey al. (1971), was used below the MLS levels. While reanalysis data below the MLS region would perhaps be preferred, sensitivity studies were performed (figures not shown), and suggested that moisture further down in the troposphere does not matter very much at all compared to moisture closer to T_C.

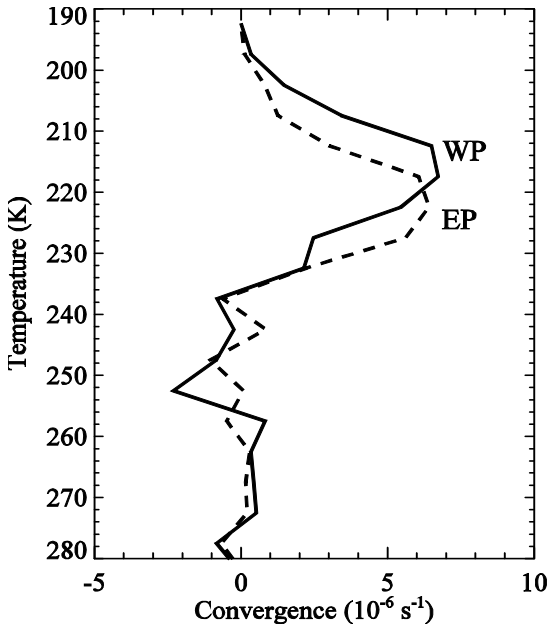

Fig. 2.12. Binned clear-sky convergence profiles for WP and EP for September 2004-July 2005.

Table 2.1. Convergence-weighted temperature (T_C) for WP and EP specific humidity and temperature profiles.

	WP Specific Humidity	EP Specific Humidity
WP Temperature Profile	216.6 K	219.2 K
EP Temperature Profile	218.1 K	220.2 K

2.9 Testing the PUSH Mechanism

The notion behind the PUSH mechanism is that the surface drives convection, by assuming that parcels of air, so long as they retain positive buoyancy, ascend undiluted until they become negatively buoyant in the upper troposphere (Riehl and Malkus 1958, Riehl and Simpson 1979). The level of neutral buoyancy in the upper troposphere is reached at the temperature aloft in which environmental θ_E is the same as θ_E at the LCL. We refer to this intersection temperature as T_{INT}. We calculate T_{INT} first by calculating θ_E profiles for the WP, CP, and EP, and then simply determining the intersecting point in the upper troposphere. Given this procedure, parcels in the WP have the potential to ascend higher, as θ_E at the LCL is 365.8 K, versus 358.4 K in the EP (these are calculated assuming that the LCL temperatures are 6K lower than the SSTs in each of the regions – the surface relative humidity in the EP and WP are very similar to one another, according to the Comprehensive Ocean-Atmosphere Data Set, making this an acceptable assumption). For the same period (September 2004 through July 2005), T_{INT} is 192.9 K in the WP, 194.9 K in the CP, and 199.8 K in the EP. These temperatures are significantly

lower than T_{ANVIL} (median anvil cloud top temperature), by 20 K or more, and even T_{THICK} (median thick cloud top temperature). Therefore, the surface air in both the EP and WP has enough energy to rise undiluted to well above the level where the anvil cloud is concentrated. One must assume a particular entrainment spectrum for plumes in order to explain the existence of the anvils. This has not been done for this particular study, however. The clear-sky radiative cooling profile is more simply related to the temperature of the anvil clouds.

2.10 Comparing the PUSH and PULL Mechanisms

It was discussed previously that clear-sky convergence profiles support a circulation connecting clear and adjacent convective regions. The peak of the clear-sky convergence should therefore correspond to the detrainment level of anvil cloud. To investigate this, we examine a subset of data, from September 2004 through July 2005, during which we have GPS, MLS, and MODIS data. In Fig. 2.13, we present the clear-sky convergence profiles along with the anvil cloud fraction profiles for the WP and EP, both as functions of temperature. The peak in upper-level convergence lines up well with the peak in anvil cloud amount in all three regions (only the WP and EP are shown for clarity). The differences in T_{ANVIL} in the WP and EP correspond well to those of the clear-sky convergence peak. Thus, vertical profiles of convergence and observed anvil cloud fractions are related to one another.

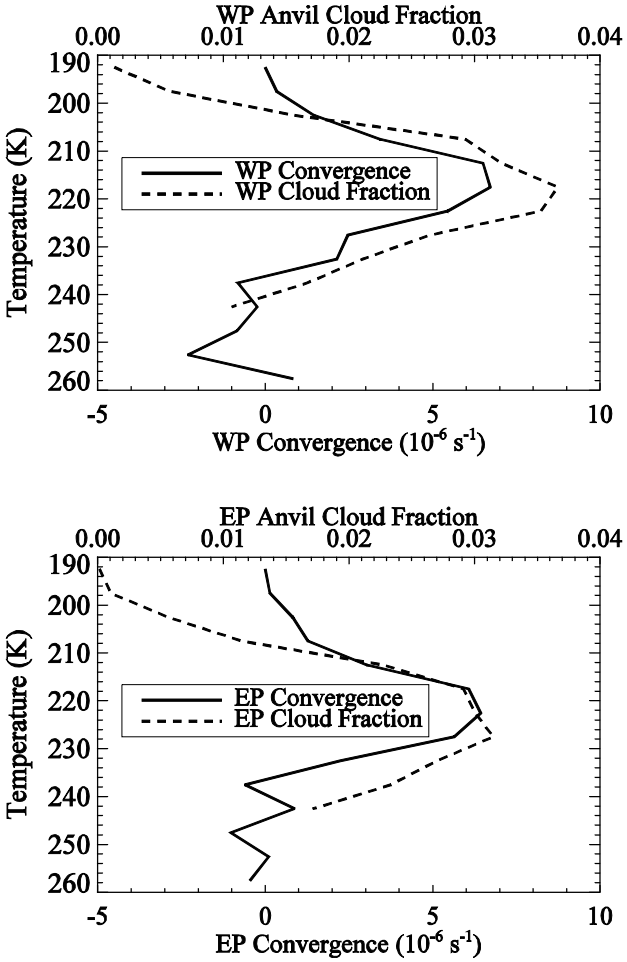

Fig. 2.13. Clear-sky convergence and anvil cloud fraction for WP (top) and EP (bottom) for September 2004-July 2005.

In order to further quantify whether or not T_C is actually a good predictor of T_{ANVIL}, we subdivide the data into seasonal datasets, so as to increase the number of samples with which to evaluate the statistical validity of the relationships between T_C and T_{ANVIL}. We present T_{ANVIL} versus T_C in Fig. 2.14, as well as the one-to-one line of these two variables. Principal component analysis is performed in this plot and subsequent ones to calculate the slopes, which makes no assumptions of dependent or independent

variables. The slope of the best linear fit is 1.06±0.41, which means that a one-to-one relationship between T_{ANVIL} and T_C cannot be ruled out. T_{ANVIL} is only about three to four degrees Kelvin warmer than T_C. Fig. 2.14 shows that the peak in clear-sky convergence corresponds well to $T_{ANVIL,}$ such that the clear-sky radiative profile seems to drive anvil cloud detrainment!

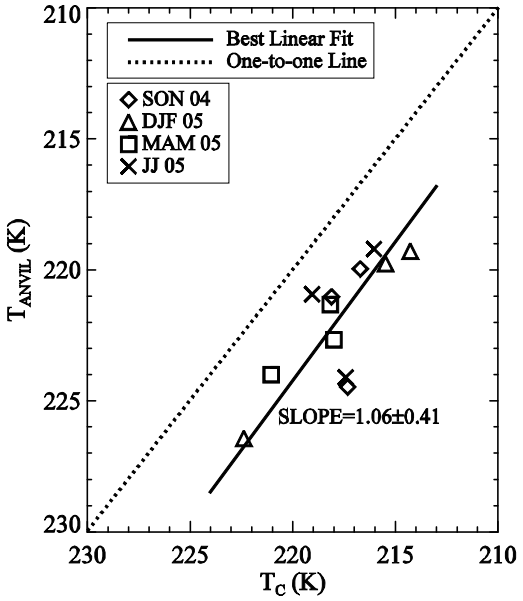

Fig. 2.14. Seasonal median anvil cloud top temperature (T_{ANVIL}) versus seasonal convergence-weighted temperature (T_C).

The PULL mechanism certainly seems to be able to predict the level of anvil cloud detrainment. Can the PUSH mechanism also be used to predict the level of convective detrainment? We address this first by plotting T_{ANVIL} versus T_{INT} for the seasonal data (Fig. 2.15), and immediately see, as suggested earlier, that T_{INT} is much lower (by 20 K or more) than T_{ANVIL}. The slope of the best linear fit line is 0.59±0.41, so that it seems that T_{INT} *does not* explain where anvil clouds are detraining.

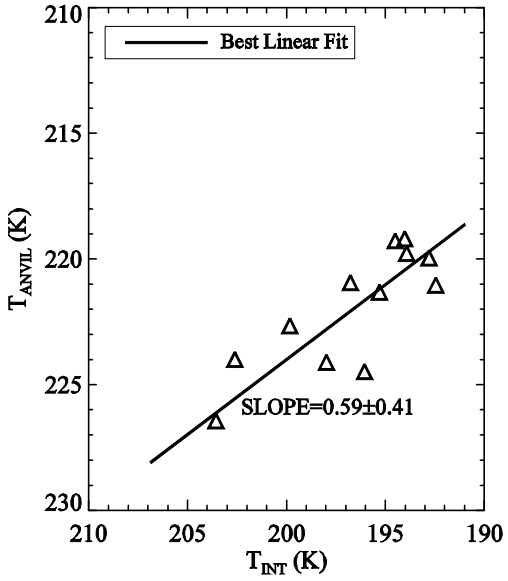

Fig. 2.15. Seasonal median anvil cloud top temperature (T_{ANVIL}) versus seasonal intersection temperature (T_{INT} is the temperature in the upper troposphere where Θ_E is the same as Θ_E at the LCL).

But, does T_{INT} have any bearing on how high the thickest clouds get? We might expect more of a linear relationship between the thickest high-topped clouds and Θ_E near the surface, since they represent the tallest convective cores, which are least affected by detrainment. Fig. 2.16 shows both T_{THICK} versus T_{INT} and the 90th percentile of the coldest thick clouds from MODIS (T_{THICK_90}) versus T_{INT}.

We immediately see that T_{INT} is significantly colder than T_{THICK} by approximately 10-15 K, but that the slope of the best linear fit is 0.96±0.41, so a one-to-one relationship cannot be ruled out. The relationship between T_{INT} and T_{THICK_90} is more convincing, especially since the 90th percentile of the thick clouds often makes it to T_{INT}. The slope of the line is 0.69±0.38. Also, the fact that T_{INT} and T_{THICK_90} are close to one another does seem to suggest

that there is a relationship between the two. The low-level θ_E thus does seem to constrain the coldest level of the convective cores, as we would expect, but the anvil cloud temperature is better predicted by the clear-sky convergence.

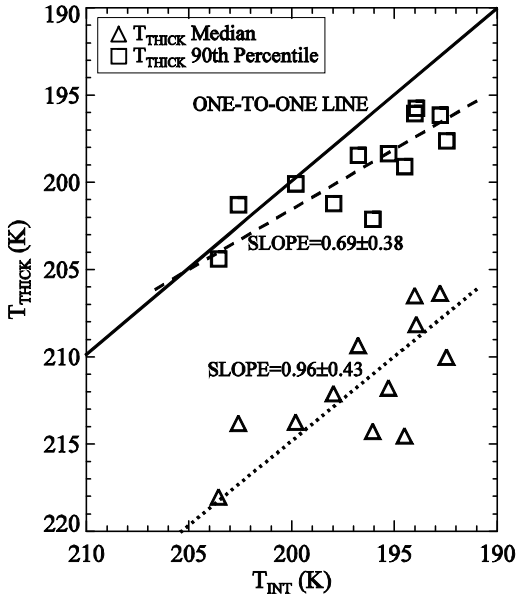

Fig. 2.16. Seasonal thick cloud top temperature (T_{THICK}) and 90th percentile of T_{THICK} versus seasonal intersection temperature (T_{INT} is the temperature in the upper troposphere where Θ_E is the same as Θ_E at the LCL).

2.11 Conclusions

We have examined structural characteristics of tropical convection in the ITCZ of the North Pacific. We have shown three modes of clouds in the WP, CP, and EP, namely trade cumulus clouds, mid-level congestus clouds, and deep convective cores and the associated detrained anvil and thin clouds. Low cloud is more prevalent in the EP, where the domain chosen is surrounded by low SST and abundant stratocumulus cloud. Congestus cloud is also somewhat more prevalent in the EP. This may be a result of the fact that

convection in the EP is more strongly driven by surface convergence (Back and Bretherton 2006).

For a given rain rate, high thin cloud is nearly twice as abundant in the WP as compared to the EP, and this makes the TOA radiative forcing due to this cloud considerably higher in the WP, on the order of 10 W m^{-2}. Anvil cloud fraction for a given rain rate is also somewhat higher in the WP compared to the EP, though because the anvil cloud is colder in the WP, the net radiative forcing of anvil cloud is about the same in the two regions. Thick cloud amount has the same relationship with rain rate in the WP, CP, and EP, making it a very good proxy for rain rate.

The differences in high-topped cloud radiative forcing in the WP and EP stem primarily from differences in high thin cloud amount. Thin and anvil clouds are systematically about 5 K colder in the WP versus the EP, and thick clouds about 6 K colder. Thick clouds are the coldest, and anvil and thin clouds are observed at similar temperatures. It seems that anvil clouds detrain from convective cores, and over time, thin cloud is the residual of the anvil cloud. We speculate that higher amounts of thin and anvil cloud in the WP are due to the broad structure of the ITCZ there, whereas the domain chosen for the EP is surrounded by subsidence regions, whose free-tropospheric air is drier, and may entrain somewhat into the EP convective zones.

We also examine how cloud top temperature is determined by examining the PUSH and PULL mechanisms. To examine the PULL

mechanism, which states that convective detrainment is driven by clear-sky convergence, we first examine upper tropospheric relative humidity. It is higher in the WP, and peaks at a lower temperature than the EP. The relative humidity structure seems to be consistent with the abundance of anvil and thin cloud, with greater humidity associated with more high-topped cloud. Also, seasonal data suggest that the temperature weighted by clear-sky convergence is a good predictor of T_{ANVIL}. The radiative cooling profiles depend on the temperature and moisture profiles, which are determined by a mixture of radiation, convection, and large-scale forcing, so that it is not possible to determine causality from such a diagnostic analysis. The large-scale motion fields may in fact be responsible for the differences between the WP and EP. It is known that the vertical velocity profile is shallower in the EP than the WP. Also, the PULL mechanism gives a simpler prediction of the anvil cloud, as it can be computed from the clear-sky radiative cooling profile. Finally, unlike the PUSH mechanism, PULL requires no assumptions about entrainment profiles.

In examining the PUSH mechanism, the temperature where near-surface air achieves neutral buoyancy is much colder than T_{ANVIL}, and Θ_E *does not* seem to control T_{ANVIL}. The thickest, coldest clouds (the 90th percentile of the thick clouds) can make it to T_{INT}, so near surface Θ_E might be controlling the altitude of the coldest convective cores.

2.12 Postscript

Since this work has been published in the *Journal of Climate*, it has come to my attention that the moisture profiles used below 316 hPa for the radiative flux calculations were from an idealized tropical profile (McClatchey et al. 1971), which is much drier in the lower and middle atmosphere compared to actual profiles of the WP, CP, and EP. Using the actual WP, CP, and EP profiles would decrease the longwave cloud forcing calculations and make the net cloud forcing more negative. Since this study was less concerned about the relative differences among the regions, however, rather than absolute cloud radiative forcing values, this is not considered a major concern.

It has also been pointed out by Mark Zelinka (personal communication, 2008) that MODIS net cloud forcing is considerably more negative compared to CERES by 8 Wm^{-2} in the WP and 27 Wm^{-2} in the EP, at least for July and August 2003-2005. From his calculations, relative to ISCCP for the collection 5 data (note that collection 4 data were used for Chapter 2, though collection 4 versus collection 5 cloud forcings are similar), MODIS minus ISCCP anvil plus thick cloud fraction is 0.18 for the WP, and 0.14 for the EP, and these cloud categories have a negative net cloud forcing. Also, according to Hartmann et al. (2001), individual ISCCP SW and LW cloud forcings compare favorably to ERBE. Thus, in an absolute sense, the net cloud forcing values shown in Fig. 2.5 from MODIS appear thus to be too negative for all regions. Fortunately for this study, however, there is *qualitative* consistency, as ISCCP,

CERES, and ERBE all show that the EP has a considerably larger negative cloud forcing compared to the WP.

Finally, the latest collection 5 MODIS anvil clouds tend to be slightly colder compared to collection 4 clouds, the latter of which was used for this study. I have calculated T_{ANVIL} for the same period as in this chapter for collection 5. In the WP, T_{ANVIL} is 219.4 K for collection 4, but 217.0 K for collection 5. In the EP, T_{ANVIL} is 224.3 K and 222.2 K collections 4 and 5, respectively. If collection 5 data are considered more accurate, this would be even more favorable for the results presented in Fig. 2.14 in that median anvil clouds from collection 4, while well-correlated with the convergence weighted temperatures, are systematically too warm by a few degrees. This would lend additional credence to the PULL mechanism described.

Chapter 3: The Vertical Structure of Tropical Oceanic Convective Clouds and its Relation to Precipitation

3.1 Introduction

Tropical convection plays an important role in the energy and moisture balances of Earth. Previous research has shown important differences between the structure of convection in the West Pacific (WP) and East Pacific (EP) ITCZ regions, as we saw in the previous chapter. The net radiative effect of clouds in the ITCZ is more nearly neutral in the WP and more negative in the EP (Hartmann et al. 2001). The inferred precipitation from microwave versus infrared techniques is very different in the WP and EP, and these differences appear to be related to differences in cloud structure (Berg et al. 2002). Schumacher and Houze (2003) indicate a possible feedback between a higher stratiform rain fraction and stronger SST gradients in the EP. Using four independent datasets, Zhang et al. (2004) have observed a shallow circulation in the EP, and Back and Bretherton (2006) have shown significant differences in the mean vertical velocity profiles in the WP and EP, with vertical motion concentrated higher in the atmosphere in the WP than in the EP. The availability of simultaneous measurements of cloud structure from CloudSat and precipitation from AMSR on the A-Train (see Stephens et al. 2002 for more) provide a new opportunity to understand the differences in convection in the WP and EP.

The extent to which cloud top heights vary is likely related to the SST, SST gradients, mesoscale and large-scale dynamics, and the intensity of convective systems. Considerable variations in SST structure are apparent across the ITCZ from 5˚-15˚N, where the WP, from 120˚-160˚, is an area of very high SSTs (median of 29.0˚C from mid June 2006 through mid June 2007), and relatively low SST gradients, as compared to the EP (210˚-260˚), where SST gradients are higher but the median SST is considerably lower (27.7˚C). SSTs are from the NOAA Optimum Interpolation Climate Diagnostics Center (web site: http://www.cdc.noaa.gov), with version two data used (Reynolds et al. 2002). It has been shown by Back and Bretherton (2006, 2008a) that while both the WP and EP are areas of mean ascent, the WP has a much more 'top-heavy' vertical velocity profile compared to the more 'bottom-heavy' vertical velocity profile in the EP. Back and Bretherton (2008b) also derive a predictive model of the tropical distribution of rainfall in which vertical motion is divided into deep and shallow modes, which are controlled by absolute SST and SST gradients, respectively. We use CloudSat cloud radar and AMSR microwave rain rate data to provide a more detailed analysis of the structure of deep and shallow convective systems in the WP and EP and its relation to precipitation.

In the previous chapter, we showed that differences in high-topped cloud fraction per unit rain rate exist in the WP and EP. For clouds with tops colder than 245K, and intermediate visible cloud optical depth between 4 and

32, cloud fraction increases with rain rate, but does so more in the WP. The most striking difference in high-topped clouds, however, is that thin high-topped clouds ($\tau<4$) in the WP are approximately twice as abundant compared to the EP for a given rain rate. Luo and Rossow (2004) estimated that 44% of tropical thin cirrus clouds are directly detrained from convection, while 56% form *in situ*, which suggests that the large-scale environment in the WP, with a more top-heavy profile of vertical motion, could be associated with the greater sustainability of high thin cloud there.

3.2 Data

We use data from CloudSat, which is the first satellite-borne cloud radar (sun-synchronous), with an operational frequency of 94 GHz, for which backscatter from clouds can be measured. It was launched in April 2006, and data have been available since June 2006. As it is part of the A-train satellite constellation, it closely follows the orbit of the satellites Aqua, PARASOL, and Aura (Stephens et al. 2002). The A-train has two equatorial passage times of approximately 1:30 a.m. and 1:30 p.m. local time. Its horizontal resolution of 1.7 km along track by 1.4 km across track, along with its effective vertical resolution of 240m, give CloudSat a small spatial footprint and good vertical resolution, but only for a nadir curtain (Cloudsat Standard Data Products Handbook available at http://www.cloudsat.cira.colostate.edu/dataHome.php). CloudSat has an estimated operational sensitivity of -30 dBZ, which prevents CloudSat from seeing some thin cirrus. Since the main focus of our study is

cloud structure as it relates to precipitation, the inability for CloudSat to sense all thin clouds is not viewed as a major drawback.

We also collocate the cloud data with instantaneous rain rate data from AMSR, aboard the Aqua satellite. AMSR data are gridded with a horizontal resolution of 25km by 25km (Wentz and Meissner 2002). Microwave sensitivity becomes saturated when instantaneous rain rates exceed 25 mm/hr, though during this one-year period of analysis (mid June 2006 through mid June 2007), observed rain rates do not exceed 15.3 mm/hr in our regions of interest.

3.3 Methodology

The CloudSat cloud mask product, which utilizes the radar reflectivity to determine cloud layers, is used to discriminate between cloudy and clear profiles. The algorithm implemented for this study can sense up to four cloud layers. For all the *cloudy* profiles in this one-year analysis, 88% in the WP and 89% in the EP have either one or two cloud layers.

The collocation methodology is straightforward, and simply matches the AMSR rain rate with all the CloudSat profiles that fall within its 25km footprint. No spatial or temporal averaging is performed, and all CloudSat profiles are assigned the precipitation of the AMSR pixel in which they fall. Not averaging the profiles preserves the high-topped cloudSat horizontal and vertical resolution.

3.4 Cloud Tops of Precipitating and Non-Precipitating Clouds

We first examine the vertical structure of clouds as a function of rain rate regime from AMSR. We examine PDFs of all cloud tops for non-precipitating clouds, for raining clouds in which the rain rate is below the 90th rain rate percentile in each region, and for clouds in which the rain rate is equal to or greater than the 90th percentile (3.8 mm/hr and 3.7 mm/hr in the WP and EP, respectively). The percentiles of rain rate are for all raining profiles, with a rain rate threshold of 0.1 mm/hr. Though by definition clouds with rain rates that exceed the 90th percentile only comprise 10% of the rain *area*, they account for 47% and 50% of total rain *amount* in the WP and EP, respectively.

Figure 3.1 shows the PDFs of cloud tops for these various rain rate categories, labeled as 'no rain', 'mod rain', and 'hvy rain'. The high mode of heavily precipitating clouds in both the WP and EP is nearly two km higher than moderate and no precipitation cases. The peak of heavily precipitating high-topped clouds in the WP is between 15 and 16 km, with only 0.8% of heavily precipitating clouds ascending to above the mean tropical tropopause of 17 km. Relatively few heavily precipitating clouds have cloud tops lower than 9.5 km (19% in the WP and 27% in the EP), and the overall cloud top height distribution has a relative minimum near 9.5 km. Moderately precipitating high-topped clouds generally have similar high-topped cloud distributions as non-precipitating high-topped clouds, though high-topped clouds are more common in the WP for both categories.

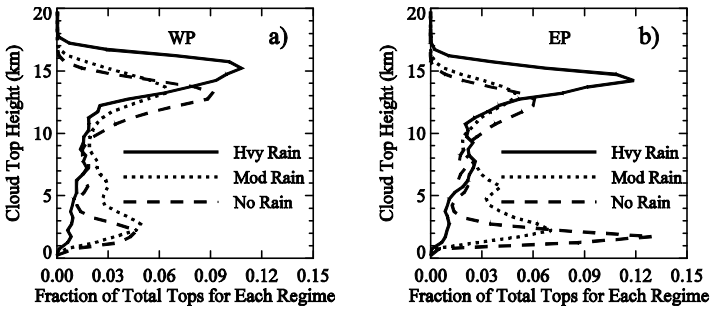

Fig. 3.1. WP (a) and EP (b) cloud top PDFs for different rain categories (categories defined in text).

Low and middle cloud (**tops lower than 9.5 km**) distributions are considerably different for moderately raining versus non-raining clouds, particularly in the EP. Non-raining clouds are mostly boundary-layer clouds (around two km), whereas moderately raining low and middle clouds are deeper, with two discernible peaks, at around three and six km. The secondary peak around six km could very well be classified as congestus clouds, as noted in such studies as Johnson et al. (1999). The greater abundance of low and middle moderately raining or non-raining clouds in the EP seems consistent with the 'bottom-heavy' vertical velocity profile there.

3.5 Contribution to Total Rain From Different Clouds

We next quantify the contribution of different cloud heights to both total rain amount and total rain area in the WP and EP. We begin by examining the prevalence of clouds as a function of rain rate. We examine three cloud types: 1) high-topped clouds only, in which the lowest top is greater than 9.5 km, 2) low and middle clouds only (tops lower than 9.5 km), and 3) high-topped clouds over low and middle clouds. Figure 3.2a shows that

as rain rate increases, the fraction of clouds that are *high-topped clouds only* increases dramatically. For a given rain rate, more clouds are high-topped clouds in the WP than the EP. For very light rain rates, more clouds are low and middle clouds than high-topped clouds in both regions, though more so in the EP (Fig. 3.2b). The fraction of only low and middle clouds decreases precipitously with increasing rain rate in both regions. High-topped clouds over low and middle clouds primarily represent situations in which high thin clouds overlie lower precipitating clouds, and their relationship with rain rate is very similar in both regions (Fig. 3.2c).

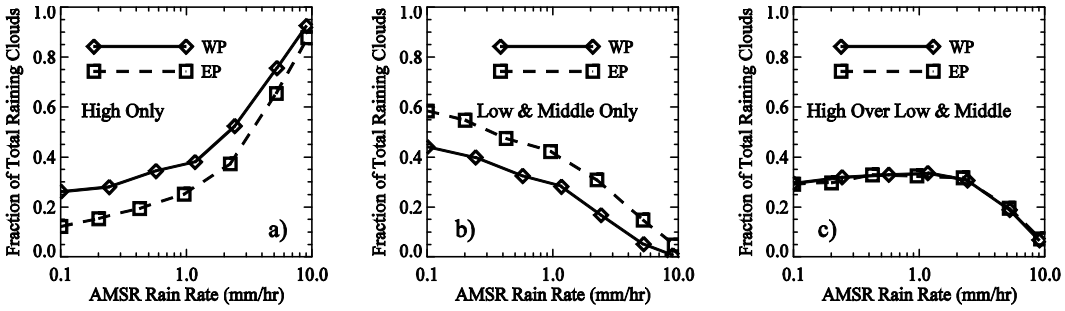

Fig. 3.2. a) Fraction of clouds versus rain rate that are **high-topped clouds** only, b) **low and middle clouds only**, and c) **high-topped clouds over low and middle clouds**. High-topped clouds have tops > 9.5km.

Next, we examine the mean rain rate as a function of cloud top, which we present in Fig. 3.3a, assuming that the cloud with the lowest top in each profile is raining. A fairly robust increase in rain rate is observed with increasing cloud top height, except for the interval between 9 and 12 km, for which rain rate is approximately constant. The increase in rain rate with cloud top height is rapid for clouds deeper than 12 km. Note the logarithmic y-axis, so that a nearly *tenfold increase* in rain rate occurs as cloud tops rise from 12 km to 17 km, from ~1 mm/hr to ~10 mm/hr. It is also noteworthy that

significantly lower rain rates in the WP are associated with a given high-topped cloud top versus the EP, which may be a result of stronger low-level convergence there. When deep convection fires up, if stronger upward motion is present, we might expect it to be balanced by stronger rain rates.

Finally, we compute the contribution to *total rain amount* as a function of cloud top height. We calculate this by multiplying the rain rate as a function of lowest cloud top height, r(z), by the probability of a given *raining* cloud top height, p(z). These are shown Fig. 3.3a and Fig. 3.3b, respectively. The contribution to total rain amount, which we call the *precipitation density* (mm/hr/km), is shown in Fig. 3.3c, and the total area under each curve is the mean rain rate for the given region. The WP and EP have large peaks in *precipitation density* at just above 15 km and near 14 km, respectively. The moderate contribution from clouds between about three and nine km represents the contribution to total rain from low and middle clouds. Low and middle clouds contribute less to total rain amount in the WP, at 38%, versus 47% in the EP. In terms of *total rain area*, low and middle clouds contribute 60% in the WP and 74% in the EP. Thus, though precipitating low and middle clouds are more widespread, high-topped clouds contribute more substantially to *total rain amount*, especially on a per unit area basis (see Lau and Wu (2003) for warm rain contribution to rain area versus rain amount).

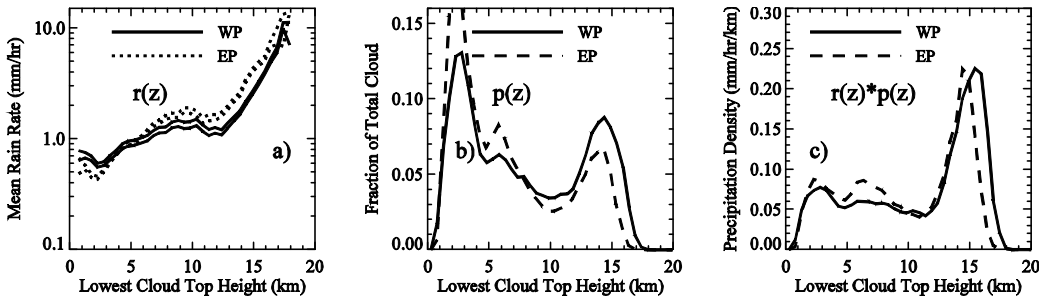

Fig. 3.3. a) Mean rain rates versus cloud top heights r(z), assuming the lowest cloud is raining. The two curves for WP and EP indicate the 99% confidence intervals. b) PDFs of cloud tops p(z) of lowest raining clouds in each profile. c) *Precipitation density,* r(z)•p(z) (mm/hr/km).

3.6 High Thick and Middle Thick Cloud Systems

We now examine *cloud systems*, which we define as a contiguous group of profiles along the flight track that is identified as cloudy. High thick convective cloud systems must contain at least one profile with a cloud thickness of at least 10km. Many deep convective systems are extensive, with a mean size of about 340 km in the WP and 370 km in the EP. While deep convective cloud systems cover 27% of the WP and 24% of the EP from mid June 2006-mid June 2007, these differences are not statistically significant at the 95% confidence level, as revealed by a t-test analysis. We compute the t-test by subdividing the data from each region into 50 subaverages and using the standard deviation of these subaverages to compute confidence limits. It should be noted that this approach of partitioning deep clouds into systems based on geometric thickness is different from the approach in Chapter 2, in which cloud fraction versus rain rate was assessed. This suggests that deep convective systems may be as horizontally extensive in the two regions, and

that the greater anvil and thin cloud fraction per unit rain rate in the WP versus EP presented in Chapter 2 may not necessarily be directly connected to deep thick systems, at least as they are defined in this chapter.

Figure 3.4a shows the PDFs of all cloud tops within high thick convective systems in the WP and EP. The distribution of high-topped clouds looks remarkably similar in the WP and EP, with only a slightly greater abundance of high-topped clouds in the WP. 67% of all deep convective system clouds are high-topped clouds in the WP, and 56% in the EP. Within deep convective cloud systems, low clouds with tops around two km are more prevalent in the EP.

Next, we examine some statistics of middle thick convective cloud systems, whose cloud thickness must exceed five km but whose cloud top must be below 9.5 km for at least one profile. While overlying high-topped clouds are permitted, no high-topped clouds with thicknesses greater than five km are allowed. Middle thick convective systems likely encompass precipitating congestus clouds or perhaps convection that is still developing, possibly into deep convection at a later time.

Figure 3.4b shows the PDFs of all cloud tops of middle thick convective cloud systems, and indicates a clear peak in cloud tops around six km. Another peak is apparent between two and three km. A very small portion of the shallow convective systems consist of high thin clouds around 12-13km that overlie lower clouds. The percent of the WP covered by middle

thick systems is 2.0%, versus 3.0% in the EP, and the t-test analysis reveals that these differences are statistically significant. The greater amount of middle thick systems in the EP is consistent with the stronger surface convergence in the EP. Also, the mean size of middle thick systems is considerably smaller in the WP at 40 km, versus 90 km in the EP.

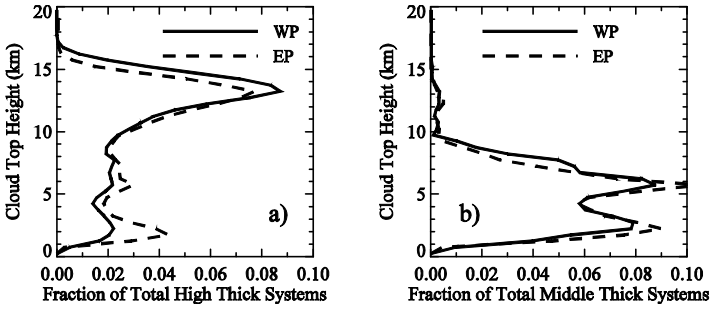

Fig. 3.4. (a) PDFs of cloud tops of all high thick convective systems and (b) middle thick convective systems in the WP and EP.

3.7 Summary and Implications

This study has demonstrated that heavily precipitating clouds in the WP and EP are rather similar qualitatively, with more precipitation coming from clouds with lower tops in the EP. The real difference lies in *moderately raining or non-raining clouds*, where the WP has a much smaller abundance of low and middle clouds relative to high-topped clouds compared to the EP. This also may suggest that deep convective cores are structurally similar in both regions, albeit a bit deeper in the WP. High thin clouds contribute the most to differences in cloud top PDFs between the WP and the EP.

We have demonstrated that low and middle clouds contribute 38% and 47% to *total rain amount* in the WP and EP, respectively. Mean rain rates

(where it is raining) are slightly higher in the WP (1.37 mm/hr versus 1.29 mm/hr in the EP), probably because there are more high-topped clouds there, which have substantially greater mean rain rates than low and middle clouds. Since rain rate increases substantially as cloud top increases, especially for clouds higher than 12 km, the mean rain rate for a particular region is related to the distribution of heights of raining clouds. We also show, however, that high-topped clouds at a given altitude have greater rain rates in the EP, which may be a result of the stronger low-level convergence there.

We have also seen that the vertical structure of high thick convective cloud systems, which are defined to be contiguous cloudy profiles with at least one cloud containing a geometric thickness of at least 10 km, are fairly similar in the WP and EP. The high thick convective cloud system fractional horizontal coverage in the WP and EP is 0.27 and 0.24, respectively, but this difference is not statistically significant. WP and EP high-topped cloud differences instead stem from high thin clouds, which cover a significantly larger fraction of the WP at 0.33 versus 0.24 in the EP, irrespective of whether they are part of a contiguous cloud system. This suggests that the optically thin high-topped cloud differences shown in Chapter 2 may be fairly well-removed from deep convective cores.

Chapter 4: Understanding the Importance of Microphysics and Macrophysics for Warm Rain in Marine Low Clouds

4.1 Introduction

Warm oceanic clouds over the tropics and subtropics are extensive and important to the Earth radiation balance, a result of their high albedo relative to the ocean surface (Hartmann and Short 1980; Slingo 1990). Single-layer marine stratiform water clouds cover nearly one-third of the global ocean surface (Charlson et al. 1987). The optical depth τ of a warm cloud is proportional to the cloud liquid water path LWP and inversely related to the cloud droplet effective radius r_e. The cloud LWP is generally considered a macrophysical variable which is controlled by both cloud-scale dynamics and the thermodynamics of the ambient air (Petty 2006). The effective radius, on the other hand, is the ratio of the third to second moments of the droplet size distribution, and is predominantly a microphysical variable (Wood 2006b). If one assumes a lognormal size distribution that does not vary in the vertical, then LWP itself is fundamentally related to both r_e and droplet concentration N_d (also a microphysical variable) as follows (Matrosov et al. 2004):

$$LWP = (4/3)\pi\rho N_d r_e^3 \exp(-3\sigma^2)\Delta h \qquad (4.1)$$

where σ is the distribution width, and Δh the cloud thickness. Thus, for a given LWP, small changes in r_e are associated with substantial increases in N_d.

If one assumes that supersaturation is sufficient to activate all cloud condensation nuclei (CCN), then the CCN, or aerosol number concentration, is

directly related to N_d. For marine clouds, this is often a reasonable assumption (Martin et al. 1994; Miles et al. 2000). Regions influenced by continental aerosols and/or anthropogenic pollution tend to be characterized by higher N_d and smaller cloud droplet size (Han et al. 1994; Miles et al. 2000; Breon et al. 2002; Bennartz 2007). For a given LWP, continental clouds thus tend to be brighter than pristine marine clouds (Twomey 1974, 1977). As a simple experiment to quantify the sensitivity of the radiative effect to changes in microphysics, Charlson et al. (1987) show that an increase in N_d of 30% (with LWP held fixed) results in a 10% reduction of r_e, which increases the solar albedo in the area covered by liquid marine stratiform clouds by 0.018, and enhances the global albedo by 0.005. This would account for a global average temperature decrease of -1.3K, after accounting for feedback effects (Charlson et al. 1987). In an observational study over western and eastern Washington State of non-raining warm clouds, Hindman et al. (1977) found an inverse relationship between cloud droplet concentration and size. It is suggested that the presence of large concentrations of small CCN in western Washington during the study inhibited the production of large cloud droplets via coalescence. Other classical studies also suggest that high droplet concentrations are almost always observed in clouds that contain few, if any, large droplets (Squires 1956, 1958), but many of such studies do not quantify what ‘few’ actually means.

In addition to the effect that droplet concentration has on the reflectivity of the cloud, droplet concentration also may be important in helping to determine the processes that form drizzle, such as collision and coalescence (Albrecht 1989). Collision efficiencies are fundamentally less efficient for smaller cloud drops (Rogers and Yau 1989). Albrecht (1989) proposes that an increase in N_d with a consequent decrease in r_e would decrease drizzle frequency and thus increase fractional cloudiness, enhancing cloud albedo. Measurements made during the First International Satellite Cloud Climatology Regional Experiment (FIRE) in horizontally homogeneous clouds in 1987 (400-500 km southwest of Los Angeles) demonstrate not only an inverse relationship between droplet size and radiation, but also that the clouds with the lowest droplet concentrations have the highest propensity to significantly drizzle (Albrecht 1989). More recent studies by Pawlowska and Brenguier (2003), Comstock et al. (2004), vanZanten et al. (2005), and Wood (2005) quantify similar behavior. Drizzle also has the effect of scavenging CCN, and low CCN concentrations seem to be important for drizzle formation, suggestive of a positive feedback (Wood 2006a).

Many observational studies attempting to show the relative importance of both the large-scale meteorology (i.e. bulk thermodynamics) versus the microphysics (CCN and consequently droplet concentration) in the brightness and drizzle properties of warm clouds have used relatively small samples. We wish to examine low cloud properties over the entire tropical and subtropical

Pacific and Gulf of Mexico utilizing collocated remote sensing instruments from the A-Train constellation (A-Train described in Stephens et al. 2002). In this way, we shall relate the meteorology and variability of cloud macrophysics and microphysics with propensity of precipitation. We use MODIS for cloud optical parameters r_e and τ, and also the CloudSat 2B-GEOPROF radar reflectivity profiles, from which we can infer not only cloud layers but also distinguish between drizzling and nondrizzling clouds.

The majority of the area that we examine in this comprehensive study can be best characterized as a pristine marine environment, which we thus would expect to have quite low CCN and low cloud droplet concentrations. However, there may still be sufficient natural droplet concentration variability to examine the role of microphysics in warm cloud structure. Our region will also encompass areas potentially subject to the influence of continental aerosols, such as the Gulf of Mexico, and also off the eastern coast of Asia, so perhaps a different set of CCN regimes might be possible in these areas, allowing for sufficient variability in our study. Our study will examine the importance of large-scale meteorology as well, as the tropics and subtropics are characterized by areas in which vertical cloud development is suppressed by pervasive strong low-level capping temperature inversions.

Our objectives of this study are multifaceted, but include

•The variability of warm cloud macrophysical (cloud top height, liquid water path) and microphysical (droplet size, concentration) properties across the tropics and subtropics

•The relative role of macrophysics and microphysics in drizzle intensity and frequency

•Whether drizzle frequency is similar for a particular cloud liquid water and droplet concentration among various meteorological regimes and background aerosol loads

4.2 Data

4.2.1 MODIS

We use the narrow-swath MODIS/Aqua level-2 Cloud subset along the CloudSat field of view track, the MAC06S0 product. The MODIS cloud data contain pixels whose horizontal resolution is either one or five km, and the narrow-swath data have an across-track width respectively of 11 km (11 one km pixels) and 15 km (three five km pixels). All of the standard level-2 MODIS cloud products are contained within this narrow-swath subset, including cloud optical and physical parameters. We primarily are concerned with the MODIS optical parameters for this study, including visible τ, effective radius r_e, and liquid water path LWP. Because only τ and r_e are independent, we devote space to discussing the physical foundation for retrieval of these variables.

MODIS is a 36-band scanning spectroradiometer aboard the Aqua satellite, which is part of the A-Train constellation (see Stephens et al. 2002 for more about the A-Train). MODIS is sun-synchronous with equatorial crossing times of 1:30 a.m. and 1:30 p.m., but as we are interested in warm cloud optical properties, we only use daytime retrievals. Four of the MODIS bands are used for the daytime shortwave cloud retrieval algorithm, including the visible band of 0.86 μm over the oceans (0.65 μm over land), and 1.64, 2.13 and 3.75 μm in the near IR (King et al. 1997). Cloud top properties, on the other hand, which include cloud cover and cloud top properties, come from the thermal wavelength bands (i.e. 8.55, 11.03, 12.02, 13.335, 13.635, 13.935, and 14.235 μm). The combination of one nonabsorbing visible band and one of the three absorbing near IR bands is used to retrieve τ and r_e, respectively. In fact, cloud radiative properties depend nearly exclusively on both τ and r_e, making retrieval of these two parameters extremely relevant (Nakajima and King 1990). A detailed examination of MODIS retrievals can be found in King et al. (1997).

Theoretically, the MODIS algorithm for retrieving optical properties is applicable to plane-parallel liquid water clouds (King et al. 1997), though of course in reality horizontal inhomogeneities of optical properties can and do occur at all horizontal scales (Pruppacher and Klett 1978). Even in partially cloudy scenes, however, Han et al. (1994) show that r_e may only be overestimated by at most 1 μm. The first step in the MODIS algorithm

includes using a radiative transfer model to compute the reflected intensity field. One assumption is that the reflection function is dependent on r_e, and somewhat on the effective variance also, as opposed to the distribution of particle sizes.

Extracting both τ and r_e from measurements of reflectance normally requires utilizing extensive look-up tables, which is computationally expensive. MODIS optical property retrievals instead use asymptotic theory for 'optically thick' layers that can be used to calculate reflection, given τ, r_e, and the underlying surface albedo A_g (King et al. 1997). For $\lambda<1$ μm, the reflection function increases with τ and has very weak dependence on r_e, whereas for absorbing wavelengths, particularly for the 3.75 μm band, the reflection function shows very little sensitivity to τ, particularly once $\tau \geq \approx 10$, and the reflectance function decreases with increasing particle size (King et al. 1997). In fact, for such optically thick conditions, τ and r_e can be determined independently.

As mentioned, the three near IR bands are 1.64, 2.13 and 3.75 μm, and r_e is sensitive to a somewhat different cloud depth depending on the choice of band used, since longer wavelength bands are more strongly absorbing and thus will be absorbed more readily and hence closer to cloud top. The 3.75 μm band is most sensitive to drops in the uppermost one to two units of visible optical depth (Han et al. 1994). In liquid water clouds, r_e often increases from cloud base to cloud top, though as Dong et al. (2008) demonstrate with surface

radiometer data, r_e may also decrease with height or even show random variation, depending on drizzle characteristics - a drizzling cloud will have its largest drops near cloud base, though these will not dominate the scattering. To thus say that satellite retrievals of 3.75 μm r_e should always be greater than in situ retrievals of mean r_e throughout the depth of the cloud is a generalization. Care though does have to be taken when comparing to *in situ* retrievals. We use the r_e produced using the 3.75 μm channel to minimize problems associated with thin and broken clouds, and to give an r_e that is most representative of cloud top (Nakajima and Nakajima 1995). Using the cloud top value is also a reflection of condensational growth of cloud droplets.

We also use MODIS as $LWP=2\rho\tau r_e/3$ (King et al. 1997). As LWP is a post-processed MODIS variable, its horizontal resolution, as for τ and r_e, is also 1 km. We also use cloud top temperature and cloud fraction, which are both 5 km variables, and are derived from bands in the thermal region (King et al. 1997). As the focus of our study is warm clouds, we only use scenes in which MODIS cloud top temperatures (in conjunction with CloudSat cloud top temperatures from ECMWF) are warmer than 273K. To ensure some horizontal homogeneity, at least at the horizontal scale in question, we also require all MODIS pixels to have a cloud fraction of one, which we discuss in greater detail in the methods section.

4.2.2 CloudSat Radar Reflectivity

CloudSat, which is the first satellite-borne cloud radar, has an operational frequency of 94 GHz, at which frequency the backscatter of clouds can be measured. We use 12 total months of CloudSat and MODIS data from two boreal autumn and winter seasons, from September 2006-February 2007, and September 2007-February 2008. Our results are insensitive to the months used. As part of the A-Train constellation, CloudSat closely follows Aqua MODIS (Stephens et al. 2002), allowing us to match this active sensor with the passive radiometer. CloudSat has a horizontal resolution of 1.7 km along track by 1.4 km across track, and an effective vertical resolution of 240 m (due to oversampling).

CloudSat has an operational sensitivity of -30 dBZ (where $dBZ=10\log_{10}Z$, with the formal definition of Z given in the next paragraph) which prevents some optically thin clouds from being seen. As we will explain in further detail in the methods section, we screen out all clouds with MODIS retrievals of $\tau<3$, perhaps partly negating this limitation of CloudSat. According to Fox and Illingworth (1997), a radar sensitivity threshold of -30 dBZ would detect 80-90% of marine stratocumulus with LWPs between 1 and 20 gm^{-2}. The lowest LWP in our study with optically thin clouds already screened out is 18 gm^{-2} as given by MODIS. We use the 2B-GEOPROF CloudSat data, which contains profiles of radar reflectivity and cloud mask (see Mace 2007 for information regarding version 5.3 cloud mask). We use

the highest confidence detections of CloudSat cloud mask to discriminate between cloudy and clear layers, in which a cloud is sensed when the reflectivity exceeds the CloudSat sensitivity. We save all values of reflectivity where clouds exist, after making a small correction for gaseous absorption, which is a standard CloudSat product. Because CloudSat is an active sensor, it can sense multiple cloud layers, and we ensure that all of our clouds are single-layer, since we are interested in the microphysical processes and drizzle characteristics of warm clouds. The vast majority (93%) of warm clouds sensed by CloudSat whose MODIS cloud fraction is one and $\tau>3$ are single-layered.

The size of the scatterers determines the magnitude of the radar reflectivity factor Z_E (e.g. Houze 1993). For the Rayleigh regime, when drop size is much smaller than the radar wavelength, Z_E is the sixth moment of the particle size distribution as follows (Fox and Illingworth 1997):

$$Z_E(mm^6m^{-3}) = \int_0^\infty N(D)D^6dD\,, \qquad (4.2)$$

in which N(D) is the number concentration of drops with diameters between D and D+dD. We should note that as D>300μm, (4.2) is no longer valid as drops scatter in the Mie regime, so that very high reflectivites are not seen with CloudSat, putting a limit on maximum observable rain rates (Comstock et al., 2004). The sixth power in (4.2) makes Z_E extremely sensitive to large drops, and in fact a small number of drizzle-sized drops (i.e. D~200 μm) would dominate the reflectivity, while adding little to the cloud liquid water content

(Fox and Illingworth 1997). In fact, only one drizzle drop per liter with a diameter of 200 μm would have a reflectivity of -12 dBZ but a LWC of only 0.04 gm^{-3} (Fox and Illingworth 1997). Specifically, drizzle becomes important when it adds to the radar reflectivity to the same extent that the cloud droplet population does, such that the reflectivity is at least doubled, e.g. an increase of 3 dBZ (Fox and Illingworth 1997). A reflectivity thresholding technique can distinguish between cloud profiles in which drizzle effects are negligible to LWC from those in which drizzle becomes significant (Fox and Illingworth 1997; Matrosov et al. 2004). Using an 8.66-mm wavelength Doppler radar, Frisch et al. (1995) show that a -15 dBZ threshold effectively discriminates between drizzling and nondrizzling clouds. Other studies have used similar dBZ values to separate nonprecipitating from precipitating clouds (e.g. Comstock et al. 2004, other studies referenced in Liu et al. 2008). We adopt this as well, and for all profiles in which the maximum profile dBZ (dBZ_{MAX}) is greater than -15 dBZ, we designate these as drizzling clouds.

4.2.3 ECMWF Analysis Profiles

ECMWF profiles of temperature and pressure, which are available with CloudSat products, have been integrated and collocated by the CloudSat team as an auxiliary set of variables, and we use these to ascertain CloudSat cloud top temperatures, though we are mostly only interested in temperatures with regards to restricting our study to nonfreezing clouds. We exclude all profiles with high thin clouds from our analysis to prevent possible cirrus

contamination (which can be particularly problematic for retrievals of optical properties), and require that the highest CloudSat cloud layer corresponds to a temperature which is not colder than 273K.

4.3 Methods

4.3.1 Collocation of MODIS and CloudSat

For τ, r_e, and LWP, which are 1 km pixels, we average all possible pixels of the 11 across CloudSat track by 5 pixels along CloudSat track (for a possible averaging of 55 pixels), and for the original 5 km pixels, we average all possible pixels of the three across the CloudSat track by the one pixel along track. This averaging technique provides an effective size of 11 km by 5 km for τ, r_e, and LWP, and 15 km by 5 km for cloud top temperature and cloud fraction. All geolocation variables have an original horizontal resolution of 5 km. We do this so that all original one km and five km MODIS pixels are on a five km along CloudSat grid.

The collocation of MODIS and CloudSat involves finding and averaging all aforementioned averaged MODIS assemblages that are located within 0.025° latitude and longitude and within 15 minutes of each CloudSat profile that actually detects a single-layer warm cloud, and averaging the MODIS variables if necessary. The vast majority of the time only one MODIS averaged quantity falls within these spatial and temporal conditions (92% of the cases), though occasionally two MODIS pixel-sets are found, due to the slight offset of the two instruments.

To reduce complications due to partially cloudy scenes at a scale which is no larger than 15 km across track by 10 km along track, the averaged MODIS cloud fraction is required to be one. Also, to preclude any possible problems with optically thin clouds, we require that all original one km τ values must be at least three, which are then averaged into the larger grid. We refer to these optical depth and cloud fraction requirements as the 'solid and thick' criteria. While our requirement of a cloud fraction of one and $\tau>3$ biases our results towards low clouds that are more horizontally extensive and homogeneous, and may exclude some small trade cumuli, it also helps reduce any optical property retrieval problems that may be associated with broken cloudiness. Of **all** the warm clouds sensed by MODIS within the CloudSat pixels, the requirements that CloudSat sense single-layer warm clouds and also that MODIS retrievals of optical depth be greater than **three** for *all* the individual MODIS pixels located within each MODIS assemblage allows us to retain 21% of all CloudSat pixels and MODIS assemblages. We refer to these as 'screened' warm clouds throughout. This approach greatly reduces optical retrieval problems associated with horizontal inhomogeneities, and also errors associated with optically thin clouds and small effective radii (King et al. 1997). Our analysis for the entire study is based on this screening of warm clouds, and values and means of all quantities are reflections of this. In Fig. 4.1a, we present a map showing the fraction of MODIS warm cloud assemblages that meet the aforementioned MODIS 'solid and thick' and

CloudSat single-layer criteria. In the deep convective regions, the fraction is relatively small (15-20%), owing to the ubiquity of trade cumuli there, which tend to be more patchy and inhomogeneous. Values are also fairly low in the far NE Pacific and the far SE Pacific, and this is primarily because warm clouds tend to be very shallow there, and we disregard cloudy pixels in the lowest three gates (up to ~720m) because of potential near-surface clutter. To elucidate this point, in Fig. 4.1b we show the fraction of MODIS warm assemblages that meet the MODIS criteria, with no information about CloudSat, and generally this looks quite similar to Fig. 4.1a, except for the aforementioned stratocumulus regions, suggesting that the clouds are solid and thick there but perhaps very shallow or otherwise not detected by CloudSat.

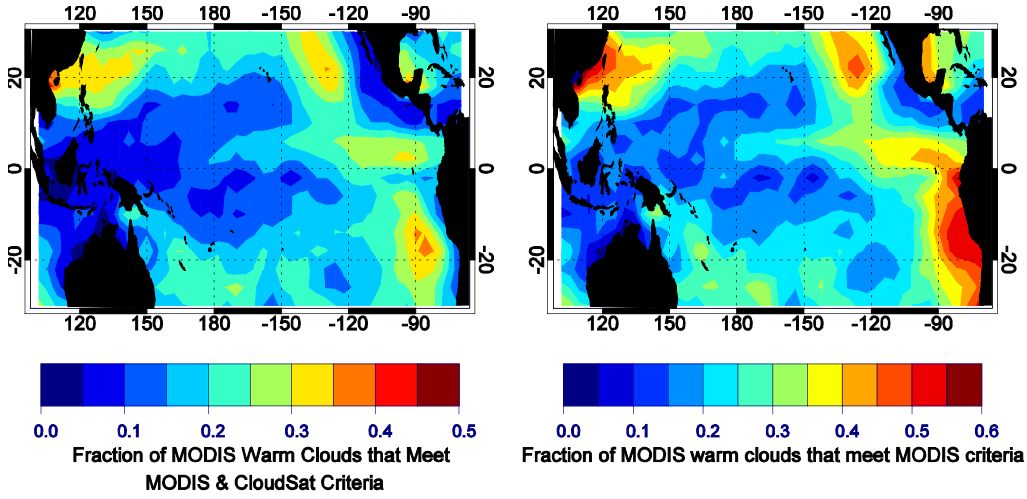

Fig. 4.1. (a) Fraction of MODIS warm clouds that CloudSat can sense that have $\tau>3$ and a cloud fraction of one for all individual MODIS pixels, (b) Fraction of MODIS warm clouds that have $\tau>3$ and a cloud fraction of one for all individual MODIS pixels. See text for details.

4.3.2 Derived Effective Droplet Concentration, N_{eff}

While MODIS mean r_e certainly conveys information about the mean size of the individual cloud droplets in the *uppermost* part of the cloud, the droplet concentration is equally important in describing the microphysical structure of a cloud. For a given cloud LWP, for instance, a small droplet size suggests a large droplet concentration, and vice versa. Droplet concentration is not retrieved by MODIS, but can be derived with knowledge of both LWP and r_e. The expression for N_{eff}, known as effective droplet concentration, is given by Wood (2006b) (see also Brenguier et al. 2000; Szczodrak and Austin 2001; Bennartz 2007) as

$$N_{eff} = \sqrt{2} B^3 \Gamma_{eff}^{1/2} \frac{LWP^{1/2}}{r_e^{3}}, \tag{4.3}$$

where $B = (3/4\pi\rho_W)^{1/3} = 0.0620$, and Γ_{eff} is the adiabatic rate of increase of liquid water content with respect to height. Three assumptions include that the liquid water content increases linearly with height above cloud base, that r_e refers to cloud top, and that r_e is equal to the geometric radius. The last assumption tends to be more inaccurate for drizzling clouds with broad drop size distributions, so that N_{eff} may be an underestimate of N_d in such conditions. In (4.3), N_{eff} is only weakly dependent on Γ_{eff}. Γ_{eff} is weakly dependent on pressure and temperature, for which we use ECMWF analysis, and is also a function of an adiabaticity factor, which can range from zero to one. Few measurements exist of the adiabaticity factor, though it is often

observed to be close to unity, particularly for nondrizzling stratocumulus clouds (Albrecht et al., 1990; Zuidema et al. 2005; Wood 2006b). In cumulus clouds, however, the adiabaticity factor can be significantly lower due to entrainment (Rauber et al. 2007). We use an adiabaticity factor of one, which means we assume that the clouds are adiabatic.

4.3.3 Regions of Study

We use pixels for which the MODIS land/water flag indicates ocean, which restricts our analysis away from the immediate coast. We also restrict our study to tropical and subtropical latitudes from 30°S to 30°N (longitude range from 100°E to 70°W). We choose such regions as we are most interested in the role that the natural variability of warm cloud macrophysics and microphysics may have on not only the cloud structure, but also on drizzle frequency and intensity. A good portion of the area that we examine can be best characterized as a remote marine environment, which we thus would expect to have quite low CCN and correspondingly low cloud droplet concentrations, save for near the Asian coast and over the Gulf of Mexico.

4.4 Geographic Distribution of Warm Cloud Properties

We now present maps of various quantities that characterize the vertical structure, macrophysical, microphysical, and drizzling characteristics of warm clouds that are seen by both MODIS and CloudSat. We begin by looking at all screened warm clouds, regardless if our CloudSat test (dBZ_{MAX}>-15) indicates the clouds to be drizzling. Figure 4.2 contains maps

of cloud top height, LWP, r_e, and $N_{eff.}$ These particular maps all contain 12 months of data and have been averaged into 4° longitude by 4° latitude bins. For slightly better clarity, these maps have been weakly smoothed with a 1-2-1 filter in the zonal direction to reduce noise. Warm cloud top heights tend to be high, even above 3 km, in regions associated with deeper convection. Even though we have screened out pixels containing overlying higher clouds via both MODIS and CloudSat, it is quite possible that these warm clouds are connected to larger, more organized deeper convective systems. In contrast, cloud top heights tend to be quite low near the South American coast and extending west, and also near and offshore of the North American/Baja California coast. Regions of suppressed cloud tops tend to be collocated with high static stability (Fig 4.3a) and cloud tops in general largely follow the structure of the underlying SST distribution (Fig. 4.3b). The cloud top distribution is consistent with our understanding of the factors controlling MBL depth (Riehl et al. 1951; Nieburger et al. 1961; Bretherton and Wyant 1997) including observations (Wood and Bretherton 2004; Wu et al. 2008).

Maps of LWP in Fig. 4.2b tend to show generally similar patterns as the cloud height maps, which should be expected for the most part, as the cloud height is likely a good indicator of cloud thickness (at least given a relatively constant cloud base height), so that a thicker cloud should contain more liquid water. Some differences exist, however, namely that LWP is especially high (approaching 300 g m^{-2} or more on average) off the coast of

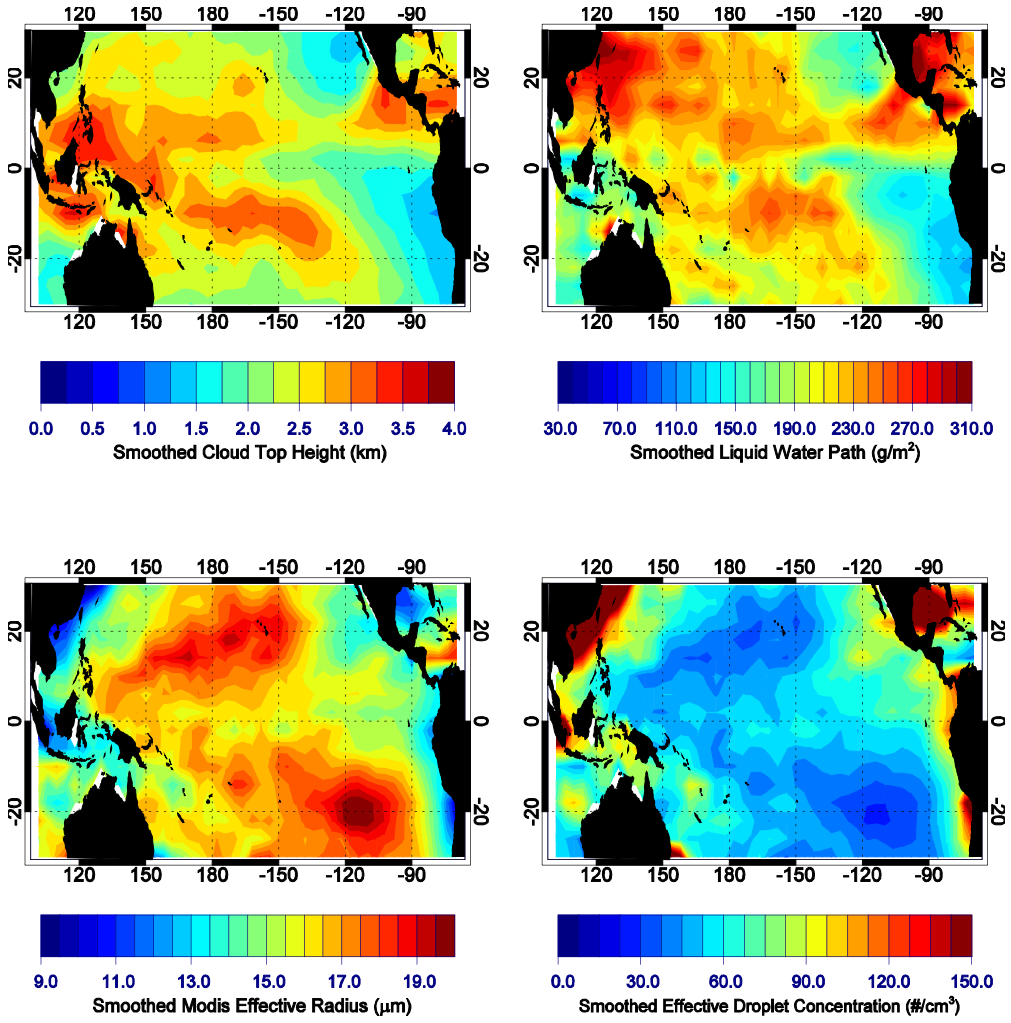

Fig. 4.2. (a) Smoothed Warm Cloud Top Height (km), (b) liquid water path (g m^{-2}), (c) r_e (μm), and (d) N_{eff} (cm^{-3}).

Asia near ~120°E, and also over the Gulf of Mexico, even though cloud tops aren't necessarily maxima in these regions. It is possible that this can be partly explained by the very large droplet concentrations near the Asian Coast and in the Gulf of Mexico (Fig. 4.2d). These regions are likely influenced by continental aerosols and pollution, which tend to be dominated by smaller

droplet and higher CCN concentrations. In fact, we see the inverse relationship between r_e and N_{eff} quite nicely when examining both Fig. 4.2c and Fig. 4.2d, which shows that variability in r_e is largely associated with N_{eff}. We also note that in much of the remote tropics and subtropics away from continents, droplet radius is quite large (r_e>15 μm) and N_{eff} is quite low (<60 cm^{-3}). Proximity to land areas tends to be important for both particle size and droplet concentration. The average geographic correlation coefficient between r_e and N_{eff} for each of the 9° by 6° boxes (map not shown) is -0.83.

We are also interested in understanding some of the background meteorology that may be responsible for controlling both the macrophysical and microphysical properties of warm clouds. We use the lower tropospheric stability (LTS), defined as Θ_{700mb} minus Θ_{1000mb} (Klein and Hartmann 1993) in Fig. 4.3a, which has been calculated by using the collocated ECMWF temperature profiles where both MODIS and CloudSat indicate that single-layer warm clouds are present. Small values are indicative of regions with either weak temperature inversions or infrequent inversions. This is the case over most of the domain, with notable exceptions being the equatorial cold tongue and far Southeastern Pacific, as well the Northeastern Pacific. As mentioned, low cloud tops are collocated with high static stability, consistent with Wood and Bretherton (2004), who find that the marine boundary layer depth is well correlated with LTS over the NE and SE Pacific.

Figure 4.3c shows the fraction of drizzling to screened warm clouds (nondrizzling and drizzling), and has very similar spatial structure to both the LTS and SST structures. Finally, Fig. 4.3d shows the median dBZ of the screened warm clouds, and looks similar spatially, as we would expect, to the drizzling warm cloud fraction. In fact, by definition, warm clouds that drizzle more than 50% of the time must have a median dBZ>-15, and vice versa. More screened warm clouds than not are drizzling across the majority of the tropics and subtropics, with the exceptions being the areas already discussed. The pervasiveness of drizzle across the tropics and subtropics has also been pointed out by Suzuki and Stephens (2008) using CloudSat data. It should also be emphasized again that drizzling clouds by our definition does not guarantee that drizzle reaches the surface, but rather that drizzle-sized drops are contained in the warm clouds. As the radar reflectivity increases above -15 dBZ, however, we would expect that a larger probability of these drops actually reach the surface. Figure 4 in Comstock et al. (2004) shows dBZ profiles of 'light' (dBZ_{MAX} of -15) and 'heavy' drizzle (dBZ_{MAX} of 0), in which drizzle reaches the surface for the heavy drizzle cases. Results examining drizzle that reaches the surface are also discussed in vanZanten et al. (2005) and Wood (2005).

What macro- and microphysical differences are there between drizzling and nondrizzling clouds? Figure 4.4 shows the mean difference of drizzling versus nondrizzling clouds of cloud top height, LWP, r_e, and N_{eff}, now in 9°

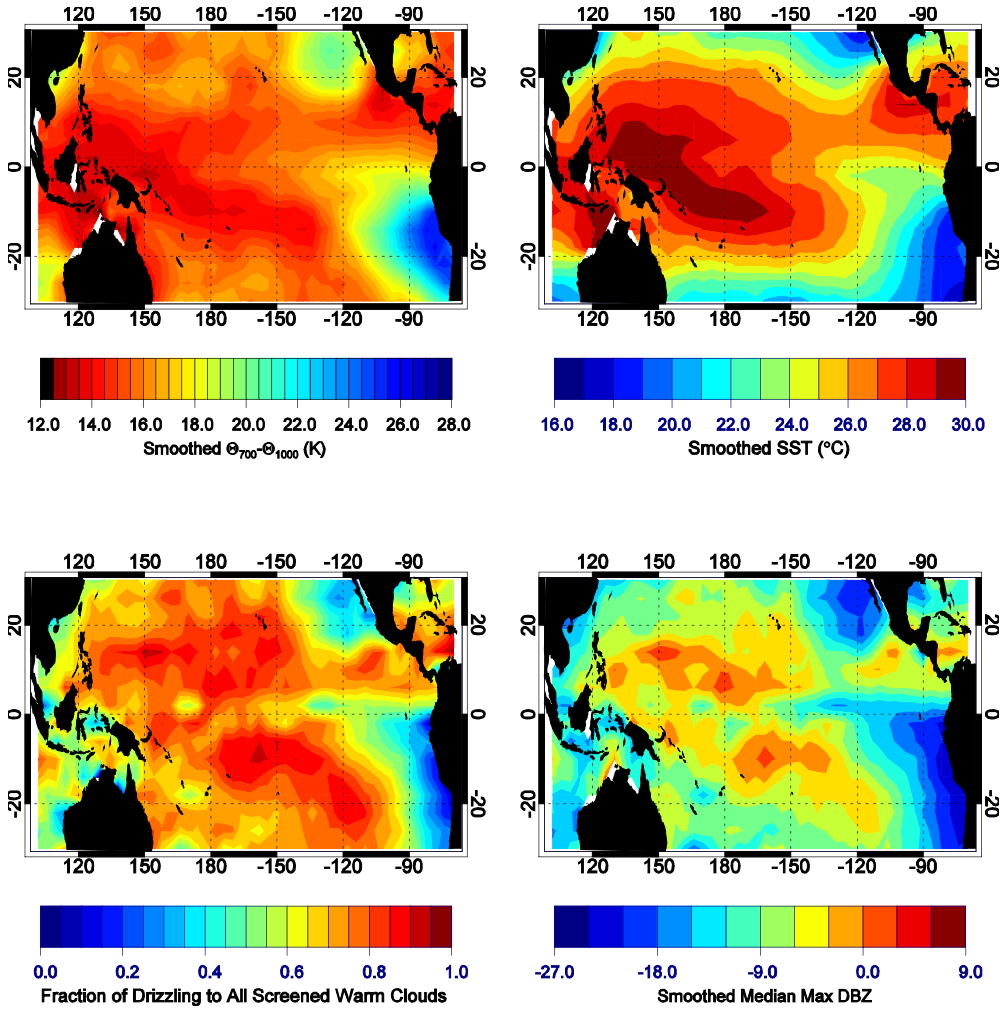

Fig. 4.3. (a) Smoothed 700mb-1000mb ΔΘ (K), (b) smoothed SST(°C), (c) fraction of drizzling to screened warm clouds, (d) median max dBZ.

longitude by 6° latitude boxes (larger boxes than in Fig. 4.2 to help ensure reasonable statistics). In most areas, drizzling clouds are deeper than nondrizzling clouds, and in some regions, especially in areas of frequent deep convection, this difference is more than one km. While the difference is positive almost everywhere, it is quite small particularly in regions where the mean cloud top height is shallow, such as the marine stratocumulus regions

(see Fig. 4.2a). In many of these areas, warm clouds are less likely to drizzle than not, and even when they do drizzle, drizzle rates are very weak. As we shall see later, cloud top heights tend to increase with dBZ, and where dBZ differences between drizzling and nondrizzling clouds are small, we would also expect cloud top height differences to be small.

The LWP of drizzling clouds is larger than the LWP of nondrizzling clouds everywhere, and the LWP difference is quite large everywhere, even in the aforementioned regions where the warm clouds are very shallow. This seems to suggest that the propensity to form drizzle is limited by the availability of cloud water, arguing for the importance of macrophysics to warm rain. It is interesting to note that in the far west Pacific (near and just south of the equator), the LWP of drizzling clouds is not all that different from the LWP of nondrizzling clouds. These are regions where the drizzling frequency is high, and the mean LWP is also high.

Figure 4.4c shows the difference of mean particle size of drizzling versus nondrizzling clouds. Generally, the r_e of drizzling clouds is several microns larger than that of nondrizzling clouds. Some increase in r_e would be

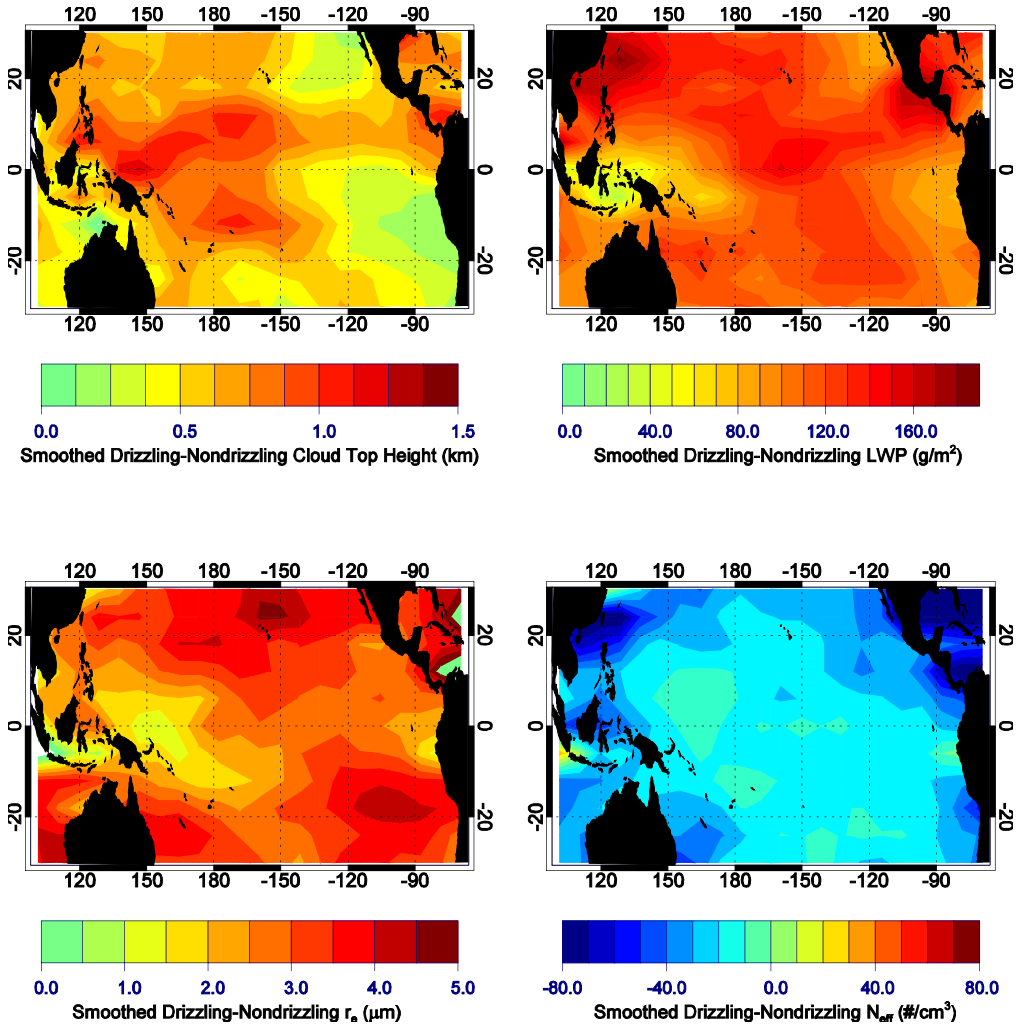

Fig. 4.4. Mean differences in drizzling and nondrizzling clouds for (a) cloud top height (km), (b) LWP (g m^{-2}), (c) r_e (μm), and d) N_{eff} (cm^{-3}).

expected by LWP alone, since deeper clouds allow more condensational growth. In some regions, namely around 20°S from about 120°W-90°W and also in regions near and poleward of 20°N, the difference approaches about 5 μm. The fact that r_e is almost always larger in drizzling clouds is consistent with the notion that since r_e represents the mean particle size near cloud top, a shift to larger droplets would imply that a larger percentage of droplets within

the entire distribution of the cloud would have a greater potential of growing to become drizzle or even rain drops, particularly since coalescence growth is more effective for larger drops.

Figure 4.4d shows the difference of N_{eff} of drizzling versus nondrizzling warm clouds. Drizzling clouds generally have somewhat lower concentrations, but in many regions, the differences are quite modest, on the order of only about 10-20 cm^{-3}. Exceptions to this include areas near the Asian Coast, the Gulf of Mexico, and also the northeastern Pacific near Baja California and Mexico where drizzling clouds have considerably lower droplet concentrations versus nondrizzling clouds. This may suggest that in regions of relatively high background number concentrations, warm rain formation effectively removes smaller droplets via collision and coalescence. Alternatively, lower number concentrations may be more conducive for drizzle, and in regions frequently impacted by higher concentrations, drizzling concentrations should be considerably lower.

We now have a sense that both cloud microphysics and macrophysics may be different in drizzling versus nondrizzling clouds, but we are also interested in the relative sensitivity of drizzle rate to both changes in LWP (macrophysics) and N_{eff} (microphysics) for the drizzling cloud population only. To quantify this, in each 9° longitude by 6° latitude box, we calculate the mean LWP and N_{eff} where the radar reflectivity is larger than the median drizzling reflectivity for each geographic box, and where the radar reflectivity is smaller

than the median drizzling reflectivity. For reference, we also present ΔdBZ as an indicator of how much the precipitation changes. Figure 4.5 gives us a sense of the fractional change in both LWP and N_{eff}, i.e. ΔLWP/LWP and $\Delta N_{eff}/N_{eff}$. The mean value of ΔLWP/LWP is 0.41. The values of ΔLWP/LWP tend to be particularly large in parts of the North Pacific, along the equator, and the southeastern Pacific. On the other hand, in Fig. 4.5b, which shows $\Delta N_{eff}/N_{eff}$, we see that fractional changes of droplet concentrations are quite small (mean value of -0.10). Larger negative values of $\Delta N_{eff}/N_{eff}$ are present over the Gulf of Mexico, the far northeast Pacific, and off the coast of Asia, which are also the areas that show larger N_{eff} differences between drizzling and nondrizzling clouds. These results suggest that changes in intensity of drizzle are much more sensitive to changes in LWP than to changes in N_{eff}. Alternatively, a cloud that is already precipitating has a considerably larger change in its liquid water than its droplet concentration as drizzle intensity increases. Thus, once drizzle has begun, the macrophysics may be more important for drizzle intensity.

4.5 PDFs of Cloud Top, LWP, r_e, and N_{eff} versus dBZ for Different Regions

Based on the aforementioned horizontal distribution of warm cloud characteristics, we divide the data into eight regions, which are illustrated in Fig. 4.6. These include the 1) Asian Coast, 2) Gulf of Mexico, 3) NE Pacific,

4) Far NE Pacific, 5) SE Pacific, 6) Far SE Pacific, 7) ITCZ and SPCZ, and 8) Equatorial Cold Tongue.

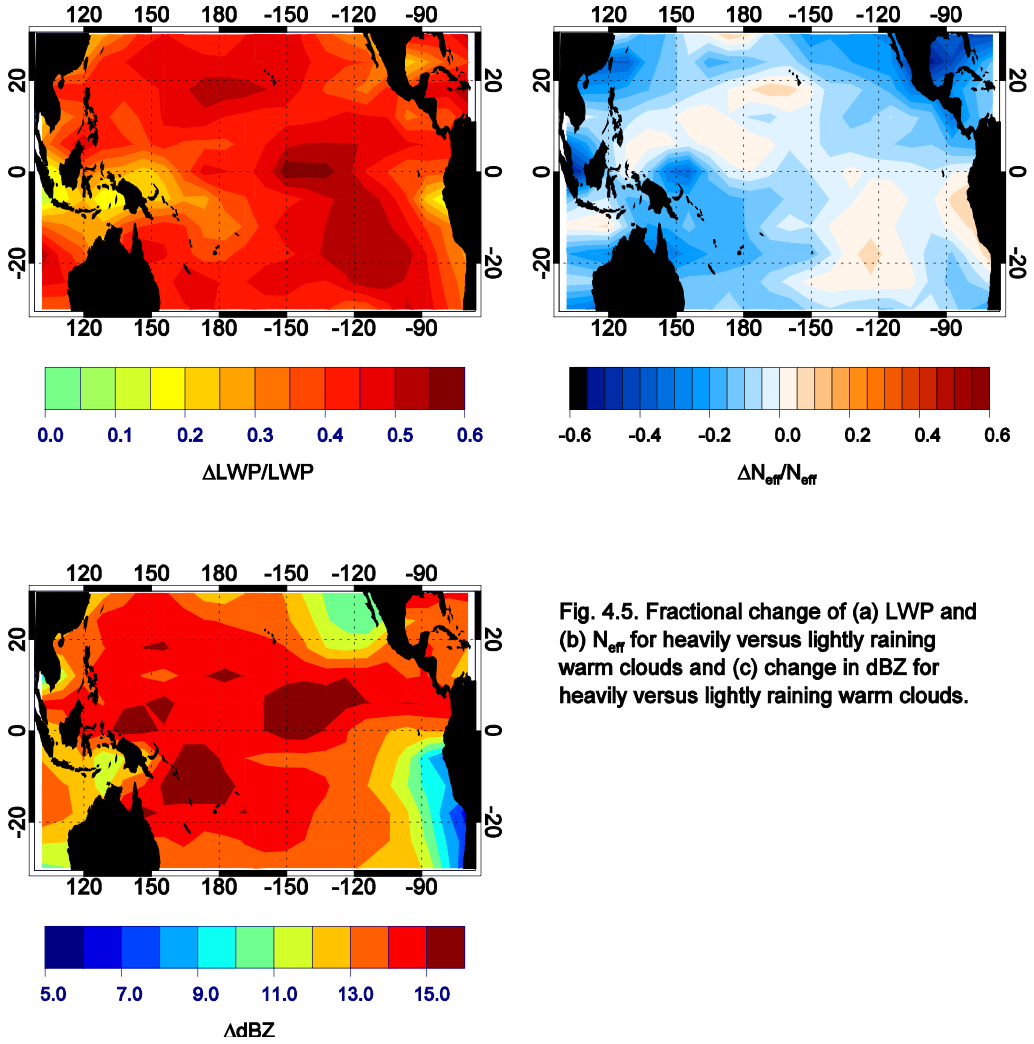

Fig. 4.5. Fractional change of (a) LWP and (b) N_{eff} for heavily versus lightly raining warm clouds and (c) change in dBZ for heavily versus lightly raining warm clouds.

To synthesize the information from the maps presented in Fig. 4.2 for each the eight regions, median values of cloud top height, LWP, r_e, and N_{eff} are presented in Table 4.1. The fraction of MODIS warm clouds that meet the aforementioned MODIS and CloudSat criteria is also shown in each of the regions. We also present various drizzling characteristics, including fraction of occurrence in which dBZ_{MAX} exceeds various dBZ thresholds, and median

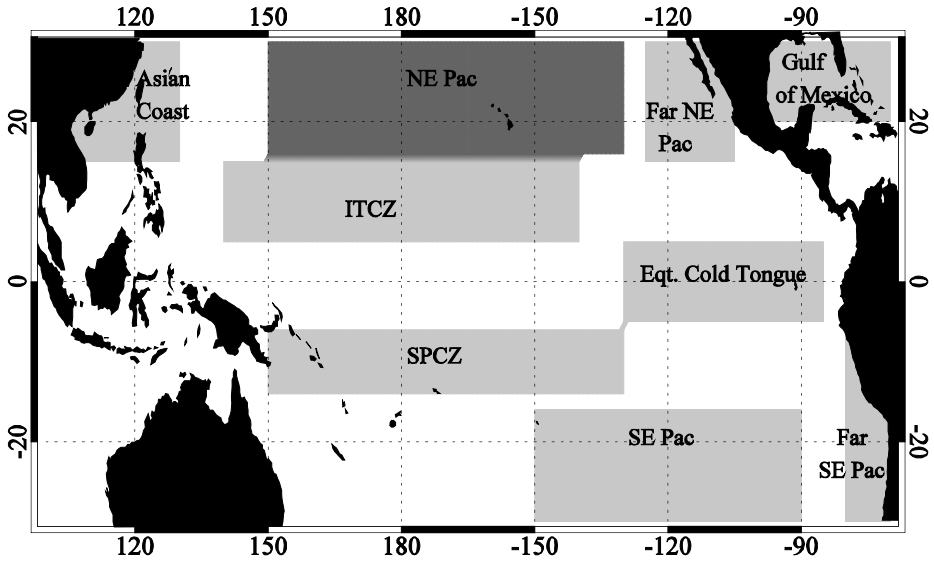

Fig. 4.6. Locations of eight regions. All pixels flagged by MODIS as coastal regions are excluded from analysis.

dBZ_{MAX} above various thresholds. The rationale of our choice of the eight regions becomes more evident from Table 4.1, including that the Asian Coast and Gulf of Mexico are characterized by considerably higher droplet concentrations, we think owing to the proximity of continental regions. Most of the open Pacific, on the other hand, is characterized by very low N_{eff}. Cloud droplet size in the SE Pacific, ITCZ and SPCZ, and NE Pacific is especially large. The Far SE Pacific and Far NE Pacific both have on average very shallow warm clouds, owing to frequent and strong low-level inversions there. In contrast, the ITCZ and SPCZ are characterized by deep warm clouds with a high drizzling frequency (83.7%) and high median dBZ (0.1).

Table 4.1. Parameters indicating the macrophysical and microphysical cloud properties and drizzle characteristics for each of the eight regions. **Bold** numbers represent the maximum value among all regions, and *italics* represent minimum values. All numerical values other than percentages represent median values for each region.

	NE Pac	Far NE Pac	Gulf of Mexico	Asian Coast	SE Pac	Far SE Pac	ITCZ/ SPCZ	Eqt. Cold Tongue
[%] of MODIS warm clouds that meet MODIS and CloudSat criteria	22.3	17.4	20.1	**31.1**	21.4	19.3	*15.0*	22.9
Cloud Top Height (km)	2.0	1.4	2.3	2.2	2.1	*1.3*	**2.7**	1.7
LWP (g m^{-2})	177	138	250	**263**	161	*108*	216	155
r_e (μm)	16.7	13.9	12.2	*11.5*	**18.0**	13.2	17.1	14.6
N_{eff} (cm^{-3})	44	71	127	**159**	*33*	72	44	61
[%] with dBZ > -15	69.7	38.1	63.9	61.9	72.5	*23.0*	**83.7**	55.7
[%] with dBZ > 0	27.5	7.4	27.7	26.9	28.4	*2.3*	**50.3**	18.6
[%] with dBZ > 7.5	11.2	2.0	10.8	9.9	10.6	*0.3*	**28.6**	7.0
dBZ for all clouds	-8.4	-18.4	-9.0	-10.1	-7.6	*-22*	**0.1**	-13.4
dBZ for dBZ>-15	-2.9	-8.1	-1.9	-1.8	-2.8	*-10.0*	**3.2**	-5.0
dBZ for dBZ>0	6.2	4.5	6.0	5.8	5.8	*3.4*	**8.5**	5.7

Based on geographical differences in meteorology and the macrophysical and microphysical differences in warm clouds, we wish to more closely examine how variables representing these change as a function of dBZ. To do this, nondrizzling clouds are first separated from drizzling clouds. Then,

the 25th, 50th, and 75th percentiles of reflectivity are determined in each region for the drizzling population only. This ensures an equal number of samples for a particular region in each drizzling category (0-25th, 25th-50th, 50-75th, 75th-100th), though because the drizzling frequency is quite variable from region to region, regions with a very low drizzling frequency (i.e. the Far SE Pacific) have many more samples in the nondrizzling category compared to each of the drizzling categories.

Figure 4.7 shows the SE Pacific PDFs of cloud top height, LWP, r_e, and N_{eff} for the aforementioned dBZ categories, and also for the nondrizzling population. We perform the calculations for all eight regions, but only show the SE Pacific in Fig. 4.7 and Asian Coast in Fig. 4.8, to illustrate differences in a remote, clean marine environment versus one influenced by continental aerosols and pollution. We also note that the SE Pacific looks similar to most of the other remote marine regions, particularly the ITCZ/SPCZ and NE Pacific, and that the Asian Coast is similar to the Gulf of Mexico.

In Fig. 4.7, we see that both the cloud top height and LWP peaks shift towards higher values as backscatter increases. The PDFs also tend to spread out with more drizzle. Increasing cloud top and LWP with reflectivity suggests, not surprisingly, that these two macrophysical quantities are quite related to one another, such that clouds grow vertically and thus contain more liquid water when more drizzle is produced.

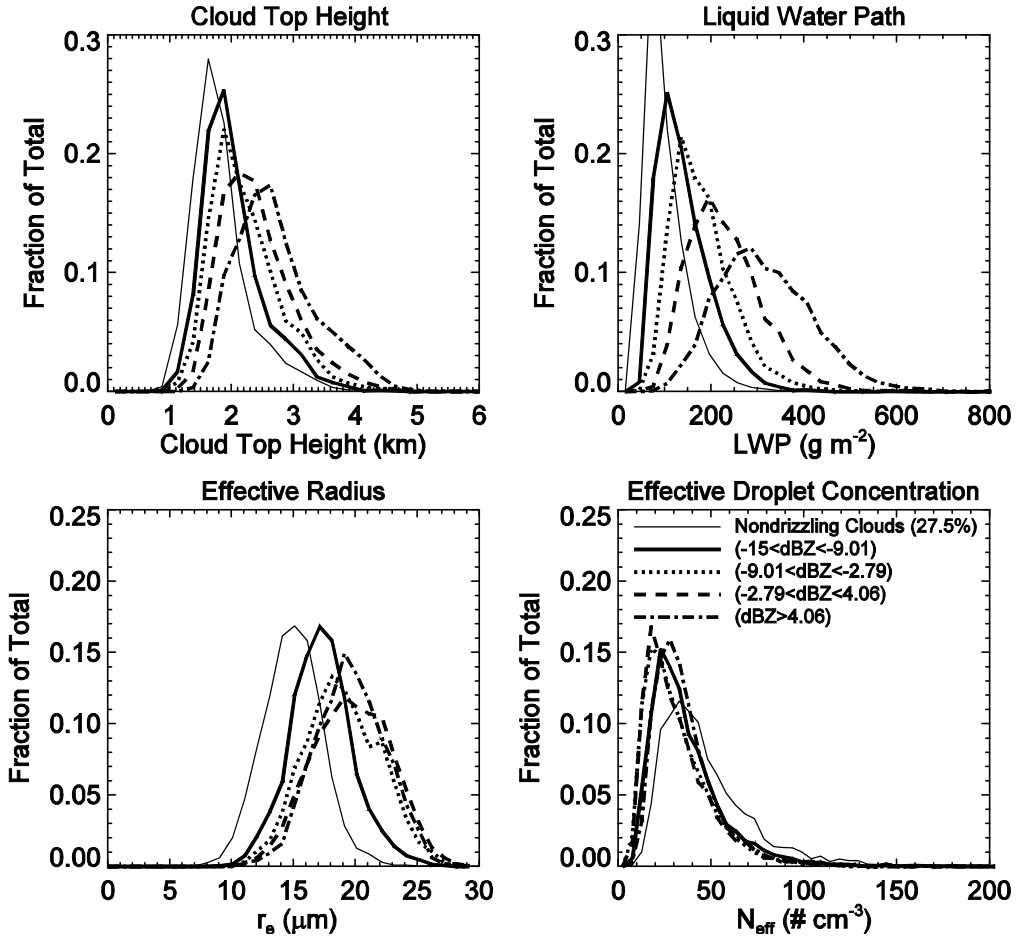

Fig. 4.7. PDFs of (a) cloud top height, (b) LWP, (c) r_e, and (d) N_{eff} for the SE Pacific for nondrizzling and drizzling dBZ quartiles. dBZ ranges for each drizzling category are given, as is the nondrizzling cloud frequency.

Turning to Fig. 4.7c, we see that the r_e peak increases from nondrizzling clouds to the lightest drizzling category, but then other r_e categories for stronger drizzle look similar to one another, peaking at a higher particle size than nondrizzling or very lightly drizzling clouds. This suggests that mean droplet size near cloud top is less related to amount of drizzle, especially if drizzle already is happening. Cloud top height and LWP appear to be more coupled with drizzle intensity than r_e or N_{eff}.

Finally, in Fig. 4.7d, we see that all the N_{eff} distributions look rather similar irrespective of dBZ, except that the nondrizzling population is shifted towards somewhat higher values. We will discuss this more thoroughly in upcoming sections, but it appears that the microphysical changes are more evident at the onset of drizzle than for changes in drizzle intensity. This suggests that increased r_e with drizzle is largely a result of greater vertical cloud development rather than changes in microphysics (N_{eff}) per se.

Figure 4.8 shows analogous PDFs, but for the Asian Coast. It is apparent that cloud top height and LWP both increase with dBZ. One difference, however, is that a large number of clouds have LWP values that surpass 600 gm^{-2}, especially for the two highest dBZ categories. Also, the LWP distributions tend to be less peaked for the Asian Coast, especially as dBZ increases. Particle size, while certainly increasing with dBZ, tends to be much smaller near the Asian Coast compared to the SE Pacific. Distributions of N_{eff} reveal great variability for the Asian Coast, and many clouds have much larger droplet concentrations than the SE Pacific, with many concentrations surpassing 400 cm^{-3}. Smaller particle sizes and higher concentrations are likely because of the continental aerosol influence in this region. The highest drizzling category has a peak at lower concentrations, which may suggest either that heavy drizzle removes a large number of smaller particles, or perhaps that a lower droplet concentration simply increases precipitation. We will explore these notions more in depth in the coming sections.

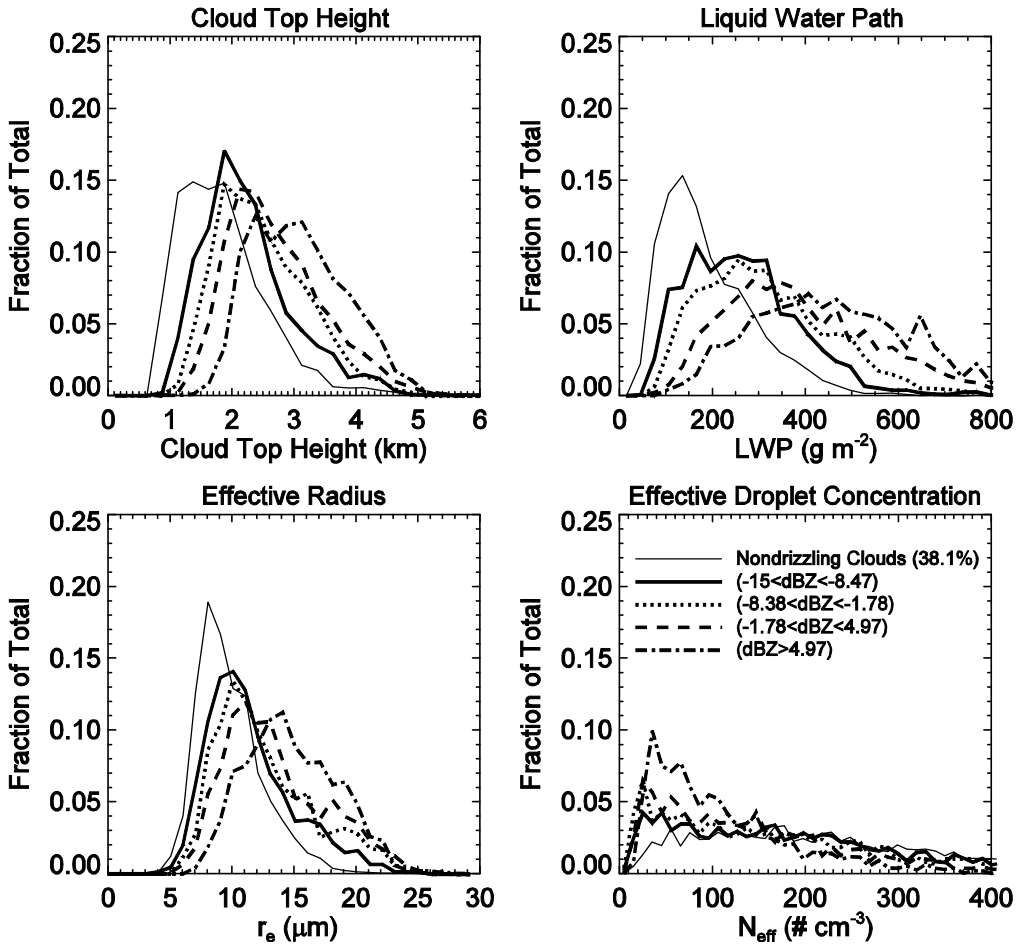

Fig. 4.8. Same as Fig. 4.7, except now for the Asian Coast.

4.6 DBZ Relationships for Different Regions

We now wish to synthesize the pertinent information from the PDFs presented in the previous section, to better understand how universal cloud macro- or microphysics relationships are as a function of drizzle. By examining the median values, we can also more easily compare all eight regions.

Figure 4.9 presents median cloud top height and LWP versus maximum dBZ for each of the eight regions. The reflectivity categories have been chosen as described in the previous section. The drizzling frequency is indicated in the legend of Fig. 4.9a, which is highest in the ITCZ and SPCZ at 84.3%, and lowest in the Far SE Pacific at only 23%. 95% confidence intervals are also shown, though we only show them for two regions with the expected largest intervals, namely the Far SE Pacific, because of its low drizzling frequency and thus smaller drizzling sample size, and also the Gulf of Mexico, which contains quite a lot of microphysical variability owing perhaps to its proximity to continental aerosols. We note that the confidence intervals even in these regions are narrow, so that curves separated visually are statistically distinct as well.

Figure 4.9a shows that cloud top height increases as radar reflectivity increases, though there are certainly height differences among the different regions. When the reflectivity exceeds -15 dBZ, the reflectivity is linearly proportional to drizzle rate (i.e. see Comstock et al. (2004) for Z-R relationships), and thus we can consider the x-axis as such. In the deep convective regions (ITCZ and SPCZ), warm clouds are approximately one km deeper for a given dBZ compared to the greatly suppressed Far SE Pacific. We also note that median cloud tops grow to ~3.5 km in the ITCZ and SPCZ for large dBZ values, certainly suggestive of the convective nature of some of

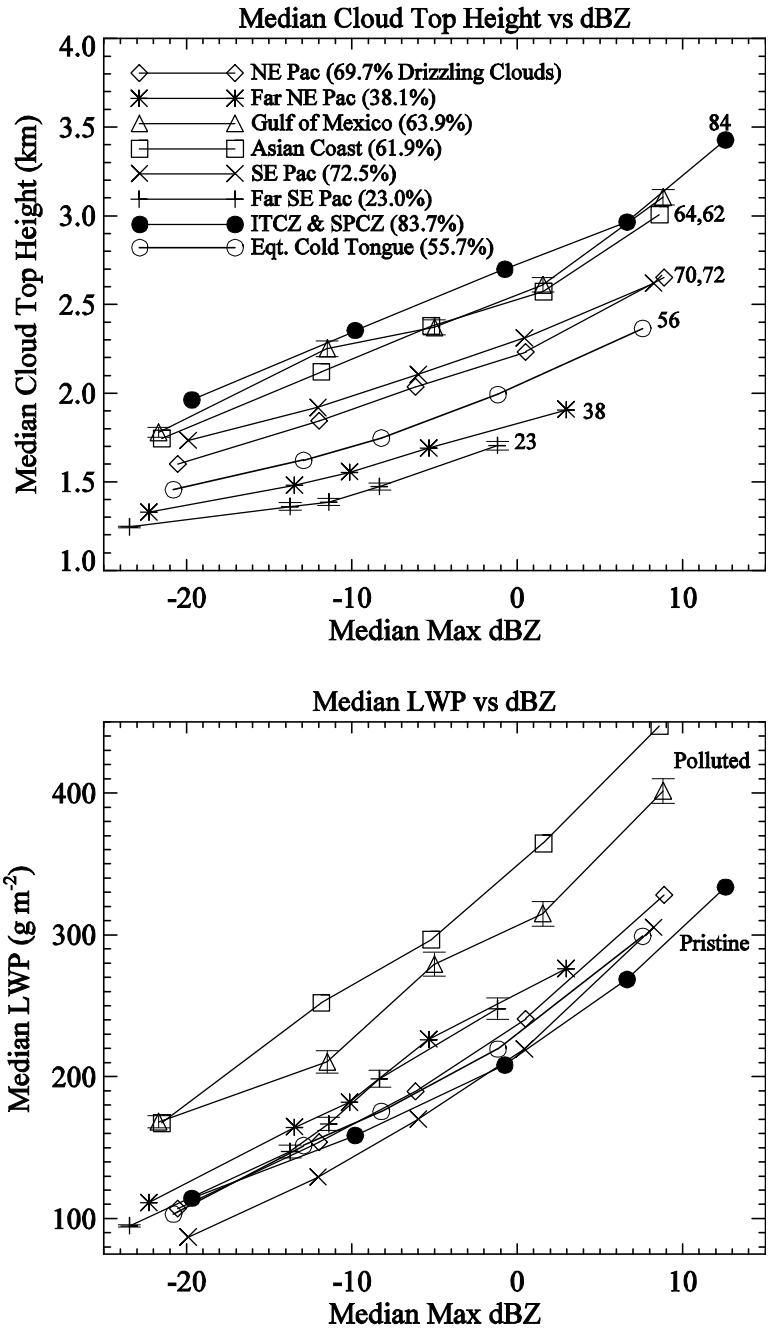

Fig. 4.9. (a) Median cloud top height, and (b) Median LWP versus median maximum dBZ for each of the eight regions. In (a), numbers/percentages indicate frequency of drizzling warm clouds in each region. 95% confidence intervals are shown for Gulf of Mexico and Far SE Pacific.

these deeper warm clouds. In the previous chapter, we also saw a strong increase of precipitation rate with cloud top height, particularly for deep convective clouds. Similarly, we see that thicker warm clouds tend to be associated with greater drizzle. Cloud top height alone, however, is not a good predictor of drizzle intensity, as the relationships are quite different among the regions.

Figure 4.9b clearly shows that LWP increases in all regions with dBZ. Some regions, such as the ITCZ and SPCZ and NE Pacific, show over a threefold increase in LWP for nondrizzling clouds to the most heavily drizzling clouds, from about 100 gm^{-2} to over 300 gm^{-2}. The Asian Coast and Gulf of Mexico stand out as having a considerably larger LWP for a given drizzle intensity compared to all the other regions, suggesting that more liquid water is needed in these regions, which have smaller mean radii and larger droplet concentrations, to produce a given amount of drizzle. This may be because there is a greater microphysical barrier to overcome. This may be indicative of the part of the Albrecht effect that large droplet concentrations inhibit drizzle.

Figure 4.10 is analogous to Fig. 4.9, except for mean r_e and N_{eff}. Particle size increases with dBZ, though certainly significant differences exist among different regions, suggesting that r_e alone is not a particularly useful indicator of drizzle intensity. The SE Pacific, for instance, stands out as having the largest droplet size for a given dBZ, and in fact r_e is 5-8 μm larger for a given amount of drizzle in the SE Pacific compared to the Asian Coast.

Most regions tend to show a fairly sharp increase of r_e with dBZ, followed by a leveling off towards higher reflectivity values, particularly as $dBZ_{MAX}>0$. This suggests that the particle size near cloud top becomes less important a determining factor of drizzle intensity than does the integrated cloud liquid. The leveling off of r_e with reflectivity is not seen for either the Asian Coast or Gulf of Mexico, and in fact mean r_e increases by 6 μm for nondrizzling warm clouds to the most heavily drizzling ones over the Gulf of Mexico.

Figure 4.10b shows the N_{eff}-dBZ relationships for all eight regions, and similar to the r_e-dBZ curves, the Asian Coast and Gulf of Mexico stand out as unique regions with N_{eff} strongly decreasing with increasing dBZ. As we might expect from the maps presented earlier, nondrizzling clouds near both the Asian Coast and over the Gulf of Mexico have much higher number concentrations (more than 100 cm^{-3} larger than the other regions), highlighting perhaps the much higher concentrations expected in areas influenced by continental aerosols compared to remote marine regions. We also observe that aside from the Asian Coast and Gulf of Mexico, N_{eff} changes very little with dBZ, especially once clouds are drizzling. If we consider the N_{eff} relationship from (3), in which $N_{eff}\sim LWP^{1/2}r_e^{-3}$, then N_{eff} changes will be more heavily weighted by changes in particle size. Despite the sharp increase of LWP with dBZ in all areas, the relative r_e-dBZ increase at both the Asian Coast and Gulf of Mexico is much greater compared to the other regions. As dBZ approaches 10, r_e and N_{eff} in the polluted regions approach values in cleaner regions. In

much of the tropics and subtropics well-removed from continental aerosols, the microphysics has perhaps some effect in determining the likelihood of drizzle, but very little impact, if any, in regulating drizzle intensity. We shall investigate the sensitivity of drizzle probability to macrophysics and microphysics more closely in the next section. Warm cloud microphysics tend to play a much greater role in determining drizzle intensity for both the Asian Coast and Gulf of Mexico.

4.7 Drizzle Probability

We attempt now to examine the drizzle probability as a function of cloud top, LWP, r_e, and N_{eff}. While an objective is to isolate the importance of each of these variables in quantifying how they relate to drizzle, this is not truly feasible with this construct, given the lack of independence among these four variables. Nonetheless, understanding drizzle probability as a function of each variable sheds additional insight on processes that may control warm rain.

Figure 4.11 contains four panels that show the frequency of drizzling clouds for cloud top, LWP, r_e, and N_{eff} categories. The five categories for each region include the 0-20th, 20th-40th, 40th-60th, 60th-80th, and 80th-100th percentiles for each variable, and the frequency is simply the number of drizzling profiles divided by the total number of screened warm cloud profiles

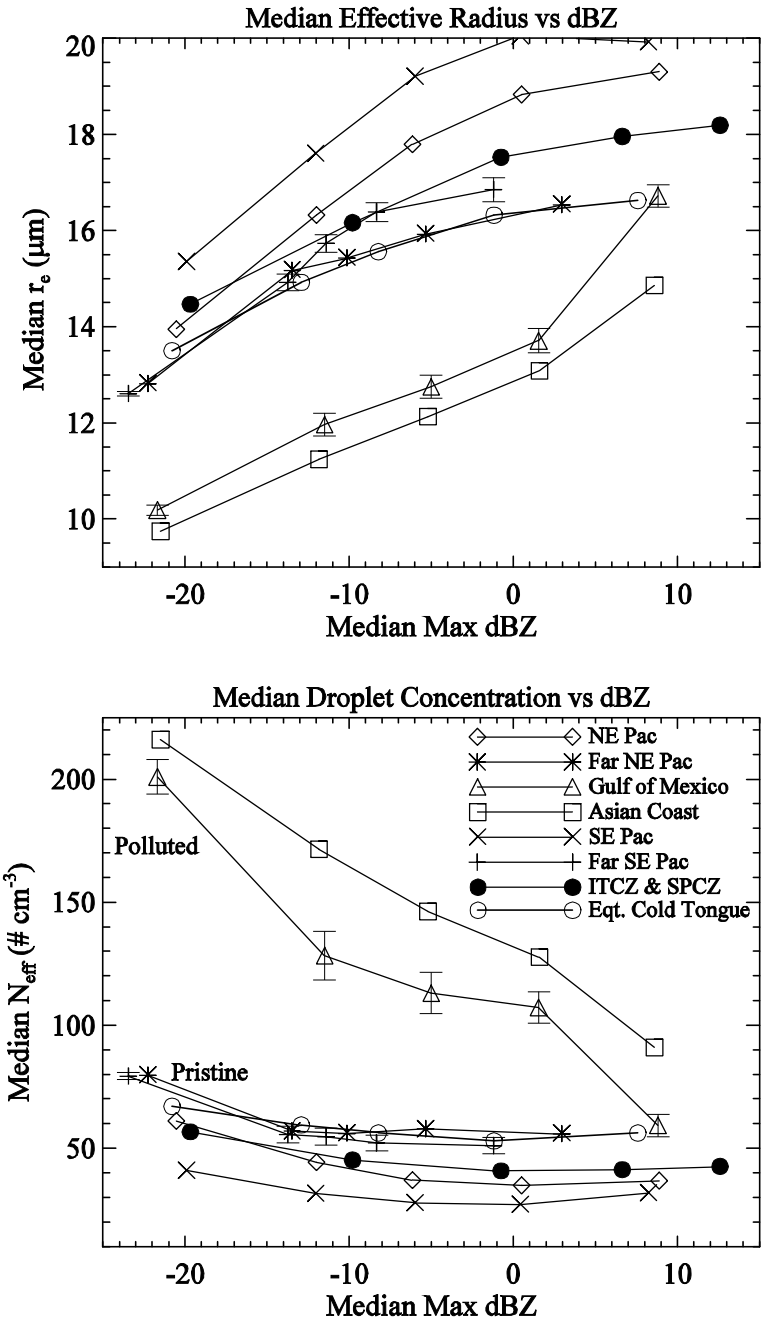

Fig. 4.10. Same as Fig. 4.9, except now for r_e and N_{eff}.

that are bounded by each category. This method ensures an equal number of samples for a particular region for each of the five categories. As an example for the equatorial cold tongue, 59% of warm clouds are drizzling when the LWP is between 132 and 181 gm^{-2} (median value of 155 gm^{-2}), but 92% are drizzling when the LWP>251 gm^{-2} (median value of 80^{th}-100^{th} LWP percentiles is 314 gm^{-2}). We also show 95% confidence intervals once again for only the Far SE Pacific and Gulf of Mexico, in which the standard error is given by $\sqrt{p(1-p)/N}$, where p in this case is the probability of drizzle, and N the total number of profiles within a given variable range (i.e. LWP).

Starting with Fig. 4.11a, we see that drizzle frequency increases dramatically with cloud top height in all areas, and in fact the relationship appears to be very tight, particularly when cloud top height is less than two km. In regions where cloud tops are higher than two km, the frequency of drizzle is greater than 80% in most regions, except for the Asian Coast, Gulf of Mexico, and equatorial cold tongue, where values are slightly lower. As cloud tops ascend to over three km, the probability of drizzle is between 90-100% in regions where clouds can get this high. Cloud top height alone thus reveals much information about drizzle frequency, consistent with Stephens et al. (2008).

The drizzle frequency plot versus LWP looks fairly similar to that of cloud top, in that drizzle frequency increases dramatically with LWP, though there is somewhat more spread among the different regions. For example,

clouds with a much higher LWP of ~350 gm^{-2} for the Asian Coast and Gulf of Mexico compared to the LWP over the ITCZ and SPCZ, NE Pacific, and SE Pacific (~150 gm^{-2}) have the same drizzle frequency of about 0.8. Even though we are now looking at whether or not a cloud will drizzle, as opposed to the drizzle rate as in the previous section, clouds near the Asian Coast and over the Gulf of Mexico contain more liquid water for the same drizzle frequency as other regions.

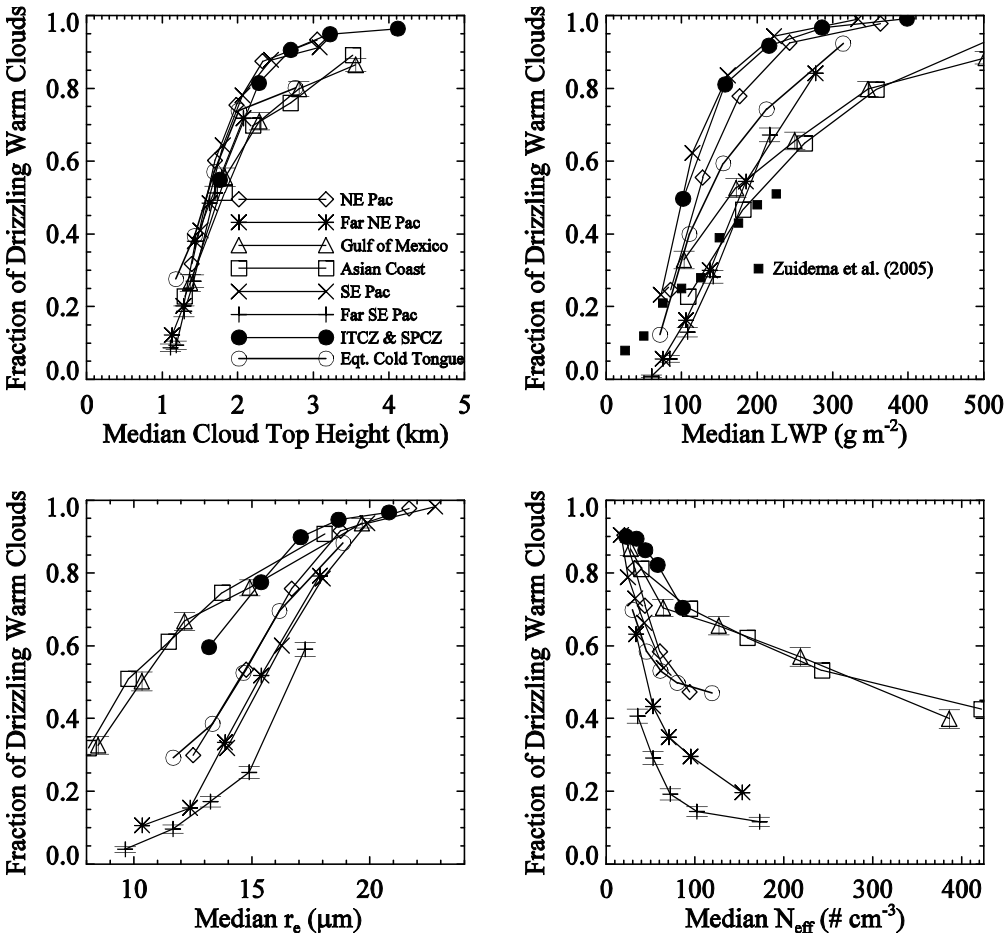

Fig. 4.11. Fraction of drizzling clouds for each region versus (a) cloud top height, (b) LWP, (c) r_e, and (d) N_{eff}. As in Fig. 4.9 and and Fig. 4.10, 95% confidence intervals shown for Gulf of Mexico and Far SE Pacific. In (b), results shown from Zuidema et al. (2005) at 20°S, 85°W.

The range of drizzle frequency versus LWP is impressive for the equatorial cold tongue, starting at only 0.12 for LWP<100 gm^{-2} and increasing to 0.92 when LWP>300 gm^{-2}, indicative of the importance of LWP and drizzle formation there. Also noteworthy is the Far SE Pacific, whose overall drizzle frequency is 0.23, where the drizzle frequency ranges from 0.0 for LWP~50 gm^{-2} to 0.67 as LWP approaches 200 gm^{-2}. Drizzle frequency versus LWP from Zuidema et al. (2005) (with drizzle defined as dBZ_{MAX}>-17 in that study) near 20°S, 85°W, an area within our Far SE Pacific, is also shown in Fig. 4.11b. Drizzle frequencies are similar to the Far SE Pacific, although somewhat lower particularly for higher LWPs. In our study, drizzle becomes much more likely even in the Far SE Pacific for more favorable macrophysical conditions, but those conditions happen rather seldom, especially compared to most of our other regions. The macrophysics alone can thus very much be a limiting factor in whether or not a cloud will rain.

Figure 4.11c shows the drizzle frequency versus r_e, and as we might expect, drizzle becomes more common with increasing droplet radius. Since there is quite a lot of variability in r_e for our selected regions, however, it is not surprising to see the amount of spread in the curves. For instance, warm clouds with smaller r_e by several μm near the Asian Coast and over the Gulf of Mexico tend to drizzle as frequently as clouds in other regions. As mean droplet size near cloud top gets larger, especially above 18 μm, warm clouds in

all regions are very likely to be drizzling (>0.9 frequency). It is also interesting to note that for a given r_e, variability in drizzle frequency seems to be related to LWP variability. For instance, for an r_e of 15 μm, the drizzling frequency in the Far SE Pacific is only about 0.25, a region where LWPs are lowest, compared to a drizzling frequency of 0.7 for the Asian Coast, Gulf of Mexico, and ITCZ/SPCZ for the same r_e, where median LWPs are over twice as large (refer to Table 4.1).

Figure 4.11d shows the drizzle frequency versus N_{eff}, and generally the probability of drizzle decreases with increasing droplet concentration. However, the range in drizzle frequency as a function of N_{eff} tends to be smaller for any particular region, indicating that microphysics alone is not as important as a factor as the cloud top height or LWP in controlling growth into drizzle-sized drops. In the ITCZ and SPCZ, for instance, drizzle frequency decreases only from 0.9 to 0.7 across the entire droplet concentration spectrum in those regions, compared to the drizzle frequency of 0.5 for small LWP to nearly 1.0 for large LWPs in that region. While drizzle frequency tends to decrease as N_{eff} increases, the microphysics seems somewhat less important compared to cloud thickness or LWP for drizzle probability.

4.8 Macrophysical Versus Microphysical Controls on Drizzle Frequency

Instead of trying to isolate the effect of individual variables on the likelihood that a nonfreezing cloud will drizzle, we now combine a macrophysical quantity (LWP) with a microphysical variable (N_{eff}) to better

understand which conditions provide the most favorable conditions for drizzle. We can also make a better attempt to hold either the cloud microphysics or macrophysics constant in order to determine the extent to which we see at least part of the Albrecht (1989) effect, which suggests that regions of low CCN tend to provide more favorable environments for drizzle formation for a given cloud thickness or LWP.

To accomplish this, we have produced contour plots of drizzle frequency as a function of both N_{eff} and LWP for each of the eight areas. Ten deciles of both N_{eff} and LWP are first computed, and then the drizzle frequency is calculated in each of the 100 categories. The fact that we use two simultaneous variables for the categories precludes an equal number of observations in each bin, but this is unavoidable for this exercise.

Figure 4.12 shows contour plots of drizzle frequency versus N_{eff} and LWP for all eight regions, and also for the entire domain. The contour lines are labeled accordingly, and each line is a 10% change in drizzle frequency, ranging from 0-100%. Coincidentally, the top three contour plots are regions of low N_{eff} regions (NE Pacific, SE Pacific, and ITCZ/SPCZ), the middle three moderate N_{eff} regions (Far NE Pacific, Far SE Pacific, Equatorial Cold Tongue), and the bottom ones high N_{eff} regions (Gulf of Mexico, Asian Coast). In all regions, we see that as N_{eff} is held constant, drizzle frequency steadily increases with LWP. Additionally, as LWP is held constant, the likelihood of drizzle tends to decrease with increasing N_{eff}, which is thus consistent with part

of the Albrecht (1989) effect. Unfortunately, with our satellite-borne observing system, we *cannot* assess whether or not cloud lifetime or fractional cloudiness changes with changes in N_{eff}. As LWP becomes sufficiently large in any region, the higher droplet concentration is less an inhibiting factor, and drizzle frequency becomes greater than 90%. It is also interesting that in the Far SE Pacific, which is a region where warm clouds on average seldom drizzle, drizzle frequency can still be very likely (>90%) if N_{eff} is small enough (<50 cm^{-3}) and LWP is large enough (>200 gm^{-2}). The fact that the 90% contour is seen in all regions gives a sense of universality of drizzle sensitivity to both the macrophysics and microphysics. Qualitatively, warm clouds with high liquid water and lower number concentration are most likely to drizzle in any region.

Some other characteristics about Fig. 4.12 are worth mentioning for clarity. Save for the Asian Coast, Gulf of Mexico, and entire domain, we have maintained the same x- and y-axes, so that the contoured regions provide a sense of the actual range of both LWP and N_{eff} for a particular region. The Asian Coast and Gulf of Mexico have a much larger N_{eff} range. For instance, the contour of drizzle frequency rarely surpasses N_{eff} values of 80 cm^{-3} in the SE Pacific, and the 9th N_{eff} decile is only 65 cm^{-3}, illustrative of a remote marine environment well-removed from continental aerosols and pollution, whereas in the Gulf of Mexico the 9th N_{eff} decile is 386 cm^{-3}, and N_{eff} can surpass 600 cm^{-3} (2.3% of the time). Also, the LWP in the Far SE Pacific only

exceeds 300 gm^{-2} about 3% of the time, but does so 38% of the time over the Gulf of Mexico. We get a sense that regions characterized by different N_{eff} regimes look rather similar to one another (i.e. the NE Pacific, SE Pacific, and ITCZ/SPCZ). The moderate N_{eff} regimes (middle row of Fig. 4.12) tend to have a smaller LWP range than other regimes, while the Gulf of Mexico and

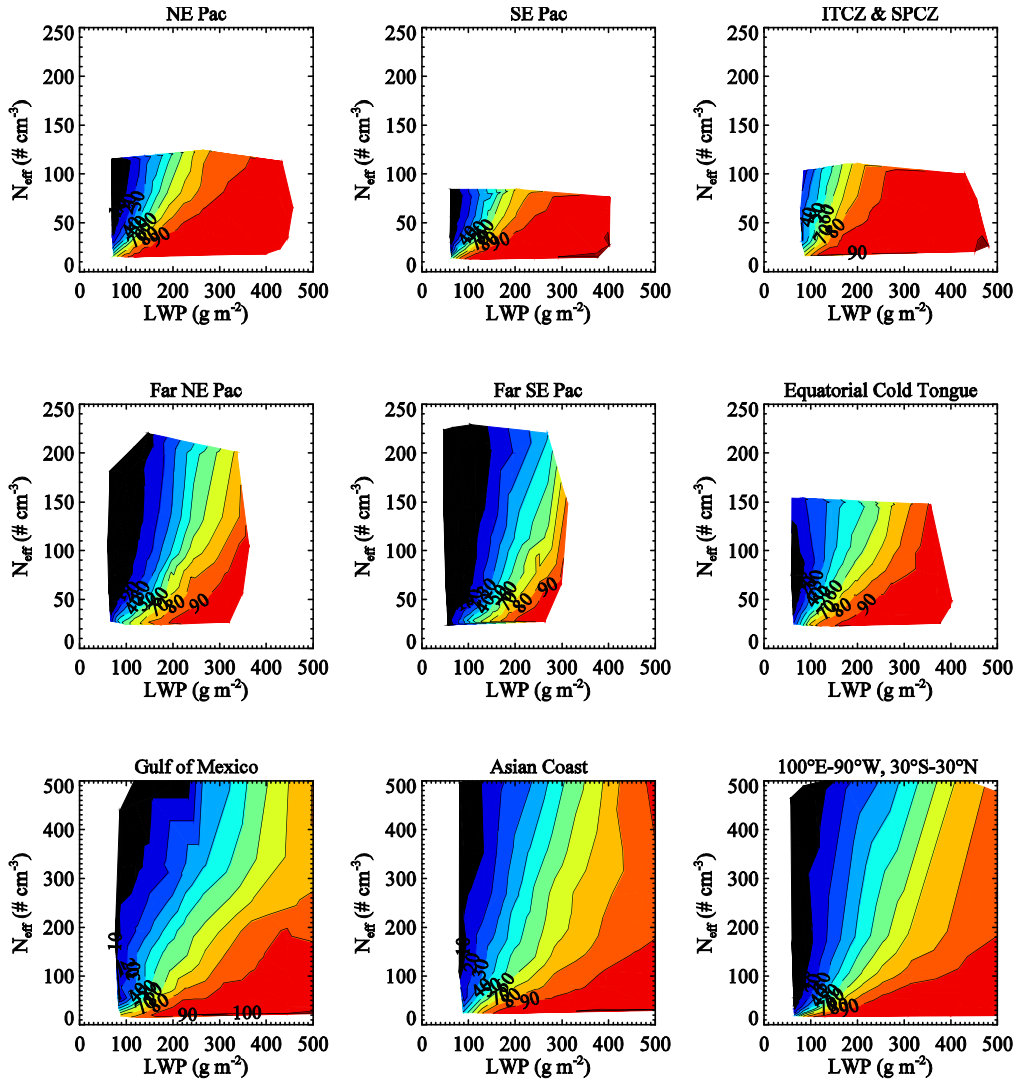

Fig. 4.12. Contours of drizzle frequency in % (from 0-100%) as a function of N_{eff} and LWP for (a) NE Pac, (b) SE Pac, (c) ITCZ and SPCZ, (d) Equatorial cold tongue, (e) Far NE Pac, (f) far SE Pac, (g) Gulf of Mexico, (h) Asian Coast, (i) entire domain.

Asian Coast have very large ranges of both LWP and N_{eff}.

Finally, even though the total drizzle frequency for a particular region can be recovered by taking the mean of all contours, the visual area of the 90% contour in a particular region provides a good sense of the drizzle frequency. This 90% contour spans a very large area in the ITCZ and SPCZ, a region where the vast majority of the screened clouds drizzle (84%), but the 90% contour only spans a tiny portion of the Far SE Pacific, where drizzle frequency of screened clouds is only 23%. The fact that the relationship between drizzle frequency, LWP, and N_{eff} is essentially the same for all regions suggests a near universality among tropical and subtropical regions. In a given location, the distribution of LWP and N_{eff} is sufficient to predict overall drizzle frequency.

4.9 Summary/Conclusions

This study has exploited a unique opportunity to utilize collocated passive radiometer optical parameter retrievals from MODIS with CloudSat radar reflectivity measurements from the A-Train system to better understand and characterize the macrophysical and microphysical factors of warm marine clouds associated with precipitation across a large part of the tropics and subtropics. We have seen that macrophysical variables cloud top height and LWP are closely related, which is expected if cloud base is nearly constant. Maps of r_e and N_{eff} demonstrate that these two variables are strongly negatively correlated, and while warm cloud r_e is generally large and N_{eff} is small across

the remote marine areas, droplets are smaller and concentrations much larger where continental aerosol influences become more likely, such as off the Asian Coast, over the Gulf of Mexico, and in close proximity to the western South American Coast and near Baja California in the Far NE Pacific. Cloud top height and LWP both tend to mirror the lower tropospheric stability rather well, with strong capping temperature inversions having the impact of restricting vertical cloud growth. Static stability is high and cloud tops shallow in the Far SE Pacific and Far NE Pacific, and to a lesser extent along the Equatorial Cold Tongue. Shallow warm clouds also drizzle much less frequently than deeper warm clouds.

This study also examines macrophysical/microphysical-dBZ relationships for eight separate tropical and subtropical regions. When the maximum reflectivity in a profile is larger than -15 dBZ, drizzle drops are present in the cloud, and reflectivity values above this threshold are proportional to drizzle intensity. Cloud top height and LWP increase substantially as drizzle intensity increases in all areas, though for a given intensity, substantially more cloud liquid water is present both near the Asian Coast and over the Gulf of Mexico. These two regions also stand out as having much higher values of N_{eff} for a given dBZ, although concentrations rapidly decrease with drizzle intensity. It thus seems that drizzle intensity is more sensitive to N_{eff} when the microphysical variability in a particular region is large. In remote marine regions, the N_{eff} range is quite small, and while it

plays a role in the likelihood of drizzle, it is much less important in controlling drizzle amount. Droplet radius also tends to level off as dBZ>0 in most regions, though the increase in droplet size is monotonic with dBZ over the Asian Coast and the Gulf of Mexico, the more polluted of the eight regions.

Also, while drizzle frequency tends to be somewhat sensitive to $N_{eff,}$ drizzle intensity and N_{eff} are only weakly related, except in regions such as the Asian Coast and Gulf of Mexico, where large background concentrations are present, and N_{eff} sharply decreases as drizzle intensity increases. It may be that the microphysics is important for drizzle rate when transitioning from a high $N_{eff,}$ high LWP regime to lower $N_{eff.}$ When N_{eff} is fairly low to begin with, a droplet concentration reduction may only have little influence on drizzle intensity.

This study also examines the controlling mechanisms behind drizzle frequency. Cloud top height appears to be the best single variable in any region in explaining the likelihood of drizzle-sized drops. Cloud LWP is also a good predictor of drizzle probability, though relationships are slightly less tight than cloud top height among the eight different regions. When drizzle frequency is calculated as a function of both LWP and $N_{eff,}$ drizzle probability is very likely (greater than 90%) when LWP is high and N_{eff} is low, and this is even seen in regions where overall drizzle frequency is very low, such as the Far SE Pacific. While drizzle frequency contours are slightly different in the different regions due to static stability and cloud top height differences, these

results reflect the macro- and microphysical conditions most favorable for warm rain initiation.

Chapter 5: Conclusions

We examined the vertical structure of clouds using MODIS (Chapter 2) and CloudSat (Chapter 3) across the ITCZ. Both instruments reveal the dominance of two primary modes, namely upper tropospheric clouds centered near 220 K (13-14 km) and shallow clouds with tops near the trade inversion. A secondary mode of congestus clouds, with tops generally above the 273 K level, or between about 6-8 km, is more populous in the EP, but is also present in the central and western ITCZ. Beyond these general features, in Chapter 2 we quantified the variability of horizontal extent and vertical depth of clouds across different dynamic and thermodynamic regimes of the ITCZ. In the WP, where SSTs are highest and SST gradients are smallest, both high thin and anvil clouds are much more pervasive per unit rain rate compared to the EP, where SSTs are lower and SST gradients larger. The presence of more high thin cloud in the WP is radiatively important, as high thin clouds have a net TOA warming effect. The combination of more high thin clouds and fewer congestus and boundary layer clouds in the WP make the net cloud forcing considerably less negative compared to the EP.

We also have found that thick high-topped cloud increases at the same rate across the ITCZ with increasing rain rate, which makes this cloud type a good proxy for rain rate over oceans. We also find that the high-topped cloud forcing becomes more negative with increasing rain rate, a result of more anvil and thick cloud fraction with precipitation, though it is *less* negative for a

given rain rate in the WP. This suggests that near convective core regions, thin anvil and high cirrus cloud are more pervasive in the WP compared to the EP. We speculated that this may be partly because the WP has a moister upper troposphere, allowing for more sustainable thin cloud spatially and temporally away from heavily precipitating regions (see Zelinka and Hartmann (2008) for similar findings).

We also showed in Chapter 2 that thin and anvil cloud top temperatures are rather insensitive to rain rate, though they are approximately 5 K colder in the WP versus the EP. On the other hand, thick high-topped clouds tend to penetrate deeper into the upper troposphere as precipitation rate increases. This seems to suggest the height of thick high-topped clouds is more fundamentally related to convective strength, with more intense storms ascending higher into the upper troposphere. We quantified the extent to which thick high-topped clouds are convectively driven by calculating the temperature corresponding to the level of neutral buoyancy across the ITCZ and comparing this to both the median and highest (90^{th} percentile) thick high-topped cloud top temperatures. The level of neutral buoyancy, which is directly related to the near-surface Θ_E, is statistically correlated with temperatures of the thickest, coldest clouds, suggesting the role of the surface in driving convective cores.

Since both anvil and thin cloud top temperature are nearly independent of rain rate, and are much warmer than the level of neutral buoyancy, we

suggested that radiative processes in the upper troposphere are more fundamentally related to temperature of anvil clouds. A circulation, in which upper-tropospheric clear-sky convergence drives convective area-divergence, is driven by the sharp decline in effective clear-sky longwave cooling by water vapor where temperatures are sufficiently low. Upper-tropospheric temperature and humidity profiles determine the level at which clear-sky convergence peaks in a particular region, and this occurs at a temperature about 4 K colder in the WP versus the EP. We computed seasonal convergence-weighted temperatures and median anvil temperatures across the ITCZ, and we quantified a robust relationship between anvil median temperature and peak in clear-sky convergence. The large-scale dynamics and thermodynamics thus appear to be important for driving the detrainment level of anvil clouds in the ITCZ.

In Chapter 3, we used an active cloud radar to explore how the vertical structure of convective clouds in the WP and EP is related to precipitation. An advantage of a cloud radar is its ability to see multiple cloud layers in a column. Cloud radar profiles corroborate some general features as retrieved from MODIS, namely that heavily raining deep clouds peak at higher levels compared to moderately or non-precipitating high-topped clouds. Heavily raining clouds are also generally characterized by a single deep mode, whereas moderately and non-precipitating clouds clearly have a shallow mode in both regions and a secondary congestus mode in the EP. The more active congestus

mode in the EP is probably related to stronger surface convergence and a more bottom-heavy vertical velocity profile as compared to the WP in which the rising motion peaks in the upper troposphere.

A minimum in cloud tops is apparent at 9.5 km, and clouds above this level become increasingly more likely in both regions as rain rate increases, although they become more likely for a given rain rate in the WP. The probability of high-topped clouds overlying low and middle clouds is about 30% and is independent of rain rate when rain rates are less than 3 mm hr^{-1}, but then multilayered clouds become less likely for heavier rain rates. This suggests that multi-layered clouds are important for mean precipitation.

We also showed that as clouds grow vertically, they tend to precipitate more heavily. This is particularly the case for clouds taller than 12 km, though for a given cloud top height, deep clouds rain more heavily in the EP. A given cloud thickness thus more efficiently rains in the EP, which is also consistent with Chapter 2 in that the ratio of optically thick to anvil plus thin is higher in the EP versus WP.

Given the larger presence of a congestus mode in the EP, it is not surprising that clouds with lower tops contribute more to total mean rainfall in the EP compared to the WP. In fact, clouds below 9.5 km contribute 47% versus 38% to total rainfall in the EP and WP, respectively. Clouds below 9.5 km are more likely to precipitate in both regions, given their contributions to total rain area of 74% and 60% in the EP and WP, respectively.

When we stratified clouds by whether or not they are connected to a contiguous deep convective system (in which at least one profile must have a cloud thickness of 10 km), the vertical structure of cloud tops is very similar in the EP and WP, with only a slightly more top-heavy cloud profile in the WP compared to the EP. When the restriction of a thick convective system was lifted, it is primarily geometrically thin high-topped cloud (e.g. thickness less than 5 km) coverage that is more pervasive in the WP, consistent with MODIS observations of more high optically thin cloud there. The physical explanation of why more high thin cloud exists in the WP certainly needs to be more thoroughly investigated, as high thin cloud is very important for the TOA radiative differences across the ITCZ.

In Chapter 4, we examined warm clouds and the relationships among large-scale meteorology, macrophysics, microphysics, and drizzle. In general, warm cloud top height is correlated spatially and temporally with LWP, though LWPs tend to be higher in regimes of higher N_{eff} near the Asian Coast and over the Gulf of Mexico. Regions of higher N_{eff} are collocated geographically with smaller r_e, and if the notion is that this combination limits the formation of drizzle-sized drops, then additional condensation may result in additional cloud water without the formation of drizzle. The frequency of drizzle is in fact observed to be reduced near the Asian Coast and over the Gulf of Mexico compared to remote marine areas that have lower LWPs (by ~100 g m^{-2}) across the tropics and subtropics. This suggests a role in microphysics limiting

drizzle formation. Drizzle frequency is also greatly reduced in stratocumulus regimes where boundary-layer inversions are strong, particularly off the coast of South America and in the Far Northeast Pacific.

Another major objective of Chapter 4 was to better understand the relative roles of microphysics and macrophysics in both drizzle formation and intensity. In areas of higher mean N_{eff}, drizzling versus nondrizzling clouds have considerably lower N_{eff}, reflecting that lower concentrations are more conducive for drizzle, and that collection and coalescence processes needed for drizzle drops actually remove smaller droplets. In lower mean N_{eff} regimes, the difference of N_{eff} between drizzling and nondrizzling drops is relatively small. In contrast, LWP is much higher in drizzling versus nondrizzling clouds in all regions, reflecting the universal importance of macrophysics. When clouds are already drizzling, the fractional change of LWP for heavily versus lightly drizzling clouds is generally greater than the fractional changes of N_{eff} for heavily versus lightly drizzling clouds. An exception to this is in high N_{eff} regimes, where N_{eff} monotonically decreases as drizzle rate increases.

Though droplet size tends to increase in most areas as dBZ increases, it levels off particularly as dBZ>0, except in high N_{eff} and low r_e regimes, where r_e monotonically increases with drizzle rate. For a given drizzle rate, r_e is much higher in remote marine areas by as much as 8 μm. Also, when we examine drizzle frequency as a function of r_e, there is much divergence among different regions, suggesting that size alone is not a good predictor of drizzle. The oft-

cited 15 μm r_e threshold that apparently partitions drizzling from nondrizzling clouds is not seen in our observations, as drizzle frequency ranges from as little at 20% for an r_e of 15 μm near the South American coast to nearly 80% in deep convective regions.

The best single predictor of drizzle frequency appears to be cloud top height, as there is a very tight relationship of increasing drizzle frequency with cloud top height among eight different regions with vastly different microphysical and macrophysical regimes. There is some divergence of the cloud top height/drizzle frequency relationship for clouds taller than 2 km, though the slightly lower drizzle frequency for deeper warm clouds is mostly in higher N_{eff} regimes. The LWP/drizzle frequency relationship is slightly less tight, and again this is likely a reflection of the role of microphysics. The fact that cloud top height though is so intimately tied to drizzle frequency certainly should be considered in climate models simulating boundary-layer dynamics. Though we did not speculate as to why this may be in Chapter 4, if the cloud base is assumed to be nearly constant, then a higher cloud top may allow for sufficient condensation to large enough sizes (i.e. a radius of 20 μm, Rogers and Yau (1989)) so that collection can become effective to form either drizzle or rain drops. A bit perplexingly, however, is that cloud top height is only a good predictor of drizzle frequency among all regions, but not of drizzle intensity. This certainly warrants future study.

Quantifying drizzle frequency as a function of both microphysics and macrophysics is the culmination of Chapter 4. For a constant LWP, drizzle frequency increases as N_{eff} decreases, and for constant N_{eff}, drizzle frequency increases as LWP increases. This is the case for all tropical and subtropical areas analyzed. Even though drizzle occurrence tends to be more correlated with LWP in general, which suggests the importance of accretion in warm rain, both N_{eff} and LWP are necessary to predict whether or not drizzle is likely. Drizzle frequencies exceed 90% in all regions when LWPs exceed 250 gm^{-2} and N_{eff} values are below 50 cm^{-1}.

Chapter 6: Future Directions

The work presented in this thesis lends itself to possible future directions. In Chapter 2, we presented evidence that indicated that the large decline in radiative cooling by water vapor is related to clear-sky convergence, which is quantitatively related to anvil cloud temperature. It would be interesting to expand this analysis to other parts of the tropics, including the SPCZ, and even perhaps the Atlantic and/or Indian Ocean sectors, to see whether or not there is a quantitative consistency more universally of clear-sky convergence and anvil cloud temperature in regions with different large-scale dynamics and thermal and moisture profiles.

Examining different tropical regions would also be enlightening to see whether or not the optically thick cloud fraction-rain rate relationship, which was the same in the WP, CP, and EP, is also applicable in other regions. As optically thick cloud fraction appears to be a good proxy for rain rate, it also appears to be a good indicator of the fraction of convective cores.

In Chapter 3, we presented evidence that the PDFs of cloud tops of raining clouds are both qualitatively and quantitatively connected to the mean rain rate in both the WP and EP. An extension of this would be to examine other regions, including deep convective and more suppressed subtropical regimes, to determine the consistency in the distribution of cloud top heights to mean precipitation. Cloud top PDFs are driven by a number of factors, including mean SST and SST gradients, as well as moisture and vertical-

velocity profiles. The sensitivity of cloud top PDFs and mean precipitation to these variables could be considered by examining 5° by 5° boxes representing various thermodynamic and dynamic regimes.

Finally, the work presented in Chapter 4 lends itself to several possible future explorations. First off, our analysis was predicated on the criterion that clouds be optically thick ($\tau>3$) and solid (cloud fraction equal to one), which allowed us to retain about 21% of all pixels along the CloudSat track identified by MODIS as warm clouds. While the remaining clouds are thus either optically thin or inhomogeneous, making optical retrievals such as effective radius potentially spurious, one could still examine the CloudSat characteristics of this large population of warm clouds, including frequency and intensity of drizzle. One may imagine many of these clouds unlikely to drizzle, but our preliminary analysis (results not shown) indicates a nontrivial portion of these clouds, as inferred from CloudSat, may be drizzling.

On a related note, the propensity of a cloud deck to drizzle could also be examined as a function of optical depth heterogeneity within each MODIS assemblage. Such an analysis would encompass MODIS assemblages already considered in our calculations in Chapter 4. Given that open-cellular warm clouds are more likely to be drizzling, it might be expected that clouds with larger optical depth variability on a small-scale may be more likely to drizzle and have higher mean drizzle rates than more homogeneous clouds.

Though we solely used the 3.75-μm channel in Chapter 4 to retrieve r_e, which is most related to cloud top cloud radius, all three channels (including 1.64-μm and 2.13-μm) could be used simultaneously to infer the vertical distribution of r_e with height. In general, mean cloud droplet size increases with height due to condensational growth, but a precipitating cloud with effective coalescence growth would likely contain droplets that are larger towards cloud base. Relating the vertical r_e distribution to both cloud top height and LWP would be useful in relating droplet growth to cloud macrophysics. The extent to which these microphysical features are observed for nondrizzling and drizzling clouds would be a natural expansion of Chapter 4.

A relatively new CloudSat product is that of rain rates, and these could be compared to using maximum dBZ as a proxy for drizzle rate. The extent to which maximum dBZ is linearly related to rain rate could be assessed as a function of cloud microphysics and macrophysics.

Bibliography

Ackerman, A. S., M. P. Kirkpatrick, D. E. Stevens, and O. B. Toon, 2004: The impact of humidity above stratiform clouds on indirect aerosol climate forcing. *Nature*, **432**, 1014-1017.

Albrecht, B. A., 1989: Aerosols, cloud microphysics, and fractional cloudiness. *Science,* **245**, 1227-1230.

Albrecht, B. A., C. W. Fairall, D. W. Thomson, and A. B. White, 1990: Surface-based remote sensing of the observed and the adiabatic liquid water content of stratocumulus clouds. *Geophys. Res. Lett.,* **17**, 89-92.

Back, L. E, and C. S. Bretherton, 2007: Geographic variability in the export of moist static energy and vertical motion profiles in the Tropical Pacific, *Geophys. Res. Lett*., *33*, L17810, doi:10.1029/2006GL026672.

Back, L. E., and C. S. Bretherton, 2008a: A simple model of climatological Precipitation and vertical motion patterns over the tropical oceans. *J. Clim.*, in press.

Back, L. E. and C. S. Bretherton, 2008b: On the relationship between SST gradients, boundary layer winds, and convergence over the tropical oceans. *J. Clim.,* in press.

Bennartz, R., 2007: Global assessment of marine boundary layer cloud droplet number concentration from satellite. *J. Geophys. Res.,* **112**, D02201, doi: 10.1029/2006JD0075472007.

Berg, W., C. Kummerow, and C. A. Morales, 2002: Differences between east and west Pacific rainfall systems. *J. Clim.*, **15**, 3659-3672.

Boehm, M. T., and J. Verlinde, 2000: Stratospheric influence on upper tropospheric tropical cirrus. *Geophys. Res. Lett,* **27**, 3209-3212.

Breon, F. M., D. Tanre, and S. Generoso, 2002: Aerosol effect on cloud droplet size monitored from satellite. *Science*, **295**, 834-838.

Brenguier, J.-L., H. Pawlowska, L. Schuller, R. Preusker, J. Fischer, and Y. Fouquart, 2000: Radiative properties of boundary layer clouds: droplet effective radius versus number concentration. *J. Atmos. Sci*., **57**, 803-821.

Bretherton, C. S., and M. C. Wyant, 1997: Moisture transport, lower-tropospheric stability, and decoupling of cloud-topped boundary layers. *J. Atmos. Sci.,* **54**, 148-167.

Charlson, R. J., J. E. Lovelock, M. O. Andreae, and S. G. Warren, 1987: Oceanic phytoplankton, atmospheric sulfur, cloud albedo, and climate. *Nature*, **326**, 655-661.

Comstock, K. K., R. Wood, S. E. Yuter, and C. S. Bretherton, 2004: Reflectivity and rain rate in and below drizzling stratocumulus. *Quart. J. Roy. Meteor. Soc.*, **130**, 2891-2918.

Comstock, K. K., C. S. Bretherton, and S. E. Yuter, 2005: Mesoscale variability and drizzle in southeast Pacific stratocumulus. *J. Atmos. Sci.,* **62**, 3792-3807.

De Roode, S. R., and P. G. Duynkerke, 1997: Observed lagrangian transition of stratocumulus into cumulus during ASTEX: mean state and turbulence structure. *J. Atmos. Sci.,* **54,** 2157-2173.

Dessler, A. E., and P. Yang, 2003: The distribution of tropical thin cirrus clouds inferred from *Terra* MODIS data. *J. Climate,* **16**, 1241-1247.

Dessler, A. E., S. P. Palm, and J. D. Spinhirne, 2006: Tropical cloud-top height distributions revealed by the Ice, Cloud, and Land Elevation Satellite (ICESat)/Geoscience Laser Altimeter System (GLAS). *J. Geophys. Res.,* **111,** D12215, doi:10.1029/2005.JD006705.

Dong, X., P. Minnis, B. Xi, S. Sun-Mack, and Y. Chen, 2008: Comparison of CERES-MODIS stratus cloud properties with ground-based measurements at the DOE ARM Southern Great Plains site, *J. Geophys. Res.*, **113**, D03204, doi:10.1029/2007JD008438.

Folkins, I., M. Loewenstein, J. Podolske, S. J. Oltmans, and M. Proffitt, 1999: A barrier to vertical mixing at 14 km in the tropics: evidence from ozonesondes and aircraft measurements. *J. Geophys. Res.*, **104**, 22095-22102.

Folkins, I., S. J. Oltmans, and A. M. Thompson, 2000: Tropical convective outflow and near surface equivalent potential temperatures. *Geophys. Res. Lett.,* **27**, 2549-2552.

Fox, N. I., and A. J. Illingworth, 1997: The potential of a spaceborne cloud radar for the detection of stratocumulus clouds. *J. Appl. Meteor.,* **36**, 676-686.

Frisch, A. S., C. W. Fairall, and J. B. Snider, 1995: Measurement of stratus cloud and drizzle parameters in ASTEX with a K_{α}-band Doppler radar and a microwave radiometer. *J. Atmos. Sci*., **52**, 2788-2799.

Fu, Q., and K. N. Liou, 1993: Parameterization of the solar radiative properties of cirrus clouds. *J. Atmos. Sci*., **50**, 2008-2025.

Han, Q., W. B. Rossow, and A. A. Lacis, 1994: Near-global survey of effective droplet radii in liquid water clouds using ISCCP data. *J. Clim.*, **7**, 465-497.

Harrison, E. F., P. Minnis, B. R. Barkstrom, V. Ramanathan, R. D. Cess, and G. G. Gibson, 1990: Seasonal variation of cloud radiative forcing derived from the Earth radiation budget experiment. *J. Geophys. Res.*, **95**, 18687-18703.

Hartmann, D. L., and D. A. Short, 1980: On the use of Earth radiation budget statistics for studies of clouds and climate. *J. Atmos. Sci.,* **37**, 1233-1250.

Hartmann, D. L. and K. Larson, 2002: An important constraint on tropical cloud-climate feedback. *Geophys. Res. Lett.*, **29**, 1195, doi: 10:1029/2002GL015835.

Hartmann, D. L., L. A. Moy, and Q. Fu, 2001: Tropical convection and the energy balance at the top of the atmosphere. *J. Clim.*, **14**, 4495-4511.

Hindman, E. E., P. V. Hobbs, and L. F. Radke, 1977: Cloud condensation nucleus size distributions and their effects on cloud droplet size distributions. *J. Atmos. Sci.,* **34**, 951-956.

Holton, J. R., 1992: *An Introduction to dynamic meteorology*. Academic Press, 511 pp.

Houze, R. A., 1993: *Cloud Dynamics*. Academic Press, 573 pp.

Hudson, J. E., 1983: Effects of CCN concentrations on stratus clouds. *J. Atmos. Sci.,* **40**, 480-486.

Johnson, R. H., T. M. Rickenbach, S. A. Rutledge, P. E. Ciesielski, and W. H. Schubert, 1999: Trimodal characteristics of tropical convection. *J. Clim.*, **12**, 2397-2418.

King, M. D., 1987: Determination of the scaled optical thickness of clouds from reflected solar radiation measurements. *J. Atmos. Sci.*, **44**, 1734–1751.

King, M. D., S.-C. Tsay, S. Platnick, M. Wang, and K.-N. Liou, 1997: Cloud retrieval algorithms for MODIS: Optical thickness, effective particle radius, and thermodynamic phase. MODIS Algorithm Theoretical Basis Doc. ATBD-MOD-05, MOD06-Cloud product, 83 pp.

Klein, S. A., 1995: Large-scale variations in boundary layer cloud cover and their relationship to meteorological parameters. Ph.D. thesis, 206 pp., Univ. of Wash., Seattle.

Klein, S. A., and D. L. Hartmann, 1993: The seasonal cycle of low stratiform clouds. *J. Clim.,* **6**, 1587-1606.

Korolev, A. V., G. A. Isaac, I. P. Mazin, and H. W. Barker, 2001: Microphysical properties of continental clouds from in situ measurements. *Q. J. R. Meteorol. Soc.,* **127,** 2117-2151.

Kubar, T. L., D. L. Hartmann, and R. Wood, 2007: Radiative and convective driving of tropical high clouds, *J. Clim.*, **20***,* 5510-5526.

Kubar, T.L. and D.L. Hartmann, 2008: The vertical structure of tropical oceanic clouds and its Relation to Precipitation. *Geophys. Res. Lett.***, 35**, L03804,doi:10.1029/2007GL032811.

Kursinski, E. R., G. A. Hajj, K. R. Hardy, J. T. Schofield, and R. Linfield, 1997: Observing Earth's atmosphere with radio occultation measurements using the Global Positioning System. *J. Geophys. Res.,* **102**, 23429-23465.

Lau, K. M., and H. T. Wu, 2003: Warm rain processes over tropical oceans and climate implications, *Geophys. Res. Lett., 30,* doi:10.1029/2003GL018567.

Lilly, D. K., 1968: Models of cloud-topped mixed layers under a strong Inversion. *Quart. J. Roy. Meteor. Soc.*, **94**, 292-309.

Liou, K. -N., 1992: *Radiation and Cloud Processes in the Atmosphere: Theory, Observation, and Modeling*. Oxford University Press, 487 pp.

Liu, C., and M. W. Moncrieff, 1998: A numerical study of the diurnal cycle of tropical oceanic convection. *J. Atmos. Sci.*, **55**, 2329-2344.

Liu, Y., B. Geerts, M. Miller, P. Daum, and R. McGraw, 2008: Threshold radar reflectivity for drizzling clouds. *Geophys. Res. Lett.,* **35**, L03807, doi: 10.1029/2007GL031201.

Livesey, N. J., W. G. Read, M. J. Filipiak, L. Froidevaux, R. S. Harwood, J. H. Jiang, C. Jimenez, H. M. Pickett, H. C. Pumphrey, M. L. Santee, M. J. Schwartz, J. W. Waters, and D. L. Wu, 2005: Version 1.5 Level 2 data quality and description document. Technical report, Jet Propulsion Laboratory, 2005. JPL D-32381.

Mace, G., 2007: Level 2 GEOPROF product process description and interface control document algorithm version 5.3, 44 pp.

Malkus, J. S., and H. Riehl, 1964: *Cloud Structure and Disturbances over the Tropical Pacific Ocean*. University of California Press, 229 pp.

Mapes, B. E., and R. A. Houze, 1993: Cloud clusters and superclusters over the oceanic warm pool. *Mon. Wea. Rev.,* **121**, 1398-1415.

Martin, G. M., D. W. Johnson, and A. Spice, 1994: The measurement and parameterization of effective radius and droplets in warm stratocumulus clouds. *J. Atmos. Sci.*, **51**, 1823-1842.

Matrosov, S. Y., T. Uttal, and D. A. Hazen, 2004: Evaluation of radar reflectivity-based estimates of water content in stratiform marine clouds. *J. Appl. Meteor.,* **43**, 405-419.

Miles, N.L., J. Verlinde, and E. E. Clothiaux, 2000: Cloud droplet size distributions in low-level stratiform clouds. *J. Atmos. Sci*., **57**, 295-311.

McClatchey, R. A., W. S. Fenn, J. E. A. Selby, F. E. Volz, and J. S. Garing, 1971: Optical properties of the atmosphere. *Rep. AFCrl-71-0279*, Air Force Cambridge Res. Lab., Bedford, Mass., 85.

McFarquhar, G. M., A. J. Heymsfield, J. Spinhirne, and B. Hart, 2000: Thin and subvisual tropopause tropical cirrus: observations and radiative impacts. *J. Atmos. Sci,* **57,** 1841-1853.

Nakajima, T., and M. D. King, 1990: Determination of the optical thickness and effective particle radius of clouds from reflected solar radiation measurements. Part I: Theory. *J. Atmos. Sci.*, **47**, 1878–1893.

Nakajima, T., and T. Nakajima, 1995: Wide-area determination of cloud microphysical properties from NOAA AVHRR measurements for FIRE and ASTEX regions. *J. Atmos. Sci.*, **52**, 4043-4059.

Neiburger, M., D. S. Johnson, and C. W. Chien, 1961: Part I: the inversion over the eastern North Pacific Ocean. Studies of the structure of the atmosphere over the eastern Pacific Ocean in summer. *Univ. of California Publications in Meteor.,* **No. 1,** University of California Press, 1-94.

Nicholls, S., 1984: Dynamics of stratocumulus: aircraft observations and comparisons with a mixed layer model. *Quart. J. Roy. Meteor. Soc.,* **110,** 783-820.

Pawlowska, H., and J.-L. Brenquier, 2003: An observational study of drizzle formation in stratocumulus clouds for general circulation model (GCM) parameterizations. *J. Geophys. Res.*, **108**, 8630, doi: 10.1029/2002JD002679.

Petty, G. W., 2006: *A First Course in Atmospheric Radiation*. 2d Ed. Sundog Publishing, 459 pp.

Pincus, R., and M. B. Baker, 1994: Effect of precipitation on the albedo susceptibility of clouds in the marine boundary layer. *Science*, **372**, 250-252.

Platnick, S., M. D. King, S. A. Ackerman, W. P. Menzel, B. A. Baum, J. C. Riedi, and R. A. Frey, 2003: The MODIS cloud products: algorithms and examples from Terra. *IEEE Trans. Geosci. Remote Sens.*, **41**, 459-473.

Pruppacher, H. R., and J. D. Klett, 1978: *Microphysics of Clouds and Precipitation.* Dordrecht, Holland, D. Reidel Publ. Co., 714 pp.

Randall, D. A., J. A. Coakley Jr., C. W. Fairall, R. A. Kropfli, and D. H. Lenschow, 1984: Outlook for research on subtropical marine stratiform clouds. *Bull. Amer. Meteor. Soc.*, **65**, 1290-1301.

Randall, D. A., and M. J. Suarez, 1984: On the dynamics of stratocumulus

formation. *J. Atmos. Sci.*, **41,** 3052-3057.

Rauber, R. M, B. Stevens, H. T. Ochs II, C. Knight, B. A. Albrecht, A. M. Blyth, C. W. Fairall, J. B. Jensen, S. G. Lasher-Trapp, O. L. Mayol-Bracero, G. Vali, J. R. Anderson, B. A. Baker, A. R. Bandy, E. Burnet, J. Brenguier, W. A. Brewer, P. R. A. Brown, P. Chuang, W. R. Cotton, L. Di Girolamo, B. Geerts, H. Gerber, S. Goeke, L. Gomes, B. G. Heikes, J. G. Hudson, P. Kollias, R. P. Lawson, S. K. Krueger, D. H. Lenschow, L. Nuijens, D. W. O'Sullivan, R. A. Rilling, D. C. Rogers, A. P. Siebesma, E. Snodgrass, J. L. Stith, D. C. Thornton, S. Tucker, C. H. Twohy, and P. Zuidema, 2007: Rain in shallow cumulus over the ocean. *Bull. Amer. Meteor. Soc*., **88,** 1912-1928.

Reed, R. J., and E. E. Recker, 1971: Structure and properties of synoptic-scale wave disturbances in the equatorial western Pacific. *J. Atmos. Sci.,* **28**, 1117-1133.

Riehl, H., and J. S. Malkus, 1958: On the heat balance in the equatorial trough zone. *Geophysica*, **6**, 503-538.

Riehl, H., T. C. Yeh, J. S. Malkus, and N. E. LaSeur, 1951: The northeast trade of the Pacific Ocean. *Quart. J. Roy. Meteor. Soc.,* **77**, 598-626.

Remote Sensing Systems, 2006: Updates to the AMSR-E V05 algorithm. Tech. Repo 020706, 5 pp. [Available online at http://www.remss.com/amsr/amsr_data_description.html#version.]

Reynolds, R. W., N. A. Rayner, T. M. Smith, D. C. Stokes, and W. Wang, 2002: An improved in-situ and satellite SST analysis for climate. *J. Clim.*, **15**, 1609-1625.

Rogers, R. R., and M. K. Yau, 1989: *A Short Course in Cloud Physics*. 3rd ed. Butterworth Heinemann, 290 pp.

Sarachik., E. S., 1978: Tropical sea surface temperature: An interactive one-dimensional atmosphere-ocean model. *Dynamics of Atmospheres and Oceans*, **2**, 455-469.

Sassi, F., M. Salby, and W. G. Read, 2001: Relationship between upper tropospheric humidity and deep convection. *J. Geophys. Res*., **106**, 17133-17146.

Savic-Jovcic, V., and B. Stevens, 2008: The structure and mesoscale organization of precipitating stratocumulus. *J. Atmos. Sci.*, **65**, 1587-

1605.

Schmidt, T., J. Wickert, G. Beyerle, and C. Reigber, 2004: Tropical tropopause parameters derived from GPS radio occultation measurements with CHAMP. *J. Geophys. Res.*, **109**, 1-13.

Schumacher, C., and R. A. Houze, 2003: Stratiform rain in the tropics as seen by the TRMM precipitation radar, *J. Clim.*, *16*, 1739-1756.

Sharon, T. M., B. A. Albrecht, H. H. Jonsson, P. Minnis, M. M. Khaiyer, T. M. VanReken, J. Seinfeld, R. Flagan, 2006: Aerosol and cloud microphysical characteristics of rifts and gradients in maritime stratocumulus clouds. *J. Clim.*, **63,** 983-997.

Slingo, A., 1990: Sensitivity of the Earth's radiation budget to changes in low clouds. *Nature*, **343**, 49-51.

Squires, P., 1956: The microstructure of cumuli in maritime and continental air. *Tellus,* **8**, 443-444.

Squires, P., 1958: The microstructure and colloidal stability of warm clouds. Part I – The relation between structure and stability. *Tellus*, **10**, 256-262.

Stephens, G. L., D. G. Vane, R. J. Boain, G. G. Mace, K. Sassen, Z. E. Wang, A. J. Illingworth, E. J. O'Connor, W. B. Rossow, S. L. Durden, S. D. Miller, R. T. Austin, A. Benedetti, and C. Mitrescu, 2002: The CloudSat mission and the A-train - a new dimension of space-based observations of clouds and precipitation. *Bull. Amer. Meteor. Soc*., **83**, 1771-1790.

Stephens, G. L., D. G. Vane, S. Tanelli, E. Im, S. Durden, M. Rokey, D. Reinke, P. Partain, G. G. Mace, R. Austin, T. L'Ecuyer, J. Haynes, M. Lebsock, K. Suzuki, D. Waliser, D. Wu, J. Kay, A. Gettleman, Z. Wang, R. Marchard, 2008: The CloudSat mission: performance and early science after the first year of operation. *J. Geophys. Res.*, in press.

Stevens, B., 2005: Atmospheric moist convection. *Ann. Rev. Earth Planet. Sci.,* **64**, 2916-2931.

Stevens, B., G. Vali, K. K. Comstock, R. Wood, M. C. vanZanten, P. H . Austin, C. S. Bretherton, and D. H. Lenschow, 2005: Pockets of open cells and drizzle in marine stratocumulus. *Bull. Amer. Meteor. Soc.*,

86, 51-57.

Suzuki, K., and G. L. Stephens, 2008: Global identification of warm cloud microphysical processes with combined use of A-Train observations. *Geophys. Res. Lett.,* **35**, L088805, doi: 10.1029/2008GL033590.

Szczodrak, M., P. H. Austin, and P. B. Krummel, 2001: Variability of optical depth and effective radius in marine stratocumulus clouds. *J. Atmos. Sci.*, **58**, 2912-2926.

Twomey, S., 1974: Pollution and the planetary albedo. *Atmos. Environ.***, 8**, 1251-1256.

Twomey, S., 1977: The influence of pollution on the shortwave albedo of clouds. *J. Atmos. Sci.,* **34**, 1149-1152.

Udelhofen, P. M., and D. L. Hartmann, 1995: Influence of tropical cloud systems on the relative humidity in the upper troposphere. *J. Geophys. Res.,* **100**, 7423-7440.4

vanZanten, M. C., B. Stevens, G. Vali, and D. H. Lenschow, 2005: Observations of drizzle in nocturnal marine stratocumulus. *J. Atmos. Sci.,* **62**, 88-106.

Wood, R., 2007: Cancellation of aerosol indirect effects in marine Stratocumulus through cloud thinning. *J. Atmos. Sci.,* **64**, 2657-2669.

Wood, R., 2005: Drizzle in stratiform boundary layer clouds. Part II: microphysical aspects, **62**, 3034-3050. *J. Atmos. Sci.*, 3034-3050.

Wood, R., 2006a: Rate of loss of cloud droplets by coalescence in warm clouds. *J. Geophys. Res.,* **111**, D21205, doi: 10.1029/2006JD007553.

Wood, R., 2006b: Relationships between optical depth, liquid water path, droplet concentration, and effective radius in adiabatic layer cloud. University of Washington, *Personal Note.*

Wood, R., and C. S. Bretherton, 2004: Boundary layer depth, entrainment, and decoupling in the cloud-capped subtropical and tropical marine boundary layer. *J. Clim.*, **17**, 3576-3588.

Wood, R., 2008: Stratocumulus clouds. *Mon. Wea. Rev. ,* in preparation.

Wu, D., Y. Hu, M. P. McCormick, Z. Liu, K. Xu, B. Smith Jr., A. Omar, and F.-L. Chang, 2008: Estimating the marine boundary layer lapse rate using CALIPSO, MODIS, and AMSR data. *Geosci. Remote Sensing Lett.,* in press.

Yanai, M., S. Esbensen, and J. -H. Chu, 1973: Determination of bulk properties of tropical cloud clusters from large-scale heat and moisture budgets. *J. Atmos. Sci*., **30**, 611-627.

Zelinka, M., D. and D. L. Hartmann, 2008: Response of humidity and clouds to tropical deep convection. *J. Clim.,* submitted 8/08.

Zhang, C. D., M. McGauley, and N. A. Bond, 2004: Shallow meridional circulation in the tropical eastern Pacific, *J. Clim.*, *17*, 133-139.

Zuidema, P., E. R. Westwater, C. Fairall, and D. Hazen, 2005: Ship-based liquid water path estimates in marine stratocumulus. *J. Geophys. Res.*, **110**, D20206, doi: 10.1029/2005JD005833.

VITA

Terence L. Kubar was born in Fresno, CA on July 18, 1981, where he attended Bullard High School and graduated Summa Cum Laude valedictorian in 1999. Since a very young age, Terence was passionate about meteorology, always observing the sky and maintaining several weather stations, as well as reading various weather and cloud books. As a president's scholar, he was able to pursue this passion by attending San Jose State University and studying meteorology. By taking a range of rigorous core meteorology courses, he acquired an increased appreciation about the complexity of both the atmosphere and climate systems. His senior research project, "The Revision of an RCM and its Coupling With a Carbon Cycle Model", under the direction of Jerry Stephens, exposed Terence to the climate modeling world, as well as the utility in using simple climate models to better understand important factors of climate sensitivity. Terence graduated from San Jose State University in May 2003 with a Bachelor of Science in meteorology and a minor in applied mathematics. Even though Terence's project dealt with climate modeling and climate change, he also thoroughly enjoyed forecasting as a hobby, and performed well in such classes as well as the National Collegiate Forecasting Contest.

Terence moved to Seattle in August 2003 to commence his graduate school career under the direction of Professor Dennis L. Hartmann. His research interests in graduate school included tropical and subtropical climate,

convection, clouds, and precipitation using a multitude of satellite sensors. His interests of convection and clouds included a diverse range of scales, ranging from shallow stratocumulus to cumulus congestus to deep cumulonimbus clouds. While at the University of Washington, Terence continued to enjoy forecasting as an avocation, and even was the atmospheric science forecasting competition champion in spring 2005. He completed his Ph.D. from the University of Washington in the field of Atmospheric Sciences in the autumn of 2008. Terence is the recipient of a NASA ORAU fellowship, and will commence his research as a Caltech postdoc at the Jet Propulsion Laboratory Campus in Pasadena, CA, under the guidance of Duane Waliser, in the autumn of 2008. He will continue expanding his remote sensing knowledge to further understand clouds, convection, and precipitation and their roles in the climate system. Terence hopes to continue his research career in atmospheric science in the long-term future.